

Electrospun carbon nanotube filled composite nanofibers by non-covalent compatibilization

by

Piere-André John Siebert

Thesis presented in partial fulfilment of the requirements for the
degree Master of Science in Polymer Science
at Stellenbosch University



Supervisor: Prof. Peter E. Mallon

March 2016

Declaration

By submitting this thesis/dissertation electronically, I declare that the entirety of the work contained therein is my own, original work, that I am the sole author thereof (save to the extent explicitly otherwise stated), that reproduction and publication thereof by Stellenbosch University will not infringe any third party rights and that I have not previously in its entirety or in part submitted it for obtaining any qualification.

March 2016

Copyright © 2016 Stellenbosch University

All rights reserved

Abstract

This study covers the successful production of poly(acrylonitrile) (PAN)/multi-walled-carbon-nanotube (MWCNT) fibrous composites by the incorporation of noncovalently functionalized MWCNTs in various loading fractions. In maintaining the sp^2 hybridization as opposed to the conventional covalent functionalization, the conjugated MWCNT structure is maintained and in doing so preserves the mechanical and conductive properties commonly associated with these fillers. This allows for the optimum transference of desired property/properties to the produced composite assuming sufficient filler dispersion. MWCNTs are functionalized by polymeric compatibilizers of mono- and multi pyrene functional character. The pyrene moiety allows for the noncovalent π - π stacking interaction to the conjugated surface of MWCNTs by strong van der Waals forces.

Mono pyrene functional poly(acrylonitrile) (Py-PAN) polymers were synthesized via Atom Transfer Radical Polymerization (ATRP) from presynthesized pyrene functional initiators namely 1-pyrenemethyl-2-bromoisobutyrate and 1-pyrenebutyl-2-bromoisobutyrate respectively. The synthesis of PAN polymers of α -chain end pyrene functionality was also attempted by the relatively unexplored redox initiated polymerization by catalytic cerium ammonium nitrate (CAN) from 1-pyrenemethanol and 1-pyrenebutanol initiators respectively. The synthesis proved challenging from the proposed initiators and with relatively low yields even after an extensive method development in an effort to achieve optimum reaction conditions. Multi pyrene functional PAN polymers (PAN-co-PyMMP) was successfully prepared via Conventional Free Radical (CFR) copolymerization of conventional acrylonitrile (AN) monomers and presynthesized (1-pyrene)methyl-2-methyl-2-propenoate (PyMMP) macromonomers in producing a PAN based polymers of protruding pyrene moieties along the polymer chain. The multi pyrene functional copolymer is successfully prepared to three predetermined PyMMP compositions (or mol% functionality) by variation of the monomer feed ratio. The synthesized initiators as well as the monomer and functional polymers were analyzed by $^1\text{H-NMR}$ analysis confirming the isolation of the hypothesized products. $^1\text{H-NMR}$ was also implemented to determine the average composition of the pyrene moiety incorporated into both of the structurally alternate functional PAN polymers presented as the mol% pyrene functionality.

Mono- and multi-functional variations of the PAN polymer were exposed to increasing amounts of MWCNTs and analyzed by $^1\text{H-NMR}$ following reported instances of a quenching phenomenon being seen in the $^1\text{H-NMR}$ spectra of signals representing protons taking part in π - π stacking interactions (protons protruding from the pyrene moiety). The analysis produced a quenching trend of the polymers as the MWCNT loading is increased. These

Abstract

trends are confirmed by the more common method of tracking these noncovalent π - π stacking interactions by the quenching phenomenon apparent from the UV-fluorescence analysis of the pyrene moieties. Trends observed are presented to be linear as the mono-functional polymer is exposed to increasing amounts of MWCNTs where as the multi-functional polymer shows a greater initial quenching followed by what seems to be an inversion point at a 20 wt% to 30 wt% MWCNT composition after which a linear trend emerges upon a further increase of MWCNT loadings comparable to what is seen for the mono-functional polymer. The quenching analysis suggests a stronger MWCNT/functional-polymer interaction for the multi-functional polymers at similar mol% pyrene functionalities.

As envisioned, electrospinning is used to prepare the fibrous composite PAN/MWCNT materials that were prepared by the noncovalent functionalization of pristine MWCNTs via the mono and multi pyrene functional PAN compatibilizers. This lead to the successful dispersion of the MWCNT filler throughout the fiber matrix in an aligned state along the fiber axis, as shown by scanning electron microscopy (SEM) and transition electron microscopy (TEM) analysis.

A preliminary study was undertaken to produce PAN/graphene fibrous nanocomposites using the novel compatibilizers, synthesized in this study. Association analysis with compatibilizers indicated weaker π - π stacking interactions when compared to the MWCNT fillers. Further analysis suggest poor graphite exfoliation and filler dispersion within the fibrous matrix.

The carbonization of noncovalently functionalized fibrous MWCNT/PAN composites was successful as shown by SEM analysis.

Opsomming

Hierdie studie dek die suksesvolle sintese van poli(akrilonitriël) (PAN)/multi-wand-koolstof-nanobuisies ("multi walled carbon nanotubes (MWCNT)") veselagtige samestellings deur die byvoeging van nie-kovalente gefunksionaliseerde MWCNTs van verskillende hoeveelhede. In teenstryding met kovalente funksionalisasie – sp^2 hibridisasie van MWCNTs word behou deur die gebruik van 'n nie-kovalente funksionalisasie metode. Die gekonjugeerde MWCNT struktuur word dus behou, en meganiese en geleidende eienskappe geassosieer met hierdie materiale word nie belemmer nie. Indien hierdie nie-kovalente gefunksionaliseerde MWCNTs gebruik word as vullers sal die eienskappe geassosieerd daarmee optimaal oorgedra word na die samestelling; indien die vuller eweredig in die samestelling versprei is. In hierdie studie is MWCNTs gefunksionaliseer met mono- en multi-pyrene om eweredige verspreiding toe te laat. Die pyrene eenheid heg aan die gekonjugeerde MWCNT struktuur deur 'n nie-kovalente π - π stapel interaksie met behulp van Van der Waals kragte wat teenwoordig is.

Mono pyrene funksionele poliakrilonitriël (Py-PAN) polimere was sintetiseer deur gebruik te maak van Atoom Oordrag Radikale Polimerisasie ("Atom Transfer Radical Polymerization (ATRP)"). Pyrene funksionele inisieerders wat vooraf gesintetiseer is, naamlik 1-pyrenemetiel-2-bromoisobuteraat en 1-pyrenebutiel-2-bromoisobuteraat, is hiervoor gebruik. In 'n poging om PAN polimere met 'n α -ketting einde pyrene funksionaliteit te sintetiseer, was 'n relatief onbekende redoks geïnisieerde polimerisasie ondersoek. Hierdie polimerisasie maak gebruik van serium ammonium nitraat ("cerium ammonium nitrate (CAN)") as katalisator en beide 1-pyrenemetanol en 1-pyrenebutanol as inisieerders. Lae opbrengste is verkry deur gebruik te maak van die bogenoemde inisieerders. Die metode was daarom aangepas en ontwikkel in 'n poging om optimale reaksie kondisies te vind, maar gewenste opbrengste is nie verkry nie. Suksesvolle sintese van multi pyrene funksionele PAN polimere (PAN-co-PyMMP) is bereik deur gebruik te maak van Konvensionele Vrye Radikaal ("Conventional Free Radical (CFR)") ko-polimerisasie. 'n PAN gebaseerde polimeer met pyrene eenhede wat uitsteek langs die lengte van die polimeer-ketting is dus gesintetiseer, en is bereik deur gebruik te maak van konvensionele akrilonitriël (AN) monomere en vooraf gesintetiseerde (1-pyrene)metiel-2-metiel-2-propenoaat (PyMMP) makro-monomere. Die multi pyrene funksionele ko-polimeer is suksesvol gesintetiseer met drie verskillende voorafbepaalde hoeveelhede van PyMMP (mol% funksionaliteit) deur die verhouding van monomeer wat toegevoeg is te verander. Die gesintetiseerde inisieerders, makro-monomere en funksionele polimere is deur ^1H -KMR analiseer, en isolasie van die voorafgestelde produk is hierdeur bevestig. ^1H -KMR analise was ook gebruik om die

Opsomming

gemiddelde hoeveelhede van die pyrene eenhede wat teenwoordig is in die mono- en multi-pyrene polimere te bepaal; waar die hoeveelhede as mol% pyrene funksionaliteit noteer is.

Daar is berig dat pieke van protone wat in die ^1H -KMR spektrum voorkom se intensiteit kleiner raak wanneer die protone deelneem aan π - π stapel interaksies. Gevolglik is mono- en multi-funksionele variasies van die PAN polimeer met toenemende hoeveelhede van MWCNTs gemeng, en daarna deur ^1H -KMR geanaliseer. In die ^1H -KMR analise is daar opgelet dat die pieke van die protone, wat by die pyrene eenheid 'uitsteek', se intensiteit kleiner raak soos die hoeveelheid MWCNTs toegevoeg meer raak. Hierdie tendens is ook bevestig deur gebruik te maak van die meer gewilde UV fluoressensie ontledings-metode, waar die π - π stapel interaksies bevestig is deur pieke vir die pyrene eenhede wat se intensiteit kleiner raak. Lineêre tendens is waargeneem vir die mono-funksionele polimeer, waar die intensiteit van die pieke kleiner raak hoe meer MWCNTs bygevoeg is. Vir die multi-funksionele polimeer word daar 'n groot aanvanklike verlaging in die intensiteit gesien, gevolg deur 'n inverse punt by 'n gewigs fraksie van 20-30 ("weight persentage (wt%)") MWCNT waarna 'n lineêre tendens na vore kom. Vergelykbare verhoudings van MWCNTs is by beide die mono- en multi-funksionele polimere bygevoeg. Die bogenoemde resultate dui daarop dat daar 'n sterker interaksie tussen die multi-funksionele polimeer en die MWCNTs voorkom in vergelyking met die mono-funksionele polimeer en die MWCNTs, waar dieselfde funksionele polimere teenwoordig is.

Die saamgestelde veselagtige PAN/MWCNT materiale is sintetiseer deur die nie-kovalente funksionalisasie van MWCNTs met mono- en multi-pyrene funksionele PAN kompatibiliseerders waarna die samestelling ge-elektrospin is. Dit het gelei tot die suksesvolle en eweredige verspreiding van MWCNT vullers deur die vesel matriks. MWCNTs wat in lyn is met die lengte van die vesels is gesien in SEM en TEM beelde.

Acknowledgements

First and foremost I would like to thank Prof. P. E. Mallon for all his guidance and enthusiasm during the timespan of this project. His open door policy and high priority towards the project, regardless of a busy schedule is greatly appreciated.

I would like to extend a sincere thanks to all of the friendly faces who made analysis a pleasure such as Elsa Malherbe who ran countless $^1\text{H-NMR}$ samples with a smile, Nadine Makan for all the GPC analysis as well as Madelein Frazenberg and Angelique Laurie for their assistance at the SEM. The staff at the Polymer Science department deserves acknowledgement specifically Deon Koen and Calvin Maart for always being willing to assist. A special thanks needs to be given to my fellow MSc. students (Carlo Botha, Chantelle Human and Nedine van Deventer) for the morning regrouping sessions and all the advice both inside the lab and out.

To all my friends outside of science, I want to say thank you for the much needed relaxation times and at sometimes showing a genuine interest in my work.

Last but certainly not least I would like to thank my parents, grandparents and brother for the support and motivation as well as Louise Malan for her love and patience.

Table of contents

| | |
|--|-----------|
| List of abbreviations..... | iv |
| List of figures..... | vi |
| List of schemes..... | x |
| List of tables..... | xi |
| 1. Introduction and objectives..... | 1 |
| 1.1 Introduction..... | 2 |
| 1.2 Objectives..... | 3 |
| 1.3 References..... | 5 |
| 2. Historical and literature review..... | 7 |
| 2.1 Polymer nanocomposites..... | 8 |
| 2.2 Carbon nanotubes..... | 9 |
| 2.3 Methods of CNT synthesis..... | 10 |
| 2.4 Functionalization of CNTs..... | 11 |
| 2.5 Covalent functionalization of CNTs..... | 12 |
| 2.6 Non-covalent functionalization of CNTs..... | 14 |
| 2.8 Synthesis of mono and multi-functional polymers..... | 17 |
| 2.8.1 Chain end functional polymer synthesis..... | 17 |
| 2.8.1.1 Anionic polymerization..... | 17 |
| 2.8.1.2 RAFT polymerization..... | 19 |
| 2.8.1.3 NMP synthesis..... | 22 |
| 2.8.1.4 ATRP synthesis..... | 23 |
| 2.8.1.5 Cerium ammonium nitrate initiated polymerization using redox initiation..... | 27 |
| 2.8.2 Multi-functional polymer synthesis..... | 29 |
| 2.8.2.1 Copolymers..... | 30 |
| 2.9 Electrospinning..... | 33 |
| 2.10 Polymer nanocomposite nanofibers..... | 35 |
| 2.11 Analysis techniques..... | 37 |
| 2.12 References..... | 39 |
| 3. Experimental..... | 47 |
| 3.1 Experimental Materials..... | 48 |
| 3.2 Material Purification..... | 49 |
| 3.2.1 Inhibitor removal from AN monomer..... | 49 |
| 3.2.2 AIBN Recrystallization..... | 49 |
| 3.2.3 Copper bromide (CuBr) purification..... | 50 |
| 3.3 Preparation of oxidized MWCNTs..... | 50 |

Table of contents

| | |
|---|-----------|
| 3.4 Synthesis of homo PAN | 51 |
| 3.5 Synthesis of pyrene functional PAN | 51 |
| 3.5.1 Ce ⁺⁴ mediated synthesis of mono pyrene functional PAN | 51 |
| 3.5.2 ATRP synthesis of mono pyrene functional PAN | 52 |
| 3.5.2.1 Synthesis of ATRP initiator..... | 52 |
| 3.5.2.2 Synthesis of mono pyrene functional PAN by ATRP | 53 |
| 3.5.3 Synthesis of multi pyrene functional PAN | 53 |
| 3.5.3.1 Synthesis of PyMMP macromonomer | 53 |
| 3.5.3.2 Synthesis of multi pyrene functional PAN by CFR copolymerization..... | 54 |
| 3.6 Electrospinning | 55 |
| 3.7 Carbonization..... | 55 |
| 3.8 Characterization (analytical techniques)..... | 55 |
| 3.8.1 ¹ H-NMR spectroscopy | 55 |
| 3.8.2 SEC..... | 56 |
| 3.8.3 UV-visible spectroscopy | 56 |
| 3.8.4 UV-Fluorescence spectroscopy | 56 |
| 3.8.5 TGA..... | 57 |
| 3.8.6 SEM | 57 |
| 3.8.7 TEM..... | 57 |
| 3.9 References..... | 58 |
| 4. Results and discussion | 59 |
| 4.1 Synthesis of py-PAN via a cerium initiated redox system | 60 |
| 4.2 Synthesis of mono pyrene chain-end functional PAN via ATRP synthesis | 68 |
| 4.2.1 Synthesis of 1-pyrenemethyl-2-bromoisobutyrate and 1-pyrenebutyl-2-bromoisobutyrate ATRP initiators | 68 |
| 4.2.2 Synthesis of py-PAN..... | 72 |
| 4.3 Synthesis of multi pyrene functional PAN via CFR copolymerization..... | 788 |
| 4.3.1 Synthesis of PyMMP macromonomer | 78 |
| 4.3.2 Synthesis of PAN-co-PyMMP | 80 |
| 4.4 Pyrene-functional-PAN/MWCNT nanocomposites by noncovalent interaction..... | 84 |
| 4.4.1 TGA analysis | 84 |
| 4.4.2 ¹ H-NMR analysis | 89 |
| 4.4.3 UV-fluorescence analysis | 94 |
| 4.5 Production of MWCNT/PAN nanocomposites by electrospinning | 99 |
| 4.6 Pyrene-functional-PAN/EG nanocomposites by noncovalent interaction | 111 |

Table of contents

| | |
|--|------------|
| 4.7 Carbonization of MWCNT/PAN precursor fibers..... | 122 |
| 4.8 References..... | 125 |
| 5. Conclusion and future prospects | 127 |
| 5.1 Conclusion | 128 |
| 5.2 Future prospects | 131 |
| Appendix..... | 132 |

List of abbreviations

| | |
|----------------------------------|--------------------------------------|
| <i>¹H-NMR</i> | Proton-nuclear magnetic resonance |
| <i>ACS</i> | American Chemical Society |
| <i>AIBN</i> | Azobisisobutyronitrile |
| <i>AN</i> | Acrylonitrile |
| <i>ATRP</i> | Atom transfer radical polymerization |
| <i>BPO</i> | Benzoyl peroxide |
| <i>Bpy</i> | 2,2'-Bipyridyl |
| <i>CAN</i> | Ceric ammonium nitrate |
| <i>CDCl₃</i> | Deuterated chloroform |
| <i>CFR</i> | Controlled free radical |
| <i>CNT</i> | Carbon nanotube |
| <i>CRP</i> | Controlled radical polymerization |
| <i>CVD</i> | Chemical vapour deposition |
| <i>DCM</i> | Dichloromethane |
| <i>DFT</i> | Density functional theory |
| <i>DMac</i> | N,N-Dimethylacetamide |
| <i>DMF</i> | Dimethylformamide |
| <i>DMSO</i> | Dimethylsulfoxide |
| <i>DMSO-d₆</i> | Deuterated dimethylsulfoxide |
| <i>EG</i> | Expandable graphite |
| <i>FTIR</i> | Fourier transform Infrared |
| <i>HPLC</i> | High-pressure liquid chromatography |
| <i>MDI</i> | 4,4-Methylene-diphenyl-diisocyanate |
| <i>MMA</i> | Methyl-methacrylate |
| <i>MWCNT</i> | Multi-walled carbon nanotubes |
| <i>NMP</i> | Nitroxide mediated polymerization |
| <i>PAN</i> | Polyacrylonitrile |

List of abbreviations

| | |
|----------------------|--|
| <i>PDMS</i> | Poly(dimethylsiloxane) |
| <i>PEG</i> | Poly(ethylene glycol) |
| <i>PEO</i> | Poly(ethylene oxide) |
| <i>PFT</i> | Polymerization filling technique |
| <i>PMMA</i> | Poly(methylmethacrylate) |
| <i>Ppm</i> | Parts per million |
| <i>PS</i> | Polystyrene |
| <i>PVP</i> | Poly(vinylpyrrolidone) |
| <i>PyMMP</i> | (1-Pyrene)methyl-2-methyl-2-propenoate |
| <i>RAFT</i> | Reversible addition-fragmentation chain transfer |
| <i>RI</i> | Refractive index |
| <i>SDS</i> | Sodium dodecyl sulphate |
| <i>SEC</i> | Size exclusion chromatography |
| <i>SEM</i> | Scanning electron microscopy |
| <i>St</i> | Styrene |
| <i>SWCNT</i> | Single-walled carbon nanotubes |
| <i>TCD</i> | Tip to collector distance |
| <i>TDI</i> | Toluene-2,4-diisocyanate |
| <i>TEA</i> | Triethylamine |
| <i>TEM</i> | Transmission electron microscopy |
| <i>TEMPO</i> | 2,2,6,6-Tetramethylpiperidinyloxy |
| <i>TGA</i> | Thermal gravimetric analysis |
| <i>THF</i> | Tetrahydrofuran |
| <i>TMS</i> | Tetramethylsilane |
| <i>UV</i> | Ultraviolet |
| <i>UV-vis</i> | Ultraviolet-visible |

List of figures

Chapter 2

| | |
|--|----|
| Figure 2.1: Schematic representation of a graphene sheet (a), a single wall carbon nanotube (b) and a multiwalled carbon nanotube (c)..... | 8 |
| Figure 2.2: Schematic representation of the armchair (a), zigzag (b) and a chiral (c) lattice conformation across the nanotube surface..... | 9 |
| Figure 2.3: Possible phisiosorptive sites for a benzene molecule onto a CNT surface are so-called a) hollow (H), b) Bridge (B) and c) Top (T) orientated..... | 15 |
| Figure 2.4: Structural layout of a typical RAFT agent | 19 |
| Figure 2.5: Graphical representations of various classes of linear and non-linear copolymers. | 31 |
| Figure 2.6: Representations of copolymer favoring a) homogeneous b) heterogeneous and c) random monomer insertions. | 32 |
| Figure 2.7: Representation of a single needle electrospinning setup..... | 34 |

Chapter 4

| | |
|---|----|
| Figure 4.1: ¹ H-NMR spectra of 1-pyrenemethanol (in CDCl ₃ , “+”) and resultant 1-pyrenemethyl-2-bromoisobutyrate (in DMSO-d ₆ , “**”) after esterification to form the ATRP macroinitiator..... | 69 |
| Figure 4.2: ¹ H-NMR spectra of both 1-pyrenebutanol (in CDCl ₃ , “+”) and resultant 1-pyrenebutyl-2-bromoisobutyrate (in DMSO-d ₆ , “**”) after esterification to form the ATRP macroinitiator..... | 70 |
| Figure 4.3: ¹ H-NMR spectra of py-PAN·2 (1.09 mol% functionality) as synthesized from 1-pyrenemethyl-2-bromoisobutyrate ATRP macroinitiator..... | 74 |
| Figure 4.4: ¹ H-NMR spectra of py-PAN·5 (3.03 mol% functionality) as synthesized from 1-pyrenebutyl-2-bromoisobutyrate ATRP macroinitiator..... | 75 |
| Figure 4.5: Elugram of SEC analysis on py-PAN·2 (1.09mol% functionality) with a dual detection system of RI and UV (365 nm)..... | 77 |
| Figure 4.6: ¹ H-NMR spectra of produced (1-pyrene)methyl-2-methyl-2-propenoate (PyMMP) to be used as mocromonomer in the production of PAN-co-PyMMP polymers. | 79 |
| Figure 4.7: ¹ H-NMR spectra of PAN-co-PyMMP·3 (2.02 mol% functionality) as polymerized from conventional AN monomer and PyMMP macromonomer. | 81 |
| Figure 4.8: Elugram of SEC on PAN-co-PyMMP·1 (0.45 mo% functionality) using a dual detection system of RI and UV (365 nm)..... | 83 |
| Figure 4.9: MWCNT dispersion ability of functional polymer by comparative representation of a (a) polymer deprived solution, a (b) PAN-co-PyMMP·2 polymer (1.22 mol% functionality) and (c) py-PAN·2 polymer (1.09 mol% functionality) containing solution. | 84 |
| Figure 4.10: Illustration of unassociated functional polymer removal during TGA sample preparation by UV analysis of diluent from consecutive washes of (b) PAN-co-PAN·2/MWCNT composites by DMF solvent..... | 86 |

List of figures

| | |
|--|-----|
| Figure 4.11: TGA thermogram representing % weight loss associated with pristine MWCNTs, py-PAN·2 (1.09 mol% functionality), PAN-co-PyMMP·2 (1.22 mol% functionality) copolymer and homo PAN polymer under inert N ₂ environment against temperature change..... | 87 |
| Figure 4.12: Overlaid ¹ H-NMR spectra of a) py-PAN·3 (0.43 mol% functionality) and b) PAN-co-PyMMP·2 (2.02 mol% functionality) polymers with each spectra representing a 0 wt% (red), 20 wt% (green), 33 wt% (blue) and 50 wt% (purple) MWCNT loading fraction relative to functional sample..... | 90 |
| Figure 4.13: ¹ H-NMR quenching trends of pyrene representing multiplets graphically represented in comparison of py-PAN·3 (0.43 mol% functionality) and PAN-co-PyMMP·2 (1.22 mol% functionality) polymers | 92 |
| Figure 4.14: Representation of florescent quenching character observed for a) PAN-co-PyMMP·3 (2.02 mol% functionality) and b) py-PAN·1 (1.97 mol% functionality) polymers when exposed to various quantities of MWCNTs..... | 95 |
| Figure 4.15: Fluorescent quenching trends graphically represented (with trends represented by guide lines) in comparison of PAN-co-PyMMP·3 (2.02 mol% functionality) and py-PAN·1 (1.97 mol% functionality) polymers. | 96 |
| Figure 4.16: Fluorescent quenching trends observed for PAN-co-PyMMP·2 (1.22 mol% functional) and py-PAN·3 (0.43 mol% functional) polymers | 98 |
| Figure 4.17: SEM images and corresponding average fiber diameter distributions of fibrous composites of 0 wt%, 1.5 wt%, 3 wt% and 5 wt% a) oxidized MWCNT composition and b) noncovalent incorporation of the same loadings of pristine MWCNTs by PAN-co-PyMMP·1 (0.45 mol% functionality) in a PAN matrix..... | 103 |
| Figure 4.18: SEM images and corresponding average fiber diameter distributions of fibrous composites of 0 wt%, 1.5 wt%, 3 wt% and 5 wt% pristine MWCNT composition in PAN matrix by noncovalent incorporation using a) PAN-co-PyMMP·2 (1.22 mol% functionality) and PAN-co-PyMMP·3 (2.02 mol% functionality) respectively | 104 |
| Figure 4.19: SEM images and corresponding average fiber diameter distributions of fibrous composites of 0 wt%, 1.5 wt%, 3 wt% and 5 wt% pristine MWCNT composition in PAN matrix by noncovalent incorporation using py-PAN·3 (0.43 mol% functionality) | 105 |
| Figure 4.20: Average fiber diameters with increased MWCNT filler for the various compatibilizing methods. The methods being covalent oxidation of MWCNT filler as well as noncovalent functionalization by PAN-co-PyMMP·1 (0.45 mol% functional), PAN-co-PyMMP·2 (1.22 mol% functional), PAN-co-PyMMP·3 (2.02 mol% functional) and py-PAN·3 (0.43 mol% functional) compatibilizers..... | 106 |
| Figure 4.21: TEM imaging of nanofiber composites imbedded with 5 wt% of a) covalently oxidized MWCNTs and b) pristine MWCNTs by noncovalent compatibilization using PAN-co-PyMMP·3..... | 110 |
| Figure 4.22: Solvation analysis by visual representation of a) polymer deprived solution and b) multi-functional compatibilizing polymer containing solution with EG. | 112 |
| Figure 4.23: TGA curves representing % weight loss associated with pristine EG, extracted graphene/functional-PAN nano hybrid and virgin functional-PAN (of 1.22 mol% PyMMP content) | 113 |

List of figures

| | |
|--|-----|
| Figure 4.24: Visual representation of $^1\text{H-NMR}$ sample prepared for noncovalent quenching analysis of EG/functional-PAN complex | 114 |
| Figure 4.25: Overlaid $^1\text{H-NMR}$ spectra of multi-functional PAN each spectra representing a 0wt% (red), 20wt% (green), 33wt%(blue) and 50wt% (purple) respective EG loading fraction relative to functional sample. | 115 |
| Figure 4.26: Representation of $^1\text{H-NMR}$ quenching character observed for 2.02 mol% multi-functional PAN when exposed to increasing loading fractions of EG filler | 116 |
| Figure 4.27: Representation of fluorescent quenching character observed for 2.02 mol% multi-functional PAN when exposed to increasing loading fractions of EG filler | 117 |
| Figure 4.28: Fluorescent quenching trends graphically presented for 2.02 mol% multi-functional PAN when exposed to various loading fractions of EG filler | 118 |
| Figure 4.29: SEM imaging of fibrous composites of 0 wt%, 1.5 wt%, 3 wt% and 5 wt% EG composition in PAN matrix by noncovalent incorporation using 1.22 mol% PyMMP comprised multi-functional copolymer | 120 |
| Figure 4.30: Representation of altering fiber diameters resulting from increasing EG filler content as noncovalently compatibilized by 1.22 mol% functional PAN..... | 121 |
| Figure 4.31: TEM imaging of nanofiber composites imbedded with 5 wt% of pristine EG by noncovalent compatibilization using PAN-co-PyMMP·2 (1.22 mol% PyMMP content) multi-functional copolymer. | 131 |
| Figure 4.32: Images of PAN fibers as spun by electrospinning with a) no compatibilizer, b) oxidized MWCNTs c) PAN-co-PyMMP·3 and d) Py-PAN·3 for compatibilization of 5 wt% of the MWCNT fillers before (1) and after (2) carbonization, with each image accompanied by a graphical representation of the fiber diameter distribution. | 123 |
| Appendix | |
| Figure A1: SEC elugrams of py-PAN·1 (1.97 mol% functionality) represented by dual RI/UV (365nm) detection. | 133 |
| Figure A2: SEC elugrams of py-PAN·3 (0.43 mol% functionality) represented by dual RI/UV (365nm) detection. | 133 |
| Figure A3: SEC elugrams of py-PAN·4 (7.14 mol% functionality) represented by dual RI/UV (365nm) detection. | 134 |
| Figure A4: SEC elugrams of py-PAN·5 (2.86 mol% functionality) represented by dual RI/UV (365nm) detection. | 134 |
| Figure A5: SEC elugrams of py-PAN·6 (2.78 mol% functionality) represented by dual RI/UV (365nm) detection. | 135 |
| Figure A6: SEC elugrams of PAN-co-PyMMP·1 (0.45 mol% functionality) represented by dual RI/UV (365nm) detection..... | 135 |
| Figure A7: SEC elugrams of "PAN-co-PyMMP·3 (2.02 mol% functionality) represented by dual RI/UV (365nm) detection..... | 136 |

List of figures

| | |
|--|-----|
| Figure A8: TGA thermograms representing % weight loss of extracted MWCNT complexes of multi pyrene functional polymers, PAN-co-PyMMP·1, PAN-co-PyMMP·2 and PAN-co-PyMMP·3 respectively | 136 |
| Figure A9: TGA thermograms representing gravimetric weight loss of PAN-co-PyMMP·1 polymer and PAN-co-PyMMP·1/MWCNT complex respectively | 137 |
| Figure A10: TGA thermograms representing gravimetric weight loss of PAN-co-PyMMP·2 polymer and PAN-co-PyMMP·2/MWCNT complex respectively | 137 |
| Figure A11: TGA thermograms representing gravimetric weight loss of PAN-co-PyMMP·3 polymer and PAN-co-PyMMP·3/MWCNT complex respectively | 138 |
| Figure A12: TGA thermograms representing gravimetric weight loss of Py-PAN·2 polymer and Py-PAN·2 /MWCNT complex respectively | 138 |
| Figure A13: Representation of florescent quenching character observed for a) PAN-co-PyMMP·2 (1.22 mol% functionality) and b) py-PAN·3 (0.43 mol% functionality) polymers when exposed to various quantities of MWCNTs | 139 |
| Figure A14: SEM images of PAN/MWCNT fibrous composites containing a 5 wt% loading fraction of MWCNTs as prepared with the PAN-co-PyMMP·1 compatibilizing specie | 140 |

List of schemes

Chapter 2

| | |
|---|----|
| Scheme 2.1: Schematic representation regarding the two step functionalization of polymeric ω -end by chlorosilanes, post anionic polymerization..... | 18 |
| Scheme 2.2: A simplified mechanistic representation of RAFT polymerization as redrawn from general image | 20 |
| Scheme 2.3: Schematic representation for general methodologies used of RAFT end group functionalization | 22 |
| Scheme 2.4: Generally accepted mechanism for NMP synthesis by bimolecular system via conventional and TEMPO initiators as adapted from Hawker et al. | 23 |
| Scheme 2.5: Simplistic representation of ATRP propagation by general transition metal catalyst. | 24 |
| Scheme 2.6: Overview scheme regarding methods (nucleophilic, electrophilic and radical reactions) used for the end group transformation from ATRP produced hydrogen terminal polymers..... | 26 |
| Scheme 2.7: Representation of molecular ceric ammonium nitrate complex..... | 27 |
| Scheme 2.8: Mechanistic representation of CAN initiated polymerization of vinyl monomer..... | 28 |

Chapter 4

| | |
|--|----|
| Scheme 4.1: The synthesis of py-PAN polymers by the redox initiated, Ce(IV) catalyzed polymerization from (a) 1-pyrenemethanol and (b) 1-pyrenebutanol initiators respectively..... | 61 |
| Scheme 4.2: Synthesis of (a) 1-pyrenemethyl-2-bromoisobutyrate and (b) 1-pyrenebutyl-2-bromoisobutyrate ATRP initiators from 1-pyrenemethanol and 1-pyrenebutanol reagents respectively. | 68 |
| Scheme 4.3: Synthesis of py-PAN polymers from (a) 1-pyrenemethyl-2-bromoisobutyrate and (b) 1-pyrenebutyl-2-bromoisobutyrate ATRP initiators | 73 |
| Scheme 4.4: Synthesis of (1-pyrene)methyl-2-methyl-2-propenoate (PyMMP) macromonomer from 1-pyrenemethanol..... | 79 |
| Scheme 4.5: Synthesis of PAN-co-PyMMP polymers by copolymerization of acrylonitrile (AN) and (1-pyrene)methyl-2-methyl-2-propenoate (PyMMP) macromonomers using CFR polymerization | 80 |

List of tables

Chapter 2

| | |
|---|----|
| Table 2.1: Table of electrospinning variables subdivided into solution properties, governing variables and ambient parameters..... | 35 |
|---|----|

Chapter 4

| | |
|--|-----|
| Table 4.1: Solvent dependent study on yields produced by redox system | 62 |
| Table 4.2: Temperature dependent study on yields produced by redox system. | 63 |
| Table 4.3: Time dependent study on yields produced by redox system. | 64 |
| Table 4.4: Quantitative catalyst dependent study on yields produced by redox system | 65 |
| Table 4.5: Initiator study using pyrene butanol initiator..... | 66 |
| Table 4.6: Study of general catalytic system study, using simple linear aliphatic alcohol initiator.. | 67 |
| Table 4.7: Specifications of py- PAN polymers as prepared from 1-pyrenemethyl-2-bromoisobutyrate and 1-pyrenebutyl-2-bromoisobutyrate ATRP macroinitiators..... | 76 |
| Table 4.8: Specifications of PAN-co-PyMMP copolymers. | 82 |
| Table 4.9: Weight loss data as presented by TGA analysis..... | 88 |
| Table 4.10: Quenching of pyrene multiplet signals for py-PAN·3 (0.43 mol% functional) and PAN-co-PyMMP·2 (1.22 mol% functional) polymers as obtained by ¹ H-NMR analysis | 91 |
| Table 4.11: Quenching of polymeric proton signals for py-PAN·3 (0.43 mol% functional) and PAN-co-PyMMP·2 (1.22 mol% functional) polymers as obtained by ¹ H-NMR analysis | 93 |
| Table 4.12: Quenching trends of pyrene emission of py-PAN·1 (1.97 mol% functionality) and PAN-co-PyMMP·3 (2.02 mol% functionality) polymers as presented by UV-fluorescent analysis.. | 96 |
| Table 4.13: Quenching trends of pyrene emission of py-PAN·3 (0.43 mol% functional) and PAN-co-PyMMP·2 (1.22 mol% functional) polymers as presented by UV-fluorescent analysis | 97 |
| Table 4.14: Data for mol% and resultant wt% of pyrene functionality, to be used in calculations for compatibilizer composition in spinning solutions | 100 |
| Table 4.15: Tabulated representation of electrospinning solution compositions of each series prepared with loading fractions of 0 wt%, 1.5 wt%, 3 wt% and 5 wt% MWCNT compositions respectively | 101 |
| Table 4.16: Electrospun nanofiber composite mats by various compatibilizing species in a series of 0 wt%, 1 wt%, 5 wt%, 3 wt% and 5 wt% MWCNT composition | 102 |
| Table 4.17: Produced fiber diameter for composites of various filler functionalization species and incremental analysis thereof | 107 |
| Table 4.18: Values obtained from quenching analysis of pyrene signals by ¹ H-NMR on samples containing 0 wt%, 20 wt%, 33 wt% and 50 wt% EG relative to functional polymer. | 115 |

List of tables

| | |
|---|-----|
| Table 4.19: Quenching trends of pyrene emission of PAN-co-PyMMP-3 (2.02 mol% functionality) polymers as presented by UV-fluorescent analysis. | 117 |
| Table 4.20: Physical representation of spun composites of various EG loading fractions | 119 |
| Table 4.21: Average fiber diameters obtained before and after carbonization of PAN/MWCNT nanocomposite fibers | 124 |

Chapter 1

Introduction and objectives

In this chapter a brief discussion into the scope and interest of carbon based nanocomposites is addressed followed by a condensed overview of the proposed study. The chapter is concluded by the proposed objectives.

1.1 Introduction

Nanotechnology has presented itself as being an increasingly important field of study, dominating research in polymer and material sciences. Endless applications of nanomaterials include biosensors, drug delivery systems,^{1,2} microelectronics, fuel cell development,³ aerospace technology, tissue engineering,⁴ mini-emulsion,⁵ polymeric layered self-assembly, as well as nanocomposite reinforcement.⁶ Recent years indicate an increasing demand attributed to the development of nanocomposites as a subfield of nanotechnology.^{6,7} This entails the incorporation of nano-sized fillers to polymer materials in an effort to obtain superior properties or alteration of existing character such as improved mechanical strength, incorporated barrier properties, optical alteration, enhanced thermal resistance and incorporated conductive properties. Reported filler types vary from exfoliated natural clays,^{8,9} silicas,¹⁰ carbon black¹¹ to graphitic carbon based materials^{6,12} all presenting various properties to nanocomposite material. The use of a carbon based filler such as graphite (or graphene) and single- or multi-walled carbon nanotubes (SWCNTs/MWCNTs) shows great capability for the property enhancement of materials based on mechanical strength as well as thermal and electrical conductive character. Enhanced properties of a material by filler embedding are strongly dependant on the solid state morphology of the composite. This refers to the filler distribution and orientation of the nano-scale filler throughout the material matrix. CNT filler dispersion proves problematic in most solvents, which was the reason for various methods of the CNT functionalization being presented as effective techniques for solubilizing these otherwise inert fillers. Functionalization of CNT surface however, leads to the conjugated surface morphology being disrupted. When depriving the carbon filler of its conjugated chemical morphology, suppression is seen in filler properties. This problem can, however, be overcome by the noncovalent incorporation of functionality to carbon fillers in order to maintain the sp^2 hybridized surface morphology.¹³⁻²²

This project aims at such noncovalent incorporation of graphitic MWCNT filler to a polymer matrix in preparation of nanocomposites. This requires the initial synthesis of functional polymer of various molecular structures yielding a compatibilizing polymer serving in effect as the interface of noncovalent interaction between the carbon based filler and the polymer matrix. In order to take full advantage of the potential regarding a nanocomposite with a noncovalent interaction between filler and matrix, it is essential to have an understanding of the processes and parameters involved in the chemical association and the limitations thereof. Analysis of the integrity of noncovalent interaction is, therefore, crucial and investigated for the different functional polymers based on various research techniques such

as fluorescence, $^1\text{H-NMR}$ and TGA analysis. Composite processing is further achieved by electrospinning to fibrous form. Electrospinning of the polymeric solutions to fibrous state was discovered and patented by Formhals,²³ as a technique capable of producing fibers of substantially high aspect ratios. This high specific area presents the capability of composite use in fields such as tissue scaffolding, filtration, bio-censoring and drug delivery amongst others.

In short this project involves the preparation of noncovalent compatibilizing polymer and functionalizing of carbon based filler materials by these macromolecules as well as by conventional covalent functionalization of filler. Preparation of the nanocomposite containing a series of increasing carbon filler composition for each compatibilization method is produced to be electrospun to a fibrous composite. Finally the effects of carbon filler incorporation to electrospun fibers are investigated regarding the composite morphology at increased filler composition.

1.2 Objectives

The study aims at producing both noncovalently as well as covalently incorporated MWCNT filler to a polyacrylonitrile (PAN) matrix during electrospinning to make the fibrous composite. Comparative studies need to be done for the various compatibilization techniques and the effect these have on the fiber morphologies. In order to achieve this goal, the following objectives need to be met:

1. The synthesis of PAN matrix by means of CFR polymerization followed by simple molecular analysis of molecular weight (M_n) and polymer dispersity index (Đ) by size exclusion chromatography (SEC).
2. The preparation of oxidized multi walled carbon nanotubes (MWCNTs) as the representation of covalently functionalized filler to be used in comparative electrospun composite to that of noncovalently incorporated filler.
3. The synthesis of a pyrene functional polymer as interfacial noncovalent compatibilizer by means of cerium initiated redox polymerization and atom transfer radical polymerization (ATRP) for α -chain end functional PAN, as well as conventional free radical (CFR) copolymerization for the multi pyrene functional copolymer respectively.

- 3.1 Experimental method development for the relatively unknown method of redox initiated polymerization by cerium ammonium nitrate (CAN) catalyst in the synthesis of pyrene chain end functional PAN.
- 3.2 Synthesis of pyrene functional ATRP initiators.
- 3.3 ATRP polymerization of pyrene chain end functional PAN by ATRP polymerization to three different molecular weights.
- 3.4 Analysis of pyrene chain end functional polymers by $^1\text{H-NMR}$ analysis and SEC in combination with an RI/UV detector system.
- 3.5 The synthesis of a pyrene functional macromonomer.
- 3.6 CFR polymerization of multi pyrene functional copolymer by copolymerization of AN and macromonomer to three variations of macromonomer incorporation.
- 3.7 Analysis of multi pyrene functional copolymer by $^1\text{H-NMR}$ analysis, as well as SEC in combination with a RI/UV dual detector system.
4. Investigation of noncovalent MWCNT/functional-polymer interactions by UV-flourescent, TGA, and $^1\text{H-NMR}$ analysis respectively.
5. Electrospinning of covalently and noncovalently compastibilized MWCNT/PAN nanofibrous nanocomposites using various loading fractions of MWCNT's.
6. Investigations of fibrous composites by SEM and TEM analysis.
7. Preliminary study into the use of graphene fillers for the production of PAN/graphene fibrous composites by the same association analysis and composite production and fiber analysis as was done for the PAN/MWCNT fiber composites.
8. Preliminary study into the carbonization of the MWCNT/PAN nanocomposite fibers to produce carbon nanofibers.

1.3 References

- 1) S. Agarwal, J. H. Wendorff and A. Greiner, *Polymer*, 2008, **49**, 5603-5621.
- 2) E. Kenawy, G. L. Bowlin, K. Mansfield, J. Layman, D. G. Simpson, E. H. Sanders and G. E. Wnek, *J. Control. Release*, 2002, **81**, 57-64.
- 3) B. P. Tripathi and V. K. Shahi, *Prog. Polym. Sci.*, 2011, **36**, 945-979.
- 4) N. J. Castro, S. A. Hacking and L. G. Zhang, *Ann. Biomed. Eng.*, 2012, **40**, 1628-1640.
- 5) J. Faucheu, C. Gauthier, L. Chazeau, J. Cavaillé, V. Mellon and E. B. Lami, *Polymer*, 2010, **51**, 6-17.
- 6) V. Choudhary and A. Gupta, in *Polymer/Carbon Nanotube Nanocomposites*, ed. S. Yellampalli, Intech, 2011, p. 66-80.
- 7) M. T. Byrne and Y. K. Gun'ko, *Adv. Mater.*, 2010, **22**, 1672-1688.
- 8) P. Liu, *Appl. Clay. Sci.*, 2007, **38**, 64-76.
- 9) A. Samakande, R. D. Sanderson and P. C. Hartmann, *Polymer*, 2009, **50**, 42-49.
- 10) M. Alexandre and P. Dubois, *Mater. Sci. Eng. R. Rep.*, 2000, **28**, 1-63.
- 11) I. Balberg, *Carbon*, 2002, **40**, 139-143.
- 12) Z. Spitalsky, D. Tasis, K. Papagelis and C. Galiotis, *Prog. Polym. Sci.*, 2010, **35**, 357-401.
- 13) E. Y. Choi, S. C. Roh and C. Kim, *Carbon*, 2014, **72**, 160-168.
- 14) T. J. Simmons, J. Bult, D. P. Hashim, R. J. Linhardt and P. M. Ajayan, *ACS Nano*, 2009, **3**, 865-870.
- 15) Y. Zhao and J. F. Stoddart, *Acc. Chem. Res.*, 2009, **42**, 1161-1171.
- 16) D. Baskaran, J. W. Mays and M. S. Bratcher, *Chem. Mater.*, 2005, **17**, 3389-3397.
- 17) X. Lou, R. Daussin, S. Cuenot, A. - Duwez, C. Pagnouille, C. Detrembleur, C. Bailly and R. Jérôme, *Chem. Mater.*, 2004, **16**, 4005-4011.
- 18) H. Murakami, T. Nomura and N. Nakashima, *Chem. Phys. Lett.*, 2003, **378**, 481-485.
- 19) P. Petrov, F. Stassin, C. Pagnouille and R. Jérôme, *Chem. Commun.*, 2003, **9**, 2904-2905.
- 20) J. Chen, H. Liu, W. A. Weimer, M. D. Halls, D. H. Waldeck and G. C. Walker, *J. Am. Chem. Soc.*, 2002, **124**, 9034-9035.
- 21) N. Nakashima, Y. Tomonari and H. Murakami, *Chem. Lett.*, 2002, **31**, 638-639.

22) R. J. Chen, Y. Zhang, D. Wang and H. Dai, *J. Am. Chem. Soc.*, 2001, **123**, 3838-3839.

23) F. Anton, *Process and apparatus for preparing artificial threads*, Google Patents, Washington, DC: U.S, 1934.

Chapter 2

Historical and literature review

In this chapter, literature is reviewed regarding the facets associated with carbon nanotube reinforced polymer-based composites, specifically that of fibrous morphology. Various reported methods of filler incorporations have been reviewed with the focus shifted to a non-destructive incorporation method concerning preservation of sp^2 hybridized CNT/MWCNT molecular structure. Advances in the production of functional polymers are presented in an effort to produce a compatibilizer for facilitating homogeneous filler distribution. The synthesis of functional polymers by both controlled (Atom Transfer Radical Polymerization (ATRP), Nitroxide Mediated Polymerization (NMP), Reversible Addition-Fragmentation chain Transfer (RAFT) and anionic polymerization) and uncontrolled methods (redox initiated polymerization and conventional Free Radical Polymerization (FRP)) are discussed in depth. The review is concluded with comments on general trends in the processing of CNT/polymer composites, with the focus finally directed to the method of electrospinning which is discussed in greater depth and eventually utilized in this study.

2.1 Polymer nanocomposites

Nanomaterials are commonly defined as compounds with at least one dimension smaller than 100 nanometers. These materials can vary in physical form from particles to sheets and fibers or cylinders. The aforementioned materials have been reportedly used as fillers in polymer matrixes to alter the inherent properties of the initial polymer. A significant increase is evident in the polymer-filler contact area with regards to filler volume, as the filler size is decreased from milli- through micro- to nano-meters. A higher interfacial area should theoretically lead to a lower volume of nanofiller required to achieve the desired property alteration of the polymer matrix, giving rise to the required composite. Nano fillers can, therefore, be used in polymer matrices to produce nanocomposite materials with enhanced mechanical, thermal, electrical and optical properties.¹

Recent years show much focus being devoted to polymer/carbon nanofiller composites.² The most popular and versatile of these fillers are graphene nanosheets and carbon nanotubes (CNTs) which are both used industrially for various applications. Graphene sheets refer to a mono atomic layer of hexagonally orientated, sp^2 hybridized carbons to form a single graphitic carbon sheet. A single walled carbon nanotube (SWCNT) refers to these sp^2 hybridized carbon sheets produced in the form of a cylinder, whereas the multiwalled carbon nanotube (MWCNT) is merely multiple of these cylinders enclosed in each other to form a single tube of these cylinders. Representative images of these compounds are presented in Figure 2.1 below.

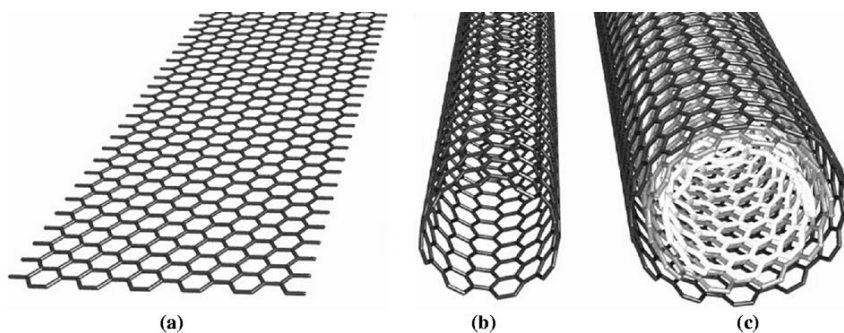


Figure 2.1: Schematic representation of a graphene sheet (a), a single wall carbon nanotube (b) and a multiwalled carbon nanotube (c).³

With the scope of this study in mind, focus is reserved to carbon nanotubes (CNTs) as a subcategory of carbon based fillers. These are the fillers set out to be used in composite development throughout this study.

2.2 Carbon nanotubes

The discovery of “needle like tubes of carbon”, now universally known as carbon nanotubes (CNTs), was presented in *Nature* by Iijima in 1991.⁴ As described, CNTs can be seen as being a graphene sheet wrapped around into a seamless tube or cylinder. The lightweight tube therefore consists, (similarly to graphene sheets) of a hexagonal, honeycomb lattice structure. These sheets are one atom thick and consist entirely of sp^2 hybridized carbons. There are three ways in which these 2-D hexagonal sheets can be arranged. Assuming the chirality along the perpendicular axis of the tubes, either an armchair, zigzag or chiral conformation can be expected (refer to Figure 2.2 below). The three variations have been estimated to have an influence on the electronic conductive ability of the nanotubes, considering the alignment of the carbon-carbon bonds and therefore the electric conducting π -bond.⁵

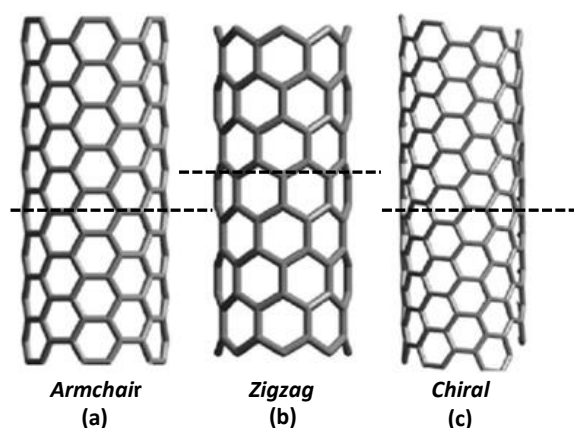


Figure 2.2: Schematic representation of the armchair (a), zigzag (b) and a chiral (c) lattice conformation across the nanotube surface.

π -Bonds assist in π - π stacking interactions between the layers in MWCNTs and it has been estimated that there are between 2 to 20 of these shells in quantity. MWCNTs have intershell spacing of about 0.34 nm (or 3.4\AA)⁶ and an internal diameter ranging in the area of 10 nm to 20 nm.⁷ Since the first reported use of these CNTs as nano fillers by Ajayan *et al.*⁸ in 1994, a large amount of research has been devoted to the use of these nanotubes in an effort to achieve polymer nanocomposites of altered mechanical and physical properties. The superior properties achievable by the incorporation of CNTs into a polymer matrix include an enhanced thermal and electrical conductivity as well as an increase in mechanical strength at a substantially low weight per volume fraction of composite.⁹

Carbon based polymer composites have been used industrially for many years in reinforcing plastics and rubber. Probably the most well-known use of carbon composites is the use of carbon fibers for reinforced products used in cars, bicycles and airplanes. Carbon black

(CB) is also known to be used as filler in rubber to produce the polymer/carbon composite tyre able to retard thermal damage. This filler is also incorporated as a conventional filler to a polymeric matrix in an effort to lend electrical properties to produced composites, such as enhanced electrical conduction or electrostatic dissipation. CNT fillers, however, prove superior in this regard by showing an enhanced electric conduction property transfer to the composite material. This is supported by Sandler *et al.*¹⁰ who showed that CNT/epoxy composites at 0.1 vol% filler loading fraction have conductivity properties superior to similar CB loading in the same epoxy matrix. CNTs present additional advantages over conventional fillers such as CB and carbon fibers. These include a greater amenability regarding processing as well as superior distribution efficiency.¹¹ The superiority over conventional carbon materials facilitates a shift in focus, in recent years, to the use of CNTs as reinforcing filler. CNTs have caught the attention of researchers due to an extraordinary mechanical as well as electrical conducting ability. It has been stated that CNTs have strengths of 10 to 100 times stronger than the toughest steel at a drastically reduced weight.² MWCNTs have been found to have a Young's modulus of about 0.27 TPa to 0.93 TPa, toughness of about 1240 J·g⁻¹ and strength of 11 to 63 GPa.¹ At a higher surface area to volume ratio SWCNTs have been reported to show an even better Young's modulus of about 0.32 TPa to 1.47 TPa, toughness of about 770 J·g⁻¹ and strengths ranging from 10 GPa to 52 GPa.¹² Referring to the electrical conducting properties, CNTs have been estimated to show conducting abilities 1000 times that of a copper wire. This character is brought about by the aforementioned universal sp² carbon bonded structure. The conjugated π -system of CNTs allows the high mobility of electrons along the tubular axis by quasi-ballistic features.^{13,14} Absolute values are, however, difficult to determine as the properties of these CNTs vary depending on the synthetic method by which they were made. These synthetic methods are presented in the upcoming section, followed by the possibilities regarding incorporation of these filler units to composite polymer matrixes.

2.3 Methods of CNT synthesis

CNTs are known to be synthesized by one of three major techniques. These are arc discharge, laser ablation and chemical vapor deposition (CVD). Arc discharge is the most mature way of CNT synthesis. This technique was used to synthesize the first nanotubes to be reported by Iijima⁴ and had initially been used in the production of C₆₀ fullerenes. Arc discharge commences under inert atmosphere and controlled pressure. The method, however, has the disadvantage of producing impurities, which include anions, fullerenes and amorphous carbon amongst the carbon soot. An advantage on the other hand is the ease at

which both MWCNTs and SWCNTs can be synthesized at moderate costs. Laser ablation produces CNTs in the form of ropes by the use of a laser pulse and small amounts of metals under an inert atmosphere and high temperatures of about 1200 °C.^{6,15} It has been claimed to produce a conversion of up to 90%¹⁶ and can be used in the synthesis of both SWCNTs as well as MWCNTs.¹⁷ The disadvantage of this technique lies in the high cost of production, and the low quality of CNTs obtained for which mandatory purification is required.¹⁵ During chemical vapor deposition, hydrocarbons are decomposed in the presence of a metal catalyst at temperatures of 700 °C to 900 °C under an inert atmosphere. The internal diameter of the produced CNTs are in correspondence to the size of the metal particles used and thus allows for more control over the CNTs produced in terms of the obtained length and diameter of the tubes. Two mechanisms of synthesis have been presented, namely the “tip growth” and the “base growth” modes, depending on the catalyst-substrate adhesion strength. As mentioned, the advantage of this technique is the degree of control over the produced CNT length achievable, although a mixture of both MWCNTs and SWCNTs are produced.^{6,15} Independent of the synthesis method, CNTs tend to agglomerate. The agglomeration tendencies of CNTs are the reason why they are often functionalized in an effort of increasing CNT/matrix interactions prior to the production of composite materials.

2.4 Functionalization of CNTs

To achieve a nanocomposite with optimum alteration of intrinsic properties, a homogeneous dispersion of filler in the matrix is needed. This is problematic in the case of CNTs and graphene sheets due to a tendency of these carbon based nanofillers to agglomerate as a result of strong van der Waal's forces existing between one another.¹⁸ Methods exist in which this problem can be overcome. Methods include vigorous mixing and sonication, thus producing temporary dispersions during nanocomposite production. A far more effective, long lasting, and viable method of facilitating carbon nanofiller dispersion is by the functionalization of the graphitic surface prior to composite processing. Solubilisation of the nanofillers in various organic and inorganic solvents can be achieved by the incorporation of certain surface functionalities. This allows for a long-term homogeneous dispersion, as a result of nanofiller/matrix interaction which leads to increased processibility as well as an optimum stress and electric transfer in the case of the CNT enhanced nanocomposites. Different methods of functionalization have been developed over the years consisting of initial covalent functionalization (section 2.5) and later the non-covalent functionalization (section 2.6) of the nanotube surfaces.^{6,19}

2.5 Covalent functionalization of CNTs

The reactivity of CNTs has proven greater than that of graphene sheets, due to the pyramidalization or misalignments of π -orbitals as a result of local strains.²⁰ Covalent functionalization of CNTs entails a chemical alteration of the nanotube sidewalls to achieve specific functionalities. The first method of direct functionalization is the one-step process of any covalent attachment, such as the hydrogenation by Birch reduction,¹⁸ cycloaddition,²¹ or functionalization by nitrene and carbene addition.¹⁹ The second and most common method for functionalization is utilizing the initial introduction of carboxylic acid (-COOH), or hydroxyl (-OH) groups to the surface by means of surface oxidation, achievable through treatment with strong acids. Oxidation treatments have been reported to include combinations of nitric acid and hydrogen peroxide ($\text{HNO}_3/\text{H}_2\text{O}_2$), or nitric acid and sulphuric acid ($\text{NO}_3/\text{H}_2\text{SO}_4$) as the most common routes to carboxylic functional CNTs.^{7,22,23} The integration of these polar groups not only leads to solubility of CNTs in various polar solvents, but also allows for greater nanotube-polymer interactions. In some cases, these polar groups act as active sites from which polymer chains can be covalently grafted. The increased associations of filler and matrix have been proven to lead to an increase in mechanical strength and Young's modulus of nanocomposites.^{24,25} The functionalization of CNTs to present functional groups of nitriles, amines, amides and oximines have also been reported, but are far less abundant in literature.^{26,27}

The incorporation of functionalities on to the CNT surfaces in the case of indirect covalent functionalization, provide in fact the possibility of functionalization by polymer entity. This is a widely popular method of compatibilizing CNTs and can be achieved via two main methods of grafting categorized as "grafting from" and "grafted to" procedures.²⁸ Multiple examples of covalent functionalization by these grafting techniques are found in literature making use of various surfaces reported as efficient initiating species to produce grafted chains. Such surfaces include carbon nanotubes,²⁹ graphene sheets³⁰ and natural clays.³¹ The methods of grafting "to" and "from" solid surfaces can be used to modify surface properties or achieve incorporation into the required matrix. In case of the latter, the grafted moieties will in effect act as a compatibilizer when creating composites.³²

During the "grafting from" technique the initiators of the polymerization are prepared on the solid surfaces or, more specific to this research, the sidewalls of the nanotubes after which in-situ polymerization commences from these points. This method can produce polymer functionalized nanotubes of a high grafting ratio, but requires stringent polymerization conditions. This process is usually achieved via conventional free radical polymerization (CRP) due to simplicity but can be done via controlled methods such as ATRP or RAFT,

dependant on the appropriate active sites.^{27,33-36} The use of this technique, therefore, is popular when synthesizing densely grafted polymers in order to achieve a brush like structure.³⁷ Using ATRP proves the dominant synthetic procedure due to the limitation of the coupling and termination reactions allowing for slow growth of grafting units.³⁸

During the “grafting to” approach, polymer functional CNTs are produced by attachment of functionalized polymer molecules to complimentary functional groups on the nanotube surface. Anionic polymerization is a popular method for the presynthesis of these sidechains based on the broad range of chain end functionalities attainable. The active species on CNT surfaces is often of an electrophilic nature which will react with nucleophilic functionalities present at the terminal position of the aspiring side chains. Functionalities reported to have been used for functionalization by the “grafting to” technique includes esters, halides, pyridines and anhydrides.³⁹ This polymer addition reaction thus represents a one-step chemistry such as esterification but leads to low polymer loadings to the nanotube surface.³⁶ This technique also usually requires the presynthesis of two macro reagents.

PMMA related polymers are used in most attempts of grafting from nanotube surfaces. Qin *et al.*⁴⁰ produced poly(*n*-butyl methacrylate) grafted SWCNTs by the ATRP synthesis of polymer from an immobilized 2-bromopropionate initiator. The produced polymer is claimed to show increased mechanical, thermal and electrical character when introduced into the parent polymer matrix in production of the nanocomposite. The same group³³ produced similar work in which ATRP was used to grow controlled polystyrene (PS) chains from SWCNTs, utilizing protruding groups of 2-bromopropionate as initiation sites. In the same publication, grafting of PS from SWCNTs was successfully achieved by the ATRP synthesis of PS chains subjected to end group transformation to PS-N₃ and finally attached to the CNT surface by cycloaddition reactions. Both techniques produced covalently functionalized SWCNTs to achieve solubility in organic solvent. Fu *et al.*⁴¹, however, converted carboxylic acid functional SCNTs to acyl chloride by reflux with thionyl chloride and subsequently were subjected to esterification with hydroxyl groups of dendritic poly(ethylene glycol) (PEG).

The advantage of the “grafting to” techniques lies in the ability to presynthesize both units of the graft copolymer, allowing for a potentially more controlled synthesis.⁴² This permits for a greater degree of control achievable over molecular architecture, when compared to the “grafting from” technique. The steric hindrance of the bulky end capped chains, however, proves a drawback as a limit in achievable density is reached which is less of a problem in the case of the “grafting from” technique. An additional problem is the removal of the unreacted end capped chains, which complicates purification of the end product together

with the initial tedious multi step grafting process. Problems, however, arise during analysis of the produced graft copolymers from either technique as direct chromatographic analysis is not possible.⁴³ Possibilities of branch severing have, however, been reported by which the side chains can be removed at the point of initiation assuming specific functionality of active site.⁴⁴⁻⁴⁶ This allows for the analysis of the severed polymer chains independently of the CNT surfaces.

The downside of covalent functionalization is the chemical alteration of the CNTs. Covalent bonds to the surface transform the sp^2 surface hybridization of the specific carbons to individual sp^3 hybridizations. Modifying CNTs in any covalent manner will result in the alteration of nanotube surface structure, in effect reducing the conjugated chemical state that will lead to inferior property transfer from the nanotube filler to the composite.⁴⁷ This is attributed to the alteration of the CNTs having drastic implications on the intrinsic properties of the filler. Such implications include the expected deterioration in the physical properties such as strain capabilities and retarding of the thermal and electrical conductivity.^{48,49}

2.6 Non-covalent functionalization of CNTs

The preservation of long range conjugation is of interest in maintaining the electronic character of CNTs. Possible associations need to be investigated that result in an interaction being non-destructive to the π - electronic surface structure. Methods for the non-covalent CNT functionalization have been reported to predominantly make use of aromatic compounds, polymers and surfactants to non-covalently attach onto the CNT surfaces via π - π stacking or hydrophobic interactions.^{50,51} Alternative methods, however, include the use of van der Waals C- π , CH- π or electrostatic CNT-polymer interactions.⁵²⁻⁵⁴ The incorporation of CNTs by this method will leave the chemical morphology of the fillers unchanged and thus the mechanical and electrical characteristics unaltered. Several methods for the non-covalent incorporation of nanotubes have been published, as great interest lies in the maintenance and partial transference of CNT properties to the composite matrix when producing the final nanocomposite.^{52,55} The methods of non-covalent incorporation of CNTs include surfactant assisted dispersion, plasma polymerization treatment, polymer wrapping and polymerization filling technique (PFT). In the surfactant assisted dispersion, a surfactant such as sodium dodecyl sulphate (SDS) or benzylalkonium chloride is used to coat the nanotubes which allows dispersion in various solvents. In the case of polymer wrapping, the conjugated and/or aromatic groups in the polymer will associate with the CNTs through van der Waal's forces and π - π stacking interactions.

Polymers reported capable of such interactions include poly(vinylpyrrolidone) (PVP), pyrene-poly(ethylene glycol) and poly(phenylenevinylene).⁶

Woods *et al.*⁵⁶ studied the energetic and electronic properties considering the non-covalent functionalization of SWCNTs with two cyclic molecules, namely 4,4-methylene diphenyl diisocyanate (MDI) and toluene-2,4-diisocyanate (TDI). The conclusion of a π - π stacking interaction was made using the density functional theory (DFT) and charge density plots. The manner of parallel adsorption, considering π - π stacking of conjugated cyclic molecules, (in this case represented by simple benzene) can commence via 3 physiosorptive sites as represented in Figure 2.3 below.

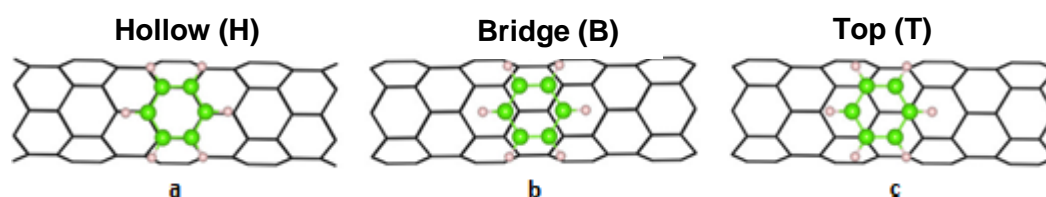


Figure 2.3: Possible physiosorptive sites for a benzene molecule onto a CNT surface are so-called a) hollow (H), b) Bridge (B) and c) Top (T) orientated.

A technique of functionalization that maintains the molecular structure best and therefore maintains the electric properties thereof, falls under the subdivision of polymer wrapping and involves the utilization of pyrene derivatives. This utilization of pyrene functionality has become one of the most popular methods for achieving polymeric surface modification of CNTs in a non-destructive manner.⁵⁷ The non-covalent functionalization is achieved by the physiosorption of these cyclic moieties, resultant from π - π stacking onto the CNT surface. Literature indicates the use of these pyrene moieties in efforts to incorporate polymer or functional groups onto CNTs and achieve efficient dispersion of the specific filler in organic solvents and polymer matrices.^{47,48,57-59} Publications include the use of various pyrene derivatives such as trimethyl-(2-oxo-2pyrene-1yl-ethyl) ammonium bromide,⁶⁰ N-succinimityl-1-pyrenebutanoate, 1-(trimethylammonium acetyl)-pyrene and pyrenecyclodextrin⁶¹ amongst others. The use of pyrene pendant polymers such as pyrene functional styrene, random copolymers of PMMA and (1-pyrene)methyl-2methyl-2-propenoate as well as block copolymers of PMMA and 4-pyrene-1-yl-methyl methacrylamide can be found amongst others.^{50,59,62,63} Chen *et al.*⁶⁴ has reported the pyrene functionalization of an amide leading to compatibilization between the CNT surface and the cyclic moiety via a non-covalent π - π stacking interaction. Due to the weak association of the noncovalent bonding, a poor load transfer from matrix to CNT filler has been reported and may lead to problems during processing of these CNT/polymer nanocomposites.⁵⁵ Choi *et al.*⁴⁷ attached 1-pyrenebutyric-chloride via π - π stacking to CNT surface preceding the condensation

reaction between these chloride groups and the terminal amide groups of introduced Nylon 66 during a twin extruder process to produce nylon functional CNTs.

The solubilizing of CNTs in organic and aqueous matrices is of interest even in the field of medicine and biological applications. Advantages lie in the compatibilization of CNTs with biological molecules such as enzymes, proteins saccharides and polysaccharides.^{61,64} Star *et al.*⁶⁵ utilized non-covalent interactions in the preparation of the biocompatible amylose wrapped SWCNTs. The group of Shinkai^{66,67} also reported the wrapping of SWCNTs by curdian and schizophyllan. These are not isolated cases, as many different saccharides and polysaccharides have been reported to be used in CNT wrapping. Such cases include amongst others the use of cyclodextrins,^{68,69} carboxymethyl amylose,⁷⁰ curdlans,^{66,67} chitosan⁷¹ and dextrans.^{72,73}

Zhao and Stoddart⁶¹ synthesized organic soluble SWCNTs by non-covalent wrapping with various polymers or dendrimers including PPyPV (poly(2,6-pyridinylenevinylene)-co-(2,5-dioctoxy-p-phenylene)vinylene), PAmPV (poly-(5-alkoxy-m-phenylenevinylene)-co-(2,5-dioctoxy-p-phenylene)-vinylene), PmPV (poly(m-phenylenevinylene)-co-(2,5-dioctoxy-p-phenylene)vinylene) and stilbene dendrimers. The PmPV wrapped CNT nanocomposite was prepared similarly by Curran *et al.*⁷⁴ who concluded that by the introduction of CNT filler, the PmPV conductivity had been increased by 8 orders of magnitude.

CNTs as well as graphene sheets show promise of industrial use in technological applications such as memory storage devices,⁷⁵ solar cells,⁷⁶⁻⁷⁸ hydrogen storage,^{79,80} chemical sensors,^{81,82} ultra-capacitors,⁸³ electromechanics, molecular switchtunnel junctions (MSTJs) as well as in various other field-effect transistor devices (FET) and photovoltaic devices.^{61,84} The concept of non-covalent incorporation of these carbon based fillers into either organic or inorganic matrices could lead to the production of nanocomposites that will greatly impact both technological and commercial fields based on the extensive electrical and heat conducting capabilities as well as the mechanical robustness of these composites.⁴⁷

Choi *et al.*⁸⁵ synthesized polymer functionalized graphene sheets by the initial chemical reduction of graphene oxide followed by non-covalent attachment of amine terminal polymers via the protonated amine bond. This noncovalent functionalization, however, resulted in the disruption in the molecular architecture of the conjugated sp^2 carbon surface structure. This technique would thus not serve as a viable method of maintaining pristine carbon properties in the produced product.

The noncovalent functionalization of CNTs seems to be the superior method of nanotube functionalization while maintaining the pristine properties of filler. The requirement then arises for the synthesis of some interface between filler and matrix. The most viable option seems to be the use of functionalities capable of strong van der Waal's π - π stacking interactions.

2.8 Synthesis of mono and multi-functional polymers

The section that follows focuses on the synthesis of both mono- and multi-functional polymers to be used as interfacial compatibilizer in the production of CNT infused polymer nanocomposites. Various methods have been reported that are capable of producing chain end functional polymer as well as multi-functional polymers of protruding functional moieties. Such methods are discussed in the following sections. ATRP and cerium initiated redox methods are discussed in more depth concerning the synthesis of chain end functional polymer whereas CRP is the area of focus concerning the multi-functional polymer synthesis, as is to be discussed in section 2.8.2.

2.8.1 Chain end functional polymer synthesis

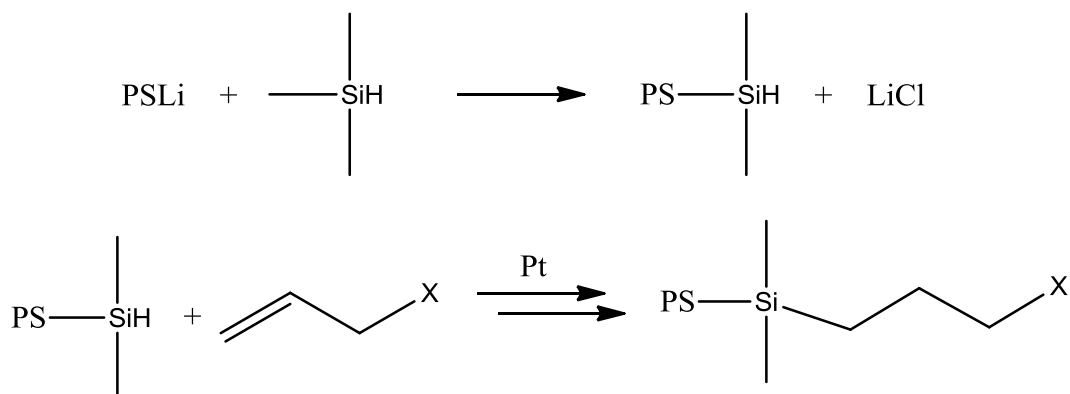
A method capable of producing chain end functional polymers is that of anionic polymer synthesis. The living character of propagation allows for polymer end capping with functional moieties. A more popular method of controlled polymer synthesis is by radical propagation. The control is achieved by limiting termination reactions as the concentration of active radical species is decreased. This is achieved by RAFT polymerization, NMP and ATRP using different mechanistic workings and allows for individual chain end functionalization by controlled polymerization.

2.8.1.1 Anionic polymerization

Polymerization reactions can be propagated via a few classified mechanisms, the first and most mature (established in the mid 1900s)^{86,87} is living anionic polymerization. The mechanism is initiated by a metal alkyl initiator, where upon dissociation will produce a positively charged metal ion as well as the negatively charged alkyl (carbanion) that will attack the monomer to produce an anionic propagation point. The most common initiator is butyllithium. Polymerizations by anionic polymerization are restricted in usable monomers, but utilize some vinyl and cyclic monomers, able to form stable anions via an electron withdrawing substituent. This indicates why polystyrene is readily used in anionic

polymerizations. The aromatic ring stabilizes the anion by delocalizing of the charges or by an induction effect. Reactions must be run under highly inert conditions to prevent termination reactions brought about by impurities such as moisture, oxygen and carbon dioxide.^{88,89} Another drawback of anionic polymerization is the probability of side reactions, specifically in the case of acrylonitrile polymerization.⁸⁹

The living character of this polymerization technique allows for the termination of polymers by functional moieties. In the case of the most popularly used lithium bases initiators, polymerization will produce a lithium associated chain end. Chain end functionality can be incorporated by facile controlled termination reactions with electrophilic reagents.⁹⁰ Common functionalities that can be incorporated to the ω -chain end include carboxylic, hydroxylic and amine functionalities amongst others.⁹¹ The incorporation of more complex functionalities includes the incorporation of functionality to the terminal chain end by the initial termination with chlorodimethylsilane compound. This ω -end functionalized silyl hydride polymer can now be reacted in a second step with various substituted alkenes to produce the desired functionality (Scheme 2.1). Terminal ω -chain end functional polymers produced by this method include perfluoroalkyl,⁹² epoxy,⁹³ cyano,⁹⁴ amine⁹⁵ and trialkoxysilyl⁹⁶ functionalities.



Scheme 2.1: Schematic representation regarding the two step functionalization of polymeric ω -end by chlorosilanes, post anionic polymerization.

Quirk *et al.*⁹⁷ reported the successful synthesis of a hydroxyl functional PS by reacting the preformed silyl hydride polymer with allyl alcohol in the presence of Karstedt's catalyst. The silyl hydride polymer was also reacted with allyl alcohol followed by additional silyl hydride PS in a multi-step process to produce multi silyl hydride in-chain functional PS. This in-chain functional PS was further functionalized by the incorporation of cyano functionality. This was achieved by reacting allyl cyanide with silyl hydride in-chain moieties in the presence of Karstedt's catalyst.

Matsuoka *et al.*⁵⁷ synthesized ω -pyrene functional PEO by anionic ring-opening polymerization from potassium tert-butoxide initiator followed by termination using

1-(bromomethyl)pyrene. The noncovalent dispersion extent of MWCNTs in THF solvent was studied by using this functional polymer as an interfacial species. The drawbacks of anionic polymerization, however, involve the stringent reaction conditions necessary to maintain the living character as well as the problem associated with the polymerization of acrylic monomers. The α -proton and polar functional groups on these conventional monomers facilitate the attack by propagating species, leading to termination of the propagation and the loss over control of the polymerization.⁹⁸

2.8.1.2 RAFT polymerization

Reversible addition-fragmentation chain transfer (RAFT) polymerization emerged as a controlled radical process in 1998⁹⁹ and has become a sought after technique for living radical polymerization. The controlled character is attributed to the reversible chain transfer polymerization step (Scheme 2.2) achieved by compounds known as a RAFT agent. Synthesis of a wide range of polymers is achievable by the use of one of the two most versatile RAFT agents. Firstly a tertiary cyanoalkyl trithiocarbonyl RAFT agent can be used in the polymeric synthesis from (meth)acrylate, styrenic and (meth)acrylamide monomers. Cyanoalkyl xanthate agents can be used for the synthesis from vinyl type monomers. The olefins, however, do prove difficult to polymerize. A wide range of RAFT agents exist representing the same general structure with a thiocarbonylthio type molecular construction. A simplified molecular layout of a RAFT agent is represented in Figure 2.4 below.

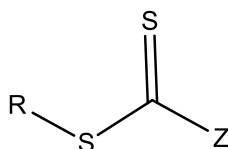
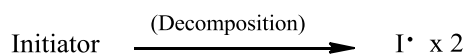
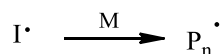
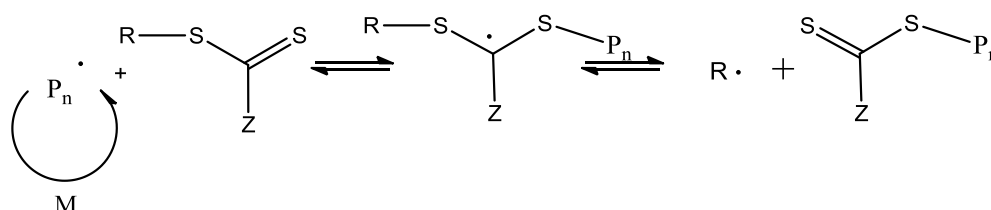
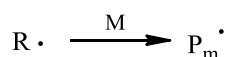
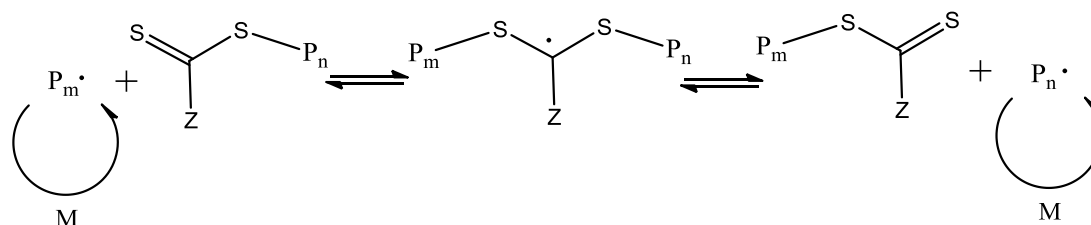
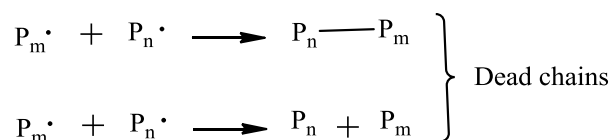


Figure 2.4: Structural layout of a typical RAFT agent.

The R-group represents the free radical leaving group, which initiates the polymerization in the presence of a monomer.¹⁰⁰ The Z-group represents a functional group providing the appropriate stability to the intermediate radical species, allowing for optimum polymerization conditions which in turn depend on the monomer reactant species.¹⁰¹ Once polymerization is initiated from initiator, propagation commences via a reversible chain transfer mechanism. This step of chain growth permits control over the polymerization reaction and the produced polymer chains by reducing the concentration of radical species (Scheme 2.2).

Initiation:**Propagation:****Reversible Chain Transfer:****Re-Initiation:****Equilibrium:****Termination:**

Scheme 2.2: A simplified mechanistic representation of RAFT polymerization as redrawn from general image.⁹⁹

The physical experimental process of RAFT polymerization is similar to that of the conventional free-radical process. The same initiators and solvents with the chosen monomer at the same temperatures are used with the addition of an appropriate RAFT-agent. Under inert conditions, low dispersities are achievable at greater and predicted

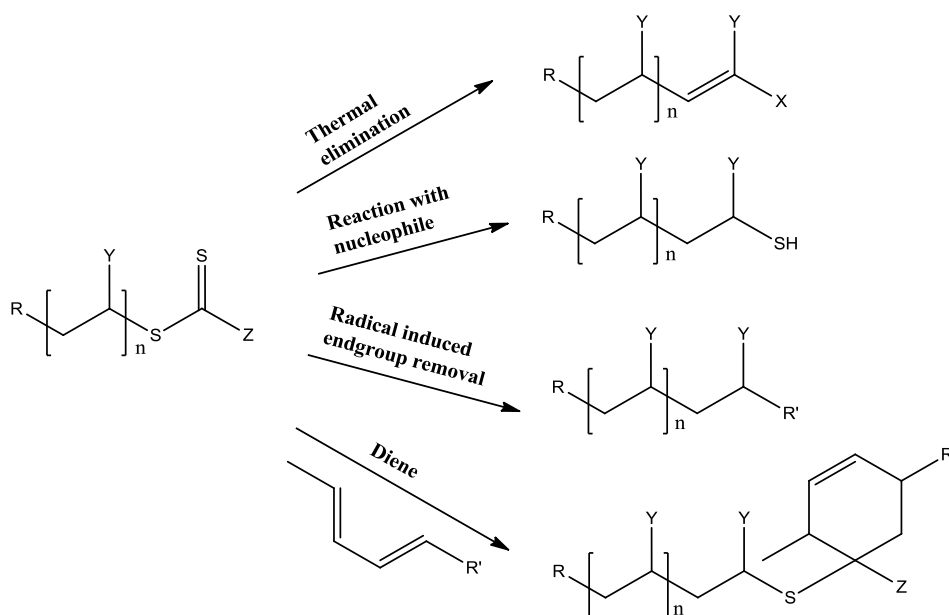
molecular weights. Molecular weights of polymer chains achieved by RAFT can theoretically be predicted from the equation below.¹⁰²

$$M_n \approx \frac{[M]_0 - [M]_f}{[I]_0} m_M \quad \text{Equation 2.1}$$

In the aforementioned equation, M_n represents the calculated molecular weight from monomer weight (m_M), the consumed monomer ($[M]_0 - [M]_f$) and the initiator concentration ($[I]_0$).

The reversible capping mechanism of the RAFT polymerization provides the possibility of introducing chain end functionality. This is achieved by utilization of either the Z-group to achieve the terminal (ω) functionality, or by the R group to produce initial (α) chain end functionality (refer to equilibrium state in Scheme 2.2). Similar to other CRP methods such as ATRP and NMP (discussed in sections 2.8.1.3 and 2.8.1.4), the incorporation of functionality to the initiating specie (the R-group in the case of a RAFT agent) will deliver the initial chain end (α) functionality. Various groups have been reportedly incorporated into the α -end of a polymeric chain by the alteration of this R-group. Such functionalities include benzyl, 2-cyanopropyl, cumyl as well as more novel alterations, such as peptides,¹⁰³ carboxylic acids¹⁰⁴ and lipid groups¹⁰⁵ to mention a few. R-groups should be capable of maintaining a stable radical during homolytical cleavage preceding polymerization. Coady *et al.*¹⁰⁶ successfully synthesized a RAFT agent containing an imidazolium R-group to produce this aforementioned pseudo-benzylic, α -chain end functional polystyrene. Zhou and Harruna¹⁰⁷ successfully synthesized terpyridine α -chain end functionalized poly(N-isopropylacrylamide) (PNIPAM) and polystyrene (PS) polymers via two variations of a terpyridine functionalized dithioester based RAFT agent.

The introduction of functionality into the ω -end proves more tedious as the alteration of thiocarbonate is required. Terminal functionalization post polymerization, however, proves possible by methods such as radical induced substitution, hetero-Diels-Alder reactions, thermolysis and most popularly the functionality incorporation by nucleophile reaction. These functionalization methods arose and are derived from methods initially used for the removal of the sulphur containing end groups which if not removed produces a colour change as well as an unpleasant odour. Methods for thiocarbonyl end group conversion are showed in Scheme 2.3, which is restructured from that obtained in the published work of Wilcock and O'Reilly.¹⁰⁸



Scheme 2.3: Schematic representation for general methodologies used of RAFT end group functionalization.

The incorporation by a nucleophile produces initial thiol functionality, which will in most cases require further modification by methods such as thiol-ene reactions, Michael addition and disulfide coupling to produce end group functionalities.¹⁰⁹⁻¹¹¹

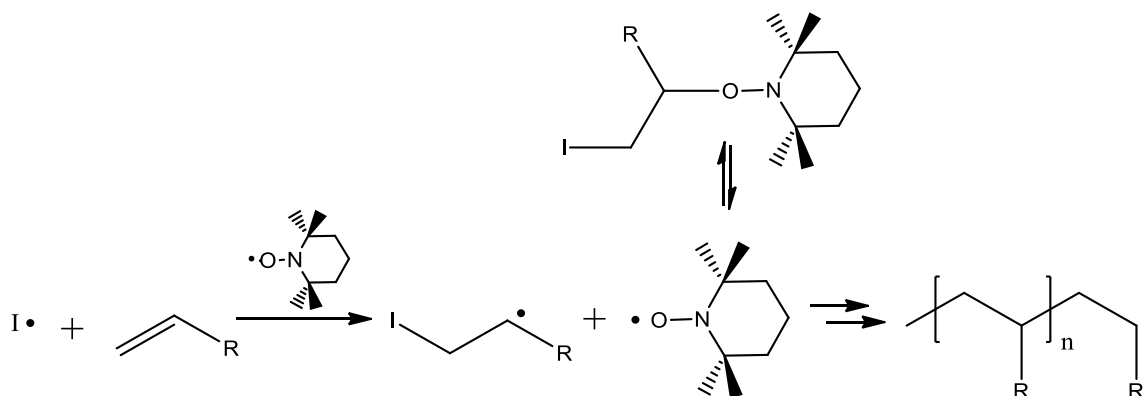
Thermolysis cleaves the sulphur moiety completely to leave an unsaturated hydrocarbon chain end. However, this requires stability of the polymeric backbone during thermal treatment. Similarly to thermolysis, radical induced reduction can be used to achieve desulfurisation in the production of a saturated hydrocarbon. It has also been reported that this technique could be utilized in the terminal end capping of a polymer by using azo-initiators.¹¹² A last method of ω -end functionalization utilizes the electron deficient character of the terminal thiocarbonylthio group acting as an efficient dienophile in a hetero-diels-alder reaction. This method suffices for the production of functional cyclic moieties.¹¹³

2.8.1.3 NMP synthesis

The rise of nitroxide mediated polymerization (NMP) as a controlled radical technique was seen in early 1990's. A comprehensive controlled technique was presented by Georges *et al.*¹¹⁴ who published work on the use of a bimolecular NMP system. This process was developed from work by Moad *et al.*¹¹⁵ who presented initiation studies of styrene polymerization by 1,1,3,3-tetramethylindolinyl-oxy agents.

The propagation process commences much like RAFT polymerization with the capping and decapping of the active polymer chain ends, producing control in the obtained chain length in much the same way as in RAFT polymerization.¹¹⁶ Generally NMP polymerization can be

divided into two separate classes. The first is classified as a unimolecular initiated system. These utilize only alkylated TEMPO (2,2,6,6-tetramethylpiperidinyloxy) initiators. The second is known as the bimolecular system and utilizes TEMPO in combination with a conventional radical initiator, such as AIBN (azobisisobutyronitrile) or BPO (benzoyl peroxide).¹¹⁷ The use of such a bimolecular system of a conventional initiator and TEMPO NMP agent in the polymer synthesis from vinyl monomer is represented by Scheme 2.4 below, altered from an image obtained in the published work by Hawker *et al.*¹¹⁷

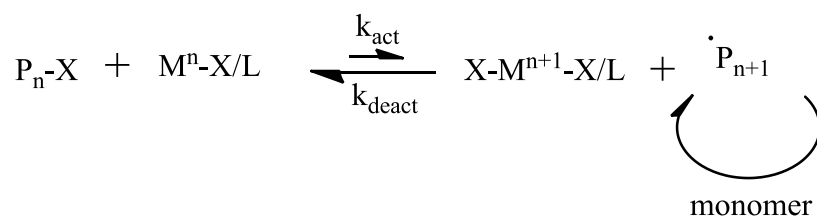


Scheme 2.4: Generally accepted mechanism for NMP synthesis by bimolecular system via conventional and TEMPO initiators as adapted from Hawker *et al.*

Hawker *et al.*¹¹⁷ successfully incorporated various substituents to the TEMPO based molecule in order to achieve α -chain end functional polymer. It was found that a methyl group located on the α -carbon was crucial in maintaining the living character of NMP synthesis. Various substituents such as benzene and functional variation thereof were, however, effectively incorporated in the β -carbon position.

2.8.1.4 ATRP synthesis

The technique of atom transfer radical polymerization (ATRP) was developed by both Sawamoto¹¹⁸ and Matyjaszewski¹¹⁹ early in the 1990's. This reaction has successfully been used to polymerize a wide range of polymers such as poly(meth)acryl-amides, poly(meth)acrylamide, polystyrene and polyacrylonitrile.¹²⁰ In this mechanism the amount of dormant to active species are controlled by the highly favoured deactivation of propagating chains by addition and abstraction of a halogen to the radical containing chain end. A representation of transition metal catalysed ATRP is presented by a simplified mechanism from that obtained in published work of Matyjaszewski and Xia¹²¹ in Scheme 2.5.



Scheme 2.5: Simplistic representation of ATRP propagation by general transition metal catalyst.

X represents a halogen, P_n , the dormant polymer chain and $\text{M}^n\text{-X/L}$ represents the ligand (L) containing transition metal (M^n) catalyst. After abstraction of the halogen, the metal becomes oxidized to M^{n+1} , and the active polymer chain (P_n^{\cdot}) is free to propagate.

This mechanism proceeds via a redox system occurring between the active polymer chain end and the catalytic metal complex. Here, the metal is oxidized to a higher state by the abstraction of a halogen from the polymer chain end. During this electron transfer to the metal complex, the $\text{P}_n\text{-X}$ bond is cleaved homolitically to yield the active chain end P_n^{\cdot} . The chain end is allowed to propagate before it is rendered dormant by the reverse of the above mentioned process, where the oxidized metal donates the abstracted halogen back to the radical possessing propagating chain end. The reverse process is preferred to be more favoured to minimize bi-molecular termination reactions and allows more control over the system regarding molecular chain lengths.¹²² The ratio of activation rate (k_{act}) to deactivation rate (k_{deact}) can be controlled in an attempt to control the polymer dispersity, by changing reaction parameters such as the temperature, initiators, transition metals, ligand and solvents used.⁸⁹ In the case of initiators, for instance, the R-X bond should be in favour of addition to dormant polymer state, therefore the use of R-Br and R-Cl initiators are preferred. Although many metal-halide complexes have been used (such as nickel (Ni), rhodium (Rh), palladium (Pd) and iron (Fe)), the copper (Cu) based complexes have become most common. The transition metal halide normally corresponds to the initiator regarding a similar halide and is used in combination with a ligand to form a complex ($\text{M}^n\text{-X/L}$). Ligands facilitate the halide addition to propagating polymer chain ends and also assist in the solubility of the complex. Considering the various complexes, nitrogen based ligands has proven to be most effective.⁸⁶

The solvent must be chosen carefully because of the fact that protic solvents will interfere with the reaction mechanism. Possible influences include chain transfer reactions or poisoning of the catalyst.¹²⁰ ATRP has the advantage over RAFT and living anionic polymerization based on the relative tolerance to additives, impurities and solvents.⁹⁹

As a result of the living character of ATRP synthesis, halogenated terminal (ω -end) functionality is presented nearly quantitatively at halide functionality of >95%. This character

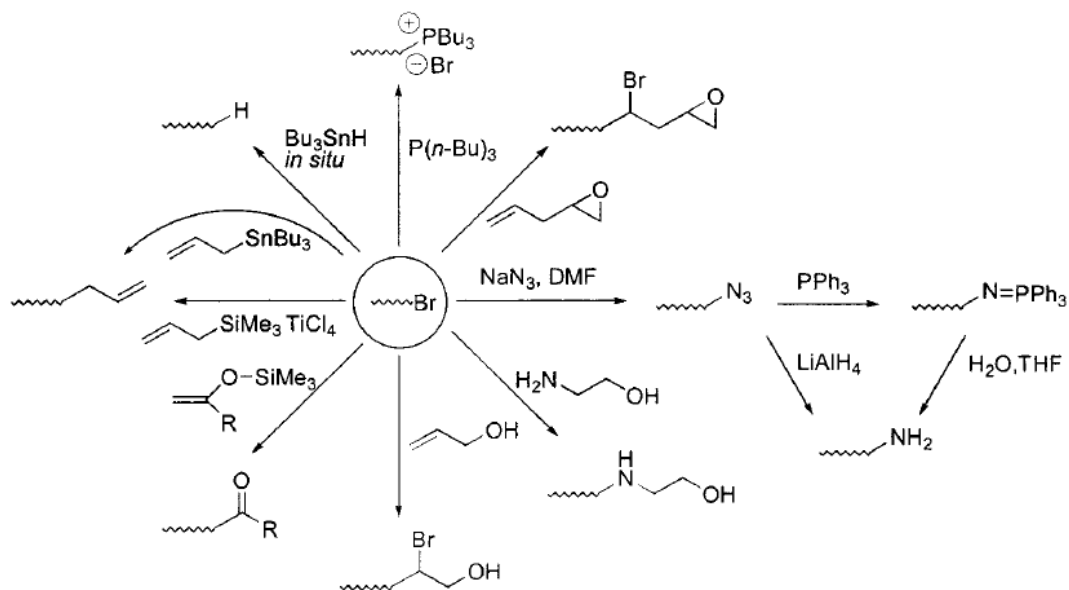
allows the ability of replacing this terminal halogen through various reactions producing a variation of ω -end functional polymers. The chemistry of halogen displacement can commence via various lewis acid catalysed electrophilic addition reactions as well as nucleophilic substitution or free radical reactions. Scheme 2.6 obtained from a review published by Matyjaszewski *et al.*¹²¹ summarize such displacement chemistry from halogenated ATRP produced polymer.

Nucleophilic substitution facilitates the incorporation of azide and amino,^{123,124} hydroxyl, acetate¹²⁵ and phosphonium¹²⁶ end groups to poly(styrene) and poly(acrylate) or methyl methacrylate polymers. Azide functionalities are shown by Coessens *et al.*¹²³ to be incorporated into poly(styrene), poly(methacrylate) and poly(methyl methacrylate) polymers via the substitution of terminal bromine end groups using sodium azide. These azide groups, in the case of poly(styrene) were further converted to amino functional groups by means of the reduction by lithium aluminium hydride. Reduction of the esters in acrylate polymers resulted in these polymers being unable to convert to the amino functionality.

The successful transformation of halogenated end groups is reported by simple electrophilic addition reactions using allyltrimethylsilane as well as the use of large variations of allyl bromides or allyl chlorides for the incorporation of these allyl functionalities into the ω -end of a polymeric chain.^{127,128}

Radical assisted transformation involves the functional incorporation of allyl end groups. The functionalities reportedly incorporated by allyl tri-*n*-butylstannanes include acetals, esters, epoxides ethers and hydroxyl groups.

Another radical induced functional transformation includes dehalogenation,¹²⁹ and insertion of unpolymerizable monomer. Coessens *et al.*¹³⁰ reported the incorporation of hydroxyl or epoxide ω -end functionality by introducing a less reactive allyl alcohol to a poly(acrylate) polymerization. Other functionalities reportedly incorporated by such a manner include *n*-maleic anhydride to a polystyrene chain¹³¹ and divinyl-benzene or ethylene to poly(methyl methacrylate).¹³² Similar radical induced transformations include the use of polymer end capping agents such as *p*-methoxy- α -(trimethylsilyloxy)styrene and α -(trimethylsilyloxy)styrene as reported by Ando *et al.*¹³³ in an effort to produce ketone-capped PMMA.



Scheme 2.6: Overview scheme regarding methods (nucleophilic, electrophilic and radical reactions) used for the end group transformation from ATRP produced hydrogen terminal polymers.¹²¹

This method of terminal, ω -end functionalization is comprised of multiple steps, with functionality being incorporated post polymerization. The far simpler technique of polymer functionalization at chain-ends would appear to be the direct α -end functionalization, incorporated by the initiator molecule.

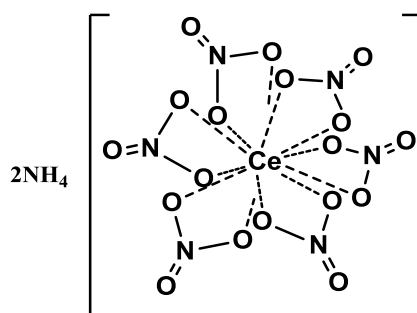
A wide variation of these commercially activated alkyl halides are available to be used for the initiation of ATRP synthesis from vinyl monomers. These initiators allow for the possibility of functionality incorporation to the α -end of a polymeric chain. The radical stabilizing fraction present on the α -carbon of the haloalkane can make up a wide range of functional groups such as nitriles, halogens, aryls, and carbonyls, tolerant of radicals and ATRP catalysts, to be incorporated as chain end functionality in polymer chains.¹²¹

Matyjaszewski *et al.*^{121,134} reported the successful synthesis of various α -chain end functional PMMA polymers by using various bromoalkane initiators. These include allyl bromide, tert-butyl-2-bromopropionate, hydroxyethyl 2-bromopropionate, α -bromo- γ -butyrolactone, 4-cyanobenzyl bromide, glycidol-2-bromopropionate and 2-bromopropanitrile each of which introduce its own specific functionality to the α -end of the PMMA chain. The use of activated sulfonyl initiators can be used in the same way by incorporating chain-end functionality, however, this proves an inefficient initiating species for polymer synthesis from acrylate based monomers.^{125,135} A deeper look into the literature surrounding this initiating system was not needed as AN is to be used as primary monomer in this study.

The α -end functionalization by initiator molecule produces a theoretical quantitative functionality of 100% compared to approximately 95% attainable functionality as expressed for the ω -end functionalization.¹²¹ This results from functional incorporation being independent of possible termination reactions such as radical coupling and disproportionation. The ease and simplicity of α -end functionalization is supported by the published work from the Matyjaszewski¹³⁶ group in which pyrene as well as hydroxyl functional groups are presented to the α -chain end of both poly(*n*-butyl acrylate)-polydivinylbenzene and poly(ethylene glycol)-poly(ethylene glycol dimethacrylate) copolymers. This is achieved by ATRP synthesis from simple alkyl halide ATRP initiators containing the respective functional groups. Following the investigation into the possible ATRP methods for the preparation of mono chain end functional polymer, the most viable technique seems to be the α -end functionalization by a functional alkyl halide initiator.

2.8.1.5 Cerium ammonium nitrate initiated polymerization using redox initiation

Ammonium hexanitratocerate(IV), more commonly known as ceric ammonium nitrate (CAN), is the most popular of the cerium reagents used in organic synthesis and is represented by the molecular formula $(\text{NH}_4)_2[\text{Ce}(\text{NO}_3)_6]$. Other forms of cerium containing oxidants include cerium(IV) ammonium sulphate, cerium(IV) sulphate and ceric perchlorate.¹³⁷ The cerium(IV) ion in CAN is stabilized by six surrounding nitrate groups forming a bulky complex with two ammonium ions in compensation of the negative formal charge. The molecular complex is represented below.



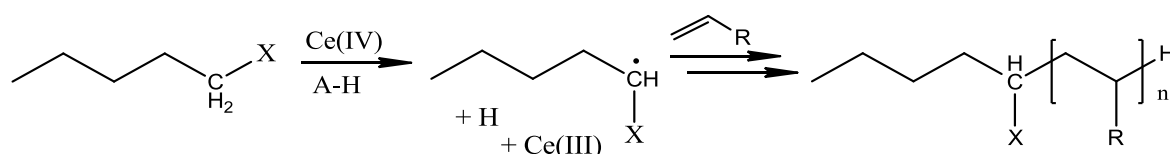
Scheme 2.7: Representation of molecular ceric ammonium nitrate complex.

CAN is in effect a one-electron oxidizing agent serving multiple purposes, with uses ranging from a nitrating agent, a remover of protecting groups as well as a initiator for the free radical mechanism in polymer synthesis. In the case of polymer synthesis, this method has reportedly been referred to as a “redox catalysed”, “redox initiated” or “redox activated” system. Compared to alternate metal based oxidants, such as chromium(VI) salts or potassium permanganate, the cerium based complexes are milder oxidizing agents and

prove to be far less toxic. The advantages of using CAN specifically among the cerium based reagents, includes the high solubility in organic solvents, allowing for frequently desired non-toxic reaction medium at low minimal cost which is easily obtainable.^{138,139} The redox method of polymerization differs from RAFT, NMP and ATRP reactions in being an uncontrolled method of synthesis. The reaction itself, however, presents properties superior to that of the controlled techniques. These attributes include the reagents allowing for not only fast reaction time, but reaction conditions at low temperatures, resulting in lower probability of undesired side reactions as well as decreasing energy consumption.¹³⁸ As this method of polymerization is extremely uncommon, more focus has been awarded to the details surrounding the synthetic procedure and conditions.

Common solvents reported for CAN utilizing reactions include water, dichloromethane (DCM), acetonitrile, tetrahydrofuran (THF) and methanol¹³⁹ of which water proves most popular.⁸⁸ Several publications indicate the use of CAN as initiation of polymerization to be possible, yielding the synthesis of homopolymers, block- as well as grafted copolymers from vinyl monomers.^{88,135,138} Because of this synthetic method serving as an uncontrolled mechanism of free radical polymerization, broad dispersities can be expected compared to the CRP methods. Possible reducing agents, compatible with such systems include alcohols, ketones, aldehydes, amides, thiols and acids.¹³⁸

The mechanism of this system commences via the initiation of polymerization by the formation of a radical centre resultant of the redox reaction taking place between the reducing agent and the ceric ion in acidic solution.⁸⁸ Theoretically by using a reducing agent functionalized with a moiety inert to the initiation and radical mediated propagation step, α -functionality incorporation to polymer chain seems possible. Below is a simple mechanistic representation of the redox initiated polymerization of vinyl monomer by the free radical system which is catalysed by a ceric ion in acetic (A-H) solution. This is achieved by using a ceric salt complex as initiator and an appropriate reducing agent to form a radical centre (Scheme 2.8). The X indicates the functionality of a simple molecule to represent the appropriate alcohol, ketone, aldehyde, amide, thiol or acid. In solution, the cerium(IV) centre is reduced to cerium(III) as the reducing agent is oxidized to produce a radical centre which will in turn polymerize in the presence of monomer until termination occurs.



Scheme 2.8: Mechanistic representation of CAN initiated polymerization of vinyl monomer.

The variables influencing this type of redox initiated free radical system were investigated in depth by Degrimenci *et al.*¹³⁸ who studied the effect of Ce(IV), reducing agent (HNO₃), monomer (AN) initiator and temperature. A CAN catalysed PAN polymerization was run in aqueous media from hydroxyl terminated initiator. The optimum conditions were found to be as follows: a CAN concentration of 0.2 M, HNO₃ concentration of 1 N, AN composition of 2.41 M at a reaction temperature of 35 °C at a runtime of 60 minutes. These conditions were, therefore, chosen as the starting conditions for CAN initiated polymerizations during this study (chapter 3).

Unsal *et al.*¹³⁵ successfully synthesizes poly(acrylonitrile-co-butylacrylate) copolymers by the CAN initiated free radical synthesis in aqueous media. Pyrole monomer was polymerized using a similar redox system in the presence of the produced copolymer to produce hydrogen bonded composites of superior electrical properties.¹³⁵ Köken *et al.*⁸⁸ used the same Ce(IV) initiated redox system to successfully synthesize poly(dimethylsiloxane)-b-poly(acrylonitrile) (PDMS-b-PAN) copolymers from hydroxyl terminal PDMS macroinitiators. Ma *et al.*¹⁴⁰ using the same methods of synthesis as Unsal and Köken, produced poly(methyl methacrylate) (PMMA) as well as poly(acrylonitrile) (PAN) grafted graphene using the redox assisted grafting from oxidized graphene sheets.

Only a few studies have been reported on these redox catalysed polymerization reactions, although it seems worth pursuing considering the appealing attributes of the reaction conditions. This section on CAN mediated polymerization concludes the review on the proposed preparation of chain-end functional polymers. A review is to follow on the synthesis of multi-functional polymer materials.

2.8.2 Multi-functional polymer synthesis

The techniques of polymerization that has been discussed up until this point include the controlled methods of RAFT polymerization, NMP and ATRP as discussed in sections 2.8.1.2, 2.8.1.3 and 2.8.1.4 respectively. These controlled techniques provide the ability for producing well controlled polymers as well as the possibility of introducing chain-end functionality. Control over these propagating chains provides the ability of incorporating both α -functional and more uniquely ω -functional polymers. The uncontrolled redox mediated polymerization by CAN has also been discussed for producing mono functional polymer (section 2.8.1.5). However, the most robust and well established uncontrolled polymerization by far, is that of conventional free radical polymerization (FRP). In the case where precise molecular weights and polymer dispersities are not necessary, conventional FRP seems

ideal based on the tolerance for impurities and the wide variety of monomers that can be polymerized by this mechanism. The technique is also commonly used for the synthesis of various types of copolymers allowing for the incorporation of multiple functionalities to a polymer chain.

2.8.2.1 Copolymers

The synthesis of copolymers presents the ability of altering the physical and/or chemical properties by incorporation of one polymer with another. Linear copolymers can be classified into broad subdivisions of statistical and segmented copolymers. Statistical copolymers include random and alternating monomer distribution where segmented linear copolymers most commonly refer to block copolymers (Figure 2.5). Gradient or tapered copolymers can be seen as a linear copolymer classified as materials between statistical and block copolymers where a gradual transition from one monomer block to another is expected. This is, however, unique to polymerizations of living character. More complex copolymers do of course exist especially in the case of segmented copolymers such as grafted copolymers (briefly discussed in section 2.5) as well as comb, multi-arm star and dendrimer type architectures.³⁵ Due to the scope of this project, however, focus will be restricted to the simple statistical copolymers.

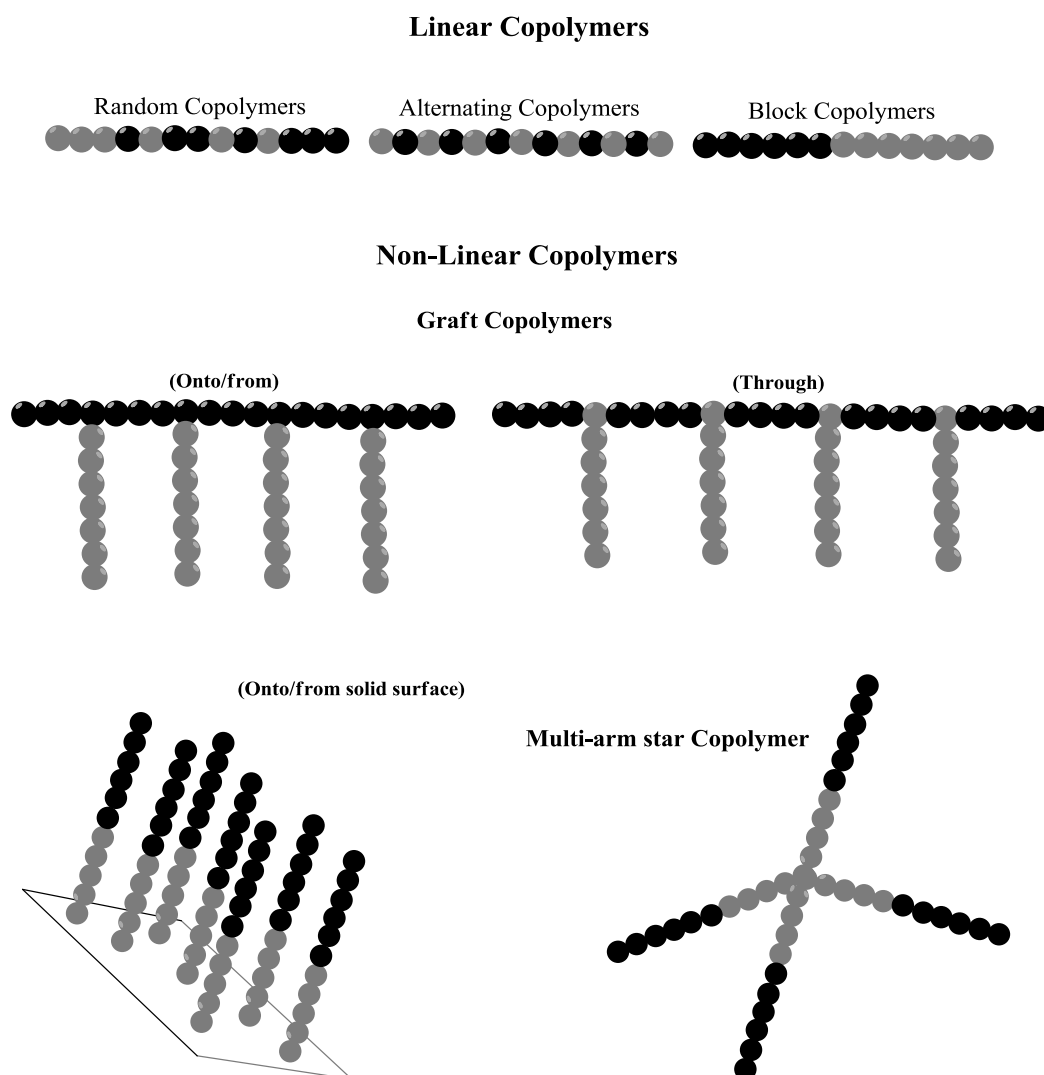


Figure 2.5: Graphical representations of various classes of linear and non-linear copolymers.

When considering simple statistical linear copolymers, monomer units are prone to distribute either alternately or completely randomly throughout the polymer. The distribution of monomer units can be attributed to the reactivity ratios of monomers regarding reactivity of homo and hetero monomeric incorporation reactions. This relative probability of addition can be represented theoretically by equations 2.2 and 2.3. Symbols r_1 and r_2 are representative of respective reactivity ratios of the probability or reactivity of monomers with identical units, (k_{11} or k_{22}) or alternately the reactivity towards the dissimilar monomer (k_{12} or k_{21}).

$$r_1 = k_{11}/k_{12} \quad \text{Equation 2.2}$$

$$r_2 = k_{22}/k_{21} \quad \text{Equation 2.3}$$

Each combination of monomers (in this case two), will have their own specific reactivity ratios, where r_1 can be seen as the reactivity of monomer unit 1 towards another unit 1. In the case of, for instance, the reactivity ratio r_1 showing high values, the homogeneous addition of monomer units 1 will be favored over inter monomer additions. This would theoretically lead to larger segments of similar monomer in the copolymer chain, assuming similarly a high reactivity for unit 2. Such a copolymer is schematically represented by Figure 2.6, “a”, assuming “errors” inevitably occurring during synthesis. Alternately, in the case of a low r_1 value (or low reactivity rate regarding monomer unit A) the incorporation of monomer units will favor heterogeneous/dissimilar reactivity. Assuming similar concentrations, this would result in an alternating addition of monomer, producing a copolymer comprising of dominantly alternating monomer units (Figure 2.6, b). Where similar reactivity ratios are evident for different monomer incorporations to one another, the competing reactivity will facilitate a random addition of monomer units to produce a heterogeneous distribution of both monomer entities along the polymer chain.³⁵ Figure 2.6 represents the various discussed linear copolymers as produced from different combinations of monomer reactivities. The representation is made by A and B representing the dissimilar monomer units 1 and 2 respectively.

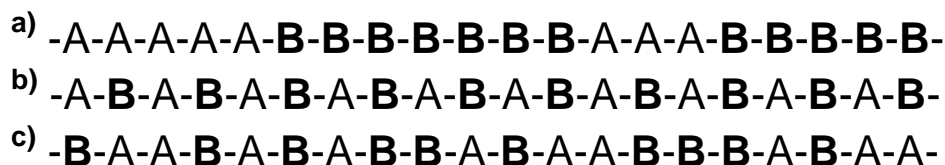


Figure 2.6: Representations of copolymer favoring a) homogeneous b) heterogeneous and c) random monomer insertions.

By using monomers of conventional functionality (or incorporated functionality) copolymerization can be used to incorporate specific characteristics to virgin polymer. The alteration or synthesis of the required functional monomer which is both compatible with the alternate monomer as well as the reaction conditions may give rise to monomers of a bulky nature. When used in concurrent polymerization with conventional monomer, the synthesis is often referred to as copolymerization with a macromonomer and could lead to additional variables to reactivity arising from steric hindrance and monomer diffusion.¹⁴¹

The copolymerization of conventional methyl methacrylate (MMA) and (1-pyrene)methyl-2-methyl-2-propenoate (PyMMP) macromonomer proved successful in the work by Lou *et al.*⁶² using the CFR synthetic approach. These poly(MMA)-co-PyMMP copolymers were used to achieve noncovalent interaction with MWCNTs. With a similar goal of noncovalent attachment, Matsuoka *et al.*⁵⁷ synthesized copolymers of α -methoxy-co-methacryloyloxyethyl, PEO and (MA-PEO1100) and ω -methacryloyloxyethyl polystyrene

(MA-PS2300) macromonomer. The use of macromonomer units may complicate copolymerization as bulky units could present sterical hindrance, affecting monomer incorporation efficiency. This phenomenon is observed specifically in the case of the grafting through technique of graft copolymerizations.

The synthesis of multi-functional polymer is relatively straight forward by CFR copolymerization of the required conventional monomer together with a compatible monomer of the prerequisite functionality.

2.9 Electrospinning

Electrospinning refers to the process of producing fine, continuous fibers by exposure of a viscoelastic material to a strong electrical field. There are alternative options of producing fibers in the range of nanometer diameters. Such options include drawing, template synthesis, phase separation and self-assembly. However, electrospinning is receiving the majority of research attention due to it being a less time consuming and tedious process. The process is a fairly recent development, only established around 1994. It is based on the production of polymeric fibers by utilizing electrostatic forces, an idea initiated about 60 years prior.¹⁴² An electrode is placed in contact with the solution to be spun while the other electrode is attached to a conductive surface. The experimental setup (illustrated in Figure 2.7) generally consists of a high voltage supply, a needle acting as a die of diameter in the sub millimetre range, which is attached to a container as well as a conductive collection surface. The container or syringe containing the material to be spun is subjected to constant pressure producing constant flow rate. The polymeric substrate is forced through the needle (or die) which is connected to the power source, in effect acting as an electrode in itself, leading to a charged fluid.

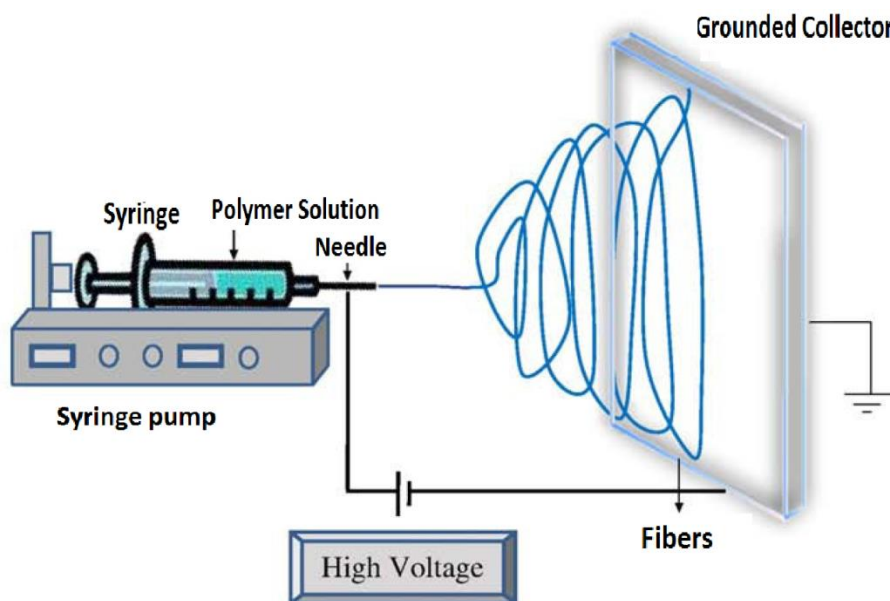


Figure 2.7: Representation of a single needle electrospinning setup.¹⁴³

The charge repulsion in the liquid results in a spherical occurrence at the needle end to elongate and form a cone type structure, commonly known as a Taylor cone.¹⁴² The grounded collector plate acts as the alternate electrode and in the case of sufficient charge, the electrostatic repulsion will overcome the surface tension to result in the eruption of a jet from the tip of the Taylor cone towards the collector plate. During the spinning process, the electric force draws the solution towards the collector plate to form thin fibers by means of destabilization of the jet.^{87,142} The destabilization of the jet leads to a higher surface area and can be divided into three modes of competing instabilities. The first is known as the axisymmetric or Reileigh break-up instability, the second as axisymmetric conducting and finally the whipping or bending instability.⁸⁷ As the jet travels from the Taylor cone to the collector plate, the polymeric solution is elongated and destabilized. Electrospinning most commonly commence from polymers in solution compared to the homogeneous melt spun alternative. Ideally the solvent should evaporate during the elongation and destabilization stage, leading to dry and charged polymeric fibers to be found in the form of a “web” of unoriented fibers. Consequently the fiber morphologies are determined by the solution properties and instabilities, brought about by various parameters. These parameters include the solution properties, governing variables, and ambient parameters. The following table lists the specific variables that can be subdivided into the appropriate spinning parameters.¹⁴²

Table 2.1: Table of electrospinning variables subdivided into solution properties, governing variables and ambient parameters.

| Solution properties | Governing variables | Ambient parameters |
|---------------------|---------------------------------|----------------------|
| Viscosity | Hydrostatic pressure | Solution temperature |
| Elasticity | Capillary | Humidity |
| Conductivity | Electric potential | Air flow |
| Surface tension | Tip to collector distance (TCD) | |

The effect of these various parameters has been investigated in depth as reported ample times in literature. The parameters most investigated in literature are the effect of altering governing variables, although the variation of the solution properties and ambient parameters is also extensively reported.^{87,142,144}

Wang *et al.*¹⁴⁴ observed a decreased fiber diameter when reducing PAN concentration and increasing solution temperature. PAN nanofibers in the sub 100 nm scale were produced by using this high temperature electrospinning procedure of the highly conductive PAN/DMF spinning solution. A decreased fiber diameter can also be achieved by using a decreased capillary, hydrostatic pressure or an increased TCD which also commonly leads to a reduction in the occurrence of fiber beading.⁸⁷ The use of the correct electric potential is essential as a voltage too small may lead to beading and a low production rate, whereas a voltage too high may lead to fiber defects. The influence of viscosity or viscosity influencing parameters has been reported. However, greater alteration on fiber diameter and morphology is seen to be resultant of parameters such as TCD, electric potential or hydrostatic pressure.^{87,145}

2.10 Polymer nanocomposite nanofibers

As stated during the introductory section, electrospinning allows for the production of fibrous materials of large aspect ratios. Successful incorporation of various fillers, with a focus on carbon based materials, allows for use in fields such as filtration, templating for nanostructures, tissue growth scaffolding, optical sensors, drug delivery systems, aerospace and ballistic materials amongst others.^{146,147} In combination with the aforementioned aspect ratios, the use of fillers in nanofibers has become a desired method of enhancing the physical and mechanical properties such as the mechanical strength and fiber conductivity. The alignment of nanotube filler in the composite matrix results in an enhanced property transfer ability of filler to matrix.¹⁴⁸ For this reason, electrospinning seems an ideal composite processing technique as the alignment of individual CNTs or bundles is expected.

The alignment is a result of concurrent dielectrophoretic and shearing forces acting on the carbon fillers.¹⁴²

Addition of fillers into the electrospinning solution alters the solution properties, thus leading to a physical change in the produced fiber. Heikkilä *et al.*⁸⁷ investigated the effect of conductivity and viscosity on the fibers by the incorporation of a ZnCl salt and MWCNTs into the spinning solution of PAN solubilized in DMF. Heikkilä found that by increasing the conductivity, an increased fiber diameter was achieved, brought about by an enhanced mass flow. This observation, however, contradicts literature stating that a decrease in the fiber diameter is obtained as reported by Ju *et al.*¹⁴⁹ and Ra *et al.*¹⁵⁰ These data are explained as being resultant of induced whipping instability brought about by the incorporated MWCNTs acting as charge carriers. Wan *et al.*¹⁴⁵ observed the alteration of flow rate had minimal effect on the fiber diameter and morphology, whereas the incorporation of MWCNT filler into a PAN and a PAN-co-N-vinyl-2-pyrrolidone functionalized polymer led to a rough surface area which is also observed by Heikkilä *et al.*⁸⁷ together with defects such as 3D structures and fiber splitting brought about by the enhanced mass flow.

Wan *et al.*¹⁴⁵ produced electrospun PAN/MWCNT as well as poly(acrylonitrile)-co-N-vinyl-2-pyrrolidone (PANCNVP)/MWCNT composites using covalently oxidized CNTs spun from a DMF solution in an effort to achieving redox mechanistic enzyme immobilization. Both composites presented a rough surface morphology justified as improper nanotube imbedding to the polymer matrix. These composites were, however, prepared at an excessive filler loading fraction, represented at a 5:1 mass ratio of polymer to MWCNT.

Dror *et al.*¹⁵¹ presented nanofibers of poly(ethylene oxide)(PEO)/MWCNTs composites electrospun from a water/ethanol mixture. Water dispersion of MWCNTs was achieved in two novel ways. The first dispersion technique used sodium dodecyl sulphate (SDS) amphiphiles as a nanotube surfactant and the second used a highly branched polymer known as "Gum Arabic". To these aqueous dispersions PEO solvated in a water/ethanol mixture was added, producing the viscoelastic solution to be spun. Alternately Wang *et al.*¹⁵² presented the synthesis of PVAc-MWCNT composites by a similar method of electrospinning from a DMF solution. MWCNTs were incorporated via oxidative functionalization to produce fibrous composites. Conductivity along the nanofiber was enhanced by ten orders of magnitude at a 0.5 wt% nanotube composition relative to the polymer matrix. Also spun from DMF solution are PAN/SWCNT and poly(lactic acid)/SWCNT continuous fiber composites. Ko *et al.*¹⁵³ constructed these composites from high-pressure CO disproportionation (HiPCO) SWCNT clusters, producing fibers in the nanoscale (< 100nm) range. An enhanced Young's modulus of 140% and a melting point is

expressed with a 4wt% nanotube inclusion. These fibers were carbonized in the production of SWCNT/carbon yarns for reinforcement applications. Similarly PAN/MWCNT composites were produced by Hou *et al.*¹⁴⁶ by inclusion of oxidized nanotubes. These fillers dispersed in nanofibers produced composites showing an increased tensile strength of 75% at 5 wt% MWCNT inclusions, and minimal heat shrinkage upon carbonization of 3%. A similarity is observed in all present observations made by Dror, Ko, Wang and Hou *et al.* all indicating both dispersed and clustered CNT fillers showing near axial alignment along fibrous composites. As expressed in previous sections these nanotube alignment facilitated enhancement of property transfer to composite material. Bayley and Mallon⁷ showed the alignment of oxidized MWCNT in electrospun composites of a polyacrylonitrile-graft-poly(dimethyl siloxane) (PAN-g-PDMS) copolymer matrix. The fiber diameter was again seen to decrease as the MWCNT fillers were increased.

Few studies have been reported concerning electrospun CNT/polymer composites of pristine (chemically unaltered) filler inclusion. In this study fibrous nanocomposites are processed using the noncovalent incorporation of CNTs to the viscoelastic solution. This composite solution is to be electrospun in an attempt to optimize the pristine character transfer to composite fibrous material. The optimum property transfer from filler to composite is based on the unaltered conjugated carbon surface structure (sp^2 hybridization), nanotube alignment and a large aspect ratio. Theoretical applications for such polymer composites of superior thermal and electrical conductivity together with mechanical integrity are numerous. PAN seems the first choice when choosing a matrix for the electrospinning production of fibrous composites because of the ease of spinning process from this polymer as well as the vast amounts of literature available on this topic. Imbedding nanotube filler into specifically a PAN matrix presents additional possibilities of converting CNT/polymer composite to CNT/carbon fibrous composite via carbonization.

2.11 Analysis techniques

In order to investigate and prove noncovalent attachment on a molecular level, various analytical techniques can be utilized, as numerous reported in literature.² This study will focus specifically on the intermolecular $\pi-\pi$ stacking associated with noncovalent interactions between the conjugated surface of CNTs and the proposed π -system, in this case exclusively the π -system of the polymer protruding pyrene moiety.

¹H-NMR has been reportedly used to indirectly detecting noncovalent $\pi-\pi$ stacking interactions by a weakening, broadening and/or shifting of the ¹H peak prior to $\pi-\pi$ stacking.

This alteration of ^1H signal can be explained by electrostatic interactions between delocalized electrons on the sp^3 hybridized carbons present at the CNT surface and the pyrene π -system.¹⁵⁴

Thermogravimetric analysis (TGA) has been reported effective in the confirmation of noncovalent, as well as covalent CNT functionalization. TGA analyses a sample based on thermal degradation, or weight loss, as a function of temperature. Therefore the degree of functionalization can be determined based on the distinct resilient thermal properties associated with CNTs relative to those of the grafted polymer.⁴²

The strong fluorescence property of pyrene enables the effective use of this method of fluorescence emission spectroscopy. As a result of π stacking interaction with pyrene moieties, a quenching phenomenon has been reported¹⁵⁵ resulting from the energy transfer within a composite, between the sp^3 hybridized carbon surface of CNTs and the cyclic pyrene moieties.^{156,157}

Microscopy techniques such as scanning electron microscopy (SEM) and transition electron microscopy (TEM) are essential in evaluation of fibrous nanocomposites. SEM is a technique capable of producing images from which fiber morphology, diameter and defects can be evaluated. TEM imaging can be utilized to study the internal morphology of fibers. Such a technique is useful in determining the distribution and alignment of the nanofiller.^{87, 150,151,153}

2.12 References

- 1) M. F. Yu, O. Lourie, M. J. Dyer, K. Moloni, T. F. Kelly and R. S. Ruoff, *Science*, 2000, **287**, 637-640.
- 2) M. T. Byrne and Y. K. Gun'ko, *Adv. Mater.*, 2010, **22**, 1672-1688.
- 3) Y. S. Duksh, B. K. Kaushik, S. Sarkar and R. Singh, *J. Eng. Des. Tech.*, 2010, **8**, 334-353.
- 4) S. Iijima, *Nature*, 1991, **354**, 56-58.
- 5) T. W. Odom, J. Huang, P. Kim and C. M. Lieber, *Nature*, 1998, **391**, 62-64.
- 6) V. Choudhary and A. Gupta, in *Polymer/Carbon Nanotube Nanocomposites*, ed. S. Yellampalli, Intech, 2011, p. 66-80.
- 7) G. M. Bayley and P. E. Mallon, *Polymer*, 2012, **53**, 5523-5539.
- 8) P. M. Ajayan, O. Stephan, C. Colliex and D. Trauth, *Science*, 1994, **265**, 1212-1214.
- 9) Z. Spitalsky, D. Tasis, K. Papagelis and C. Galiotis, *Prog. Polym. Sci.*, 2010, **35**, 357-401.
- 10) J. Sandler, J. Kirk, I. Kinloch, M. Shaffer and A. Windle, *Polymer*, 2003, **44**, 5893-5899.
- 11) P. Harris, *Int. Mater. Rev.*, 2004, **49**, 31-43.
- 12) M. F. Yu, B. S. Files, S. Arepalli and R. S. Ruoff, *Phys. Rev. Lett.*, 2000, **84**, 5552-5555.
- 13) H. Murakami, T. Nomura and N. Nakashima, *Chem. Phys. Lett.*, 2003, **378**, 481-485.
- 14) D. M. Guldi, M. Marcaccio, D. Paolucci, F. Paolucci, N. Tagmatarchis, D. Tasis, E. Vázquez and M. Prato, *Angew. Chem. Int. Ed.*, 2003, **115**, 4338-4341.
- 15) W. Liu, S. Chai, A. R. Mohamed and U. Hashim, *J. Ind. Eng. Chem.*, 2014, **20**, 1171-1185.
- 16) A. Thess, R. Lee, P. Nikolaev, H. Dai, P. Petit, J. Robert, C. Xu, Y. H. Lee, S. G. Kim, A. G. Rinzler, D. T. Colbert, G. E. Scuseria, D. Tománek, J. E. Fischer and R. E. Smalley, *Science*, 1996, **273**, 483-487.
- 17) F. Kokai, I. Nozaki, T. Okada, A. Koshio and T. Kuzumaki, *Carbon*, 2011, **49**, 1173-1181.
- 18) Y. Chen, R. C. Haddon, S. Fang, A. M. Rao, P. C. Eklund, W. H. Lee, E. C. Dickey, E. A. Grulke, J. C. Pendergrass, A. Chavan, B. E. Haley and R. E. Smalley, *J. Mater. Res.*, 1998, **13**, 2423-2431.
- 19) D. Tasis, N. Tagmatarchis, A. Bianco and M. Prato, *Chem. Rev.*, 2006, **106**, 1105-1136.
- 20) S. Banerjee, T. Hemraj-Benny and S. S. Wong, *Adv. Mater.*, 2005, **17**, 17-29.

- 21) V. Georgakilas, A. Bourlinos, D. Gournis, T. Tsoufis, C. Trapalis, A. Mateo-Alonso and M. Prato, *J. Am. Chem. Soc.*, 2008, **130**, 8733-8740.
- 22) J. Feng, J. Sui, W. Cai and Z. Gao, *J. Compos. Mater.*, 2008, **42**, 1587-1595.
- 23) W. S. Hummers Jr and R. E. Offeman, *J. Am. Chem. Soc.*, 1958, **80**, 1339-1339.
- 24) A. Rasheed, H. G. Chae, S. Kumar and M. D. Dadmun, *Polymer*, 2006, **47**, 4734-4741.
- 25) A. Rasheed, M. D. Dadmun and P. F. Britt, *J. Polym. Sci. Part B*, 2006, **44**, 3053-3061.
- 26) B. Ruelle, A. Felten, J. Ghijsen, W. Drube, R. L. Johnson, D. Liang, R. Erni, G. Van Tendeloo, P. Sophie, P. Dubois, T. Godfroid, M. Hecq and C. Bittencourt, *Micron*, 2009, **40**, 85-88.
- 27) B. Ruelle, S. Peeterbroeck, R. Gouttebaron, T. Godfroid, F. Monteverde, J. P. Dauchot, M. Alexandre, M. Hecq and P. Dubois, *J. Mater. Chem.*, 2007, **17**, 157-159.
- 28) J. N. Coleman, U. Khan, W. J. Blau and Y. K. Gun'ko, *Carbon*, 2006, **44**, 1624-1652.
- 29) G. Wang, S. Huang, Y. Wang, L. Liu, J. Qiu and Y. Li, *Polymer*, 2007, **48**, 728-733.
- 30) H. M. Etmimi, M. P. Tonge and R. D. Sanderson, *J. Polym. Sci. A Polym. Chem.*, 2011, **49**, 1621-1632.
- 31) A. Samakande, R. D. Sanderson and P. C. Hartmann, *Polymer*, 2009, **50**, 42-49.
- 32) M. Ejaz, K. Ohno, Y. Tsujii and T. Fukuda, *Macromolecules*, 2000, **33**, 2870-2874.
- 33) S. Qin, D. Qin, W. T. Ford, D. E. Resasco and J. E. Herrera, *Macromolecules*, 2004, **37**, 752-757.
- 34) M. Salami-Kalajahi, V. Haddadi-Asl, F. Behboodi-Sadabad, S. Rahimi-Razin and H. Roghani-Mamaqani, *Polym. Compos.*, 2012, **33**, 215-224.
- 35) K. A. Davis and K. Matyjaszewski, *Statistical, gradient, block, and graft copolymers by controlled/living radical polymerizations*, Springer, Berlin, 2002.
- 36) L. Sun, G. L. Warren, J. Y. O'Reilly, W. N. Everett, S. M. Lee, D. Davis, D. Lagoudas and H. J. Sue, *Carbon*, 2008, **46**, 320-328.
- 37) C. Grigoriadis, A. Nese, K. Matyjaszewski, T. Pakula, H. Butt and G. Floudas, *Macromol. Chem. Phys.*, 2012, **213**, 1311-1320.
- 38) K. L. Beers, S. G. Gaynor, K. Matyjaszewski, S. S. Sheiko and M. Möller, *Macromolecules*, 1998, **31**, 9413-9415.
- 39) M. Pitsikalis, S. Pispas, J. W. Mays and N. Hadjichristidis, in *Blockcopolymers-Polyelectrolytes-Biodegradation*, ed. V. Bellon-Maurel, A. Calmon-Decriaud, V. Chandrasekhar, N. Hadjichristidis, J. W. Mays, S. Pispas, M. Pitsikalis and F. Silvestre, Springer, Berlin, 1998, p. 1-137.

- 40) S. Qin, D. Qin, W. T. Ford, D. E. Resasco and J. E. Herrera, *J. Am. Chem. Soc.*, 2004, **126**, 170-176.
- 41) K. Fu, W. Huang, Y. Lin, L. A. Riddle, D. L. Carroll and Y. Sun, *Nano Lett.*, 2001, **1**, 439-441.
- 42) G. Xu, W. Wu, Y. Wang, W. Pang, Q. Zhu, P. Wang and Y. You, *Polymer*, 2006, **47**, 5909-5918.
- 43) P. De, M. Li, S. R. Gondi and B. S. Sumerlin, *J. Am. Chem. Soc.*, 2008, **130**, 11288-11289.
- 44) E. Ruckenstein and H. Zhang, *Macromolecules*, 1999, **32**, 6082-6087.
- 45) R. B. Grubbs, C. J. Hawker, J. Dao and J. M. Fréchet, *Angew. Chem. Int. Ed.*, 1997, **36**, 270-272.
- 46) U. M. Stehling, E. E. Malmström, R. M. Waymouth and C. J. Hawker, *Macromolecules*, 1998, **31**, 4396-4398.
- 47) E. Y. Choi, S. C. Roh and C. Kim, *Carbon*, 2014, **72**, 160-168.
- 48) P. D. Petrov, G. L. Georgiev and A. H. Müller, *Polymer*, 2012, **53**, 5502-5506.
- 49) Y. Sun, K. Fu, Y. Lin and W. Huang, *Acc. Chem. Res.*, 2002, **35**, 1096-1104.
- 50) C. Ehli, G. A. Rahman, N. Jux, D. Balbinot, D. M. Guldi, F. Paolucci, M. Marcaccio, D. Paolucci, M. Melle-Franco and F. Zerbetto, *J. Am. Chem. Soc.*, 2006, **128**, 11222-11231.
- 51) D. W. Steurman, A. Star, R. Narizzano, H. Choi, R. S. Ries, C. Nicolini, J. F. Stoddart and J. R. Heath, *J. Phys. Chem. B*, 2002, **106**, 3124-3130.
- 52) D. Baskaran, J. W. Mays and M. S. Bratcher, *Chem. Mater.*, 2005, **17**, 3389-3397.
- 53) J. Zhang, J. K. Lee, Y. Wu and R. W. Murray, *Nano Lett.*, 2003, **3**, 403-407.
- 54) G. Klopman, *J. Am. Chem. Soc.*, 1968, **90**, 223-234.
- 55) A. Eitan, K. Jiang, D. Dukes, R. Andrews and L. S. Schadler, *Chem. Mater.*, 2003, **15**, 3198-3201.
- 56) L. Woods, Ş. Bădescu and T. Reinecke, *Phys. Rev. B: Condens. Matter*, 2007, **75**, 155415.
- 57) M. Matsuoka, M. Yamamoto, K. Adachi, Y. Tsukahara and T. Konno, *Des. Monomers Polym.*, 2010, **13**, 387-397.
- 58) Y. Yan, J. Cui, P. Pötschke and B. Voit, *Carbon*, 2010, **48**, 2603-2612.
- 59) S. Meuer, L. Braun and R. Zentel, *Macromol. Chem. Phys.*, 2009, **210**, 1528-1535.
- 60) N. Nakashima, Y. Tomonari and H. Murakami, *Chem. Lett.*, 2002, **31**, 638-639.

- 61) Y. Zhao and J. F. Stoddart, *Acc. Chem. Res.*, 2009, **42**, 1161-1171.
- 62) X. Lou, R. Daussin, S. Cuenot, A. - Duwez, C. Pagnouille, C. Detrembleur, C. Bailly and R. Jérôme, *Chemistry of Materials*, 2004, **16**, 4005-4011.
- 63) T. J. Simmons, J. Bult, D. P. Hashim, R. J. Linhardt and P. M. Ajayan, *ACS Nano*, 2009, **3**, 865-870.
- 64) R. J. Chen, Y. Zhang, D. Wang and H. Dai, *J. Am. Chem. Soc.*, 2001, **123**, 3838-3839.
- 65) A. Star, D. W. Steuerman, J. R. Heath and J. F. Stoddart, *Angew. Chem. Int. Ed.*, 2002, **41**, 2508-2512.
- 66) S. Tamesue, M. Numata, K. Kaneko, T. D. James and S. Shinkai, *Chem. Commun.*, 2008, **37**, 4478-4480.
- 67) M. Numata, M. Asai, K. Kaneko, A. Bae, T. Hasegawa, K. Sakurai and S. Shinkai, *J. Am. Chem. Soc.*, 2005, **127**, 5875-5884.
- 68) G. Chambers, C. Carroll, G. F. Farrell, A. B. Dalton, M. McNamara, M. in het Panhuis and H. J. Byrne, *Nano Lett.*, 2003, **3**, 843-846.
- 69) H. Dodziuk, A. Ejchart, W. Anczewski, H. Ueda, E. Krinichnaya, G. Dolgonos and W. Kutner, *Chem. Commun.*, 2003, **9**, 986-987.
- 70) O. Kim, J. Je, J. W. Baldwin, S. Kooi, P. E. Pehrsson and L. J. Buckley, *J. Am. Chem. Soc.*, 2003, **125**, 4426-4427.
- 71) L. Y. Yan, Y. F. Poon, M. Chan-Park, Y. Chen and Q. Zhang, *J. Phys. Chem. C*, 2008, **112**, 7579-7587.
- 72) P. W. Barone and M. S. Strano, *Angew. Chem. Int. Ed.*, 2006, **118**, 8318-8321.
- 73) A. P. Goodwin, S. M. Tabakman, K. Welsher, S. P. Sherlock, G. Prencipe and H. Dai, *J. Am. Chem. Soc.*, 2008, **131**, 289-296.
- 74) S. A. Curran, P. M. Ajayan, W. J. Blau, D. L. Carroll, J. N. Coleman, A. B. Dalton, A. P. Davey, A. Drury, B. McCarthy and S. Maier, *Adv. Mater.*, 1998, **10**, 1091-1093.
- 75) B. Standley, W. Bao, H. Zhang, J. Bruck, C. N. Lau and M. Bockrath, *Nano Lett.*, 2008, **8**, 3345-3349.
- 76) X. Wang, L. Zhi and K. Müllen, *Nano Lett.*, 2008, **8**, 323-327.
- 77) Z. Liu, Q. Liu, Y. Huang, Y. Ma, S. Yin, X. Zhang, W. Sun and Y. Chen, *Adv. Mater.*, 2008, **20**, 3924-3930.
- 78) J. Wei, Y. Jia, Q. Shu, Z. Gu, K. Wang, D. Zhuang, G. Zhang, Z. Wang, J. Luo and A. Cao, *Nano Lett.*, 2007, **7**, 2317-2321.
- 79) G. K. Dimitrakakis, E. Tylianakis and G. E. Froudakis, *Nano Lett.*, 2008, **8**, 3166-3170.

- 80) C. Liu, Y. Y. Fan, M. Liu, H. T. Cong, H. M. Cheng and M. S. Dresselhaus, *Science*, 1999, **286**, 1127-1129.
- 81) F. Schedin, A. Geim, S. Morozov, E. Hill, P. Blake, M. Katsnelson and K. Novoselov, *Nat. Mater.*, 2007, **6**, 652-655.
- 82) P. G. Collins, K. Bradley, M. Ishigami and A. Zettl, *Science*, 2000, **287**, 1801-1804.
- 83) M. D. Stoller, S. Park, Y. Zhu, J. An and R. S. Ruoff, *Nano Lett.*, 2008, **8**, 3498-3502.
- 84) M. P. Anantram and F. Léonard, *Rep. Prog. Phys.*, 2006, **69**, 507-561.
- 85) E. Choi, T. H. Han, J. Hong, J. E. Kim, S. H. Lee, H. W. Kim and S. O. Kim, *J. Mater. Chem.*, 2010, **20**, 1907-1912.
- 86) W. Woishnis and S. Ebnesajjad, *Chemical Resistance of Thermoplastics*, William Andrew, Waltham, 2011.
- 87) P. Heikkilä and A. Harlin, *Express Polym. Lett.*, 2009, **3**, 437-445.
- 88) N. Köken, S. Karagöz, N. Kizilcan and B. Ustamehmetoglu, *J. Appl. Polym. Sci.*, 2013, **127**, 3790-3797.
- 89) K. Matyjaszewski, S. M. Jo, H. J. Paik and D. A. Shipp, *Macromolecules*, 1999, **32**, 6431-6438.
- 90) R. P. Quirk and D. L. Gomochak, *Rubber Chem. Technol.*, 2003, **76**, 812-831.
- 91) J. Jagur-Grodzinski, *J. Polym. Sci., Part A: Polym. Chem.*, 2002, **40**, 2116-2133.
- 92) R. P. Quirk, H. Kim, S. R. Chowdhury, M. J. Polce and C. Wesdemiotis, *Polym. Prepr.*, 2005, **46**, 583.
- 93) R. Jayaraman, J. Facinelli, J. Riffle and S. George, *J. Polym. Sci., Part A: Polym. Chem.*, 1996, **34**, 1543-1552.
- 94) R. P. Quirk, J. Janoski, S. R. Chowdhury, C. Wesdemiotis and D. E. Dabney, *Macromolecules*, 2008, **42**, 494-501.
- 95) R. P. Quirk, H. Kim, M. J. Polce and C. Wesdemiotis, *Macromolecules*, 2005, **38**, 7895-7906.
- 96) R. P. Quirk, M. Ocampo, R. L. King, M. J. Polce and C. Wesdemiotis, *Rubber Chem. Technol.*, 2008, **81**, 77-95.
- 97) R. P. Quirk, J. Janoski, M. Olechnowicz, H. Kim, D. E. Dabney and C. Wesdemiotis, *Macromol. Symp.*, 2009, **283**, 78-87.
- 98) O. W. Webster, *Science*, 1991, **251**, 887-893.
- 99) J. Chiefari, Y. Chong, F. Ercole, J. Krstina, J. Jeffery, T. P. Le, R. T. Mayadunne, G. F. Meijs, C. L. Moad and G. Moad, *Macromolecules*, 1998, **31**, 5559-5562.

- 100) Y. Chong, J. Krstina, T. P. Le, G. Moad, A. Postma, E. Rizzardo and S. H. Thang, *Macromolecules*, 2003, **36**, 2256-2272.
- 101) J. Chiefari, R. T. Mayadunne, C. L. Moad, G. Moad, E. Rizzardo, A. Postma, M. A. Skidmore and S. H. Thang, *Macromolecules*, 2003, **36**, 2273-2283.
- 102) G. Moad, Y. K. Chong, A. Postma, E. Rizzardo and S. H. Thang, *Polymer*, 2005, **46**, 8458-8468.
- 103) J. Hentschel, K. Bleek, O. Ernst, J. Lutz and H. G. Börner, *Macromolecules*, 2008, **41**, 1073-1075.
- 104) R. K. O'Reilly, *Chem. Commun.*, 2008, **35**, 4183-4185.
- 105) M. Bathfield, D. Daviot, F. D'Agosto, R. Spitz, C. Ladavière, M. Charreyre and T. Delair, *Macromolecules*, 2008, **41**, 8346-8353.
- 106) D. J. Coady, B. C. Norris, V. M. Lynch and C. W. Bielawski, *Macromolecules*, 2008, **41**, 3775-3778.
- 107) G. Zhou and I. I. Harruna, *Macromolecules*, 2005, **38**, 4114-4123.
- 108) H. Willcock and R. K. O'Reilly, *Polym. Chem.*, 2010, **1**, 149-157.
- 109) Z. Wang, J. He, Y. Tao, L. Yang, H. Jiang and Y. Yang, *Macromolecules*, 2003, **36**, 7446-7452.
- 110) M. Llauro, J. Loiseau, F. Boisson, F. Delolme, C. Ladavière and J. Claverie, *J. Polym. Sci., Part A: Polym. Chem.*, 2004, **42**, 5439-5462.
- 111) C. W. Scales, A. J. Convertine and C. L. McCormick, *Biomacromolecules*, 2006, **7**, 1389-1392.
- 112) K. L. Heredia, G. N. Grover, L. Tao and H. D. Maynard, *Macromolecules*, 2009, **42**, 2360-2367.
- 113) S. Sinnwell, A. J. Inglis, T. P. Davis, M. H. Stenzel and C. Barner-Kowollik, *Chem. Commun.*, 2008, **17**, 2052-2054.
- 114) M. K. Georges, R. P. Veregin, P. M. Kazmaier and G. K. Hamer, *Macromolecules*, 1993, **26**, 2987-2988.
- 115) G. Moad, E. Rizzardo and D. H. Solomon, *Polym. Bull.*, 1982, **6**, 589-593.
- 116) R. P. N. Veregin, M. K. Georges, P. M. Kazmaier and G. K. Hamer, *Macromolecules*, 1993, **26**, 5316-5320.
- 117) C. J. Hawker, G. G. Barclay, A. Orellana, J. Dao and W. Devonport, *Macromolecules*, 1996, **29**, 5245-5254.
- 118) M. Kato, M. Kamigaito, M. Sawamoto and T. Higashimura, *Macromolecules*, 1995, **28**, 1721-1723.

- 119) D. Greszta, D. Mardare and K. Matyjaszeaski, *Macromolecules*, 1994, **27**, 638-644.
- 120) K. Matyjaszewski, T. E. Patten and J. Xia, *J. Am. Chem. Soc.*, 1997, **119**, 674-680.
- 121) K. Matyjaszewski and J. Xia, *Chem. Rev.*, 2001, **101**, 2921-2990.
- 122) R. J. Young and P. A. Lovell, CRC press, London, 2011, p. 105-108.
- 123) V. Coessens, Y. Nakagawa and K. Matyjaszewski, *Polym. Bull.*, 1998, **40**, 135-142.
- 124) K. Matyjaszewski, Y. Nakagawa and S. G. Gaynor, *Macromol. Rapid Commun.*, 1997, **18**, 1057-1066.
- 125) V. Coessens and K. Matyjaszewski, *Macromol. Rapid Commun.*, 1999, **20**, 127-134.
- 126) V. Coessens and K. Matyjaszewski, *J. Macromol. Sci. A*, 1999, **36**, 653-666.
- 127) Y. Nakagawa, S. Gaynor and K. Matyjaszewski, *The synthesis of end functional polymers by "living" radical polymerization*, Amer Chemical Soc 1155 16th st, NW, Washington, DC 20036, 1996.
- 128) V. Coessens, T. Pintauer and K. Matyjaszewski, *Prog. Polym. Sci.*, 2001, **26**, 337-377.
- 129) V. Coessens and K. Matyjaszewski, *Macromol. Rapid Commun.*, 1999, **20**, 66-70.
- 130) V. Coessens, J. Pyun, P. J. Miller, S. G. Gaynor and K. Matyjaszewski, *Macromol. Rapid Commun.*, 2000, **21**, 103-109.
- 131) E. Koulouri, J. Kallitsis and G. Hadziioannou, *Macromolecules*, 1999, **32**, 6242-6248.
- 132) S. A. Bon, A. G. Steward and D. M. Haddleton, *J. Polym. Sci., Part A: Polym. Chem.*, 2000, **38**, 2678-2686.
- 133) T. Ando, M. Kamigaito and M. Sawamoto, *Macromolecules*, 1998, **31**, 6708-6711.
- 134) K. Matyjaszewski, V. Coessens, Y. Nakagawa, J. Xia, J. Qiu, S. Gaynor, S. Coca and C. Jasieczek, *Macromol. Chem. Phys.*, 1998, **200**, 642-651.
- 135) C. Unsal, F. Kalaoglu, H. Karakas and A. Sezai Sarac, *Adv. Polym. Technol.*, 2013, **32**, E784-E792.
- 136) H. Gao and K. Matyjaszewski, *Macromolecules*, 2007, **40**, 399-401.
- 137) A. Sarac, *Prog. Polym. Sci.*, 1999, **24**, 1149-1204.
- 138) M. Degirmenci, E. Taskesen, S. Hicri and H. Yilmaz, *J. Polym. Sci. Part A*, 2008, **46**, 5404-5413.
- 139) K. Deleersnyder, S. Schaltin, J. Fransaer, K. Binnemans and T. N. Parac-Vogt, *Tetrahedron Lett.*, 2009, **50**, 4582-4586.

- 140) L. Ma, X. Yang, L. Gao, M. Lu, C. Guo, Y. Li, Y. Tu and X. Zhu, *Carbon*, 2013, **53**, 269-276.
- 141) Z. Li, K. Zhang, J. Ma, C. Cheng and K. L. Wooley, *J. Polym. Sci., Part A: Polym. Chem.*, 2009, **47**, 5557-5563.
- 142) Z. M. Huang, Y. Z. Zhang, M. Kotaki and S. Ramakrishna, *Composites Sci. Technol.*, 2003, **63**, 2223-2253.
- 143) N. Zhu and X. Chen, in *Advances in Biomaterials Science and Biomedical Applications*, ed. R. Pignatello, InTech, 2013, p. 315-328.
- 144) C. Wang, H. Chien, C. Hsu, Y. Wang, C. Wang and H. Lu, *Macromolecules*, 2007, **40**, 7973-7983.
- 145) L. Wan, B. Ke and Z. Xu, *Enzyme Microb. Technol.*, 2008, **42**, 332-339.
- 146) H. Hou, J. J. Ge, J. Zeng, Q. Li, D. H. Reneker, A. Greiner and S. Z. D. Cheng, *Chem. Mater.*, 2005, **17**, 967-973.
- 147) A. A. Ali, *Int. J. Adv. Manuf. Tech.*, 2014, **70**, 1731-1738.
- 148) I. S. Chronakis, *J. Mater. Process. Technol.*, 2005, **167**, 283-293.
- 149) Y. Ju, G. Choi, H. Jung and W. Lee, *Electrochim. Acta*, 2008, **53**, 5796-5803.
- 150) E. J. Ra, K. H. An, K. K. Kim, S. Y. Jeong and Y. H. Lee, *Chem. Phys. Lett.*, 2005, **413**, 188-193.
- 151) Y. Dror, W. Salalha, R. L. Khalfin, Y. Cohen, A. L. Yarin and E. Zussman, *Langmuir*, 2003, **19**, 7012-7020.
- 152) G. Wang, Z. Tan, X. Liu, S. Chawda, J. Koo, V. Samuilov and M. Dudley, *Nanotechnology*, 2006, **17**, 5829.
- 153) F. Ko, Y. Gogotsi, A. Ali, N. Naguib, H. Ye, G. Yang, C. Li and P. Willis, *Adv. Mater.*, 2003, **15**, 1161-1165.
- 154) R. Haddon, *Nature*, 1995, **378**, 249-255.
- 155) D. M. Guldi, G. A. Rahman, N. Jux, D. Balbinot, U. Hartnagel, N. Tagmatarchis and M. Prato, *J. Am. Chem. Soc.*, 2005, **127**, 9830-9838.
- 156) T. Ogoshi, Y. Takashima, H. Yamaguchi and A. Harada, *J. Am. Chem. Soc.*, 2007, **129**, 4878-4879.
- 157) M. Assali, M. P. Leal, I. Fernández, R. Baati, C. Mioskowski and N. Khier, *Soft Matter*, 2009, **5**, 948-950.

Chapter 3

Experimental

Throughout this chapter focus is directed to the various chemicals, instrumentation and methods employed during synthetic as well as the analytical processes used. Experimental reagent purity and origins are presented together with detailed experimental methods and multiple characterization techniques to be used. Specifications of relevant analytical equipment are discussed regarding topics such as hardware construction and operational software.

3.1 Experimental Materials

Raw materials that were used are represented in order of appearance throughout the experimental section. These chemicals consist of the following:

Pristine short multi-walled carbon nanotubes (MWCNTs) at a proclaimed purity of >95% is obtained from Chengdu Organic Chemicals Co. Ltd. The MWCNT is successfully oxidized by using the following chemicals: 30% sulfuric acid (H_2SO_4 , purum) in H_2O , hydrogen peroxide (H_2O_2) of 30 wt% in H_2O and 70% ACS nitric acid (HNO_3) all received from Sigma-Aldrich. Sodium Nitrate (NaNO_3) at a purity of >99% is obtained from NT laboratory supplies and potassium permanganate (KMnO_4 , >99%) from Scienceworld.

Regarding the synthesis of poly(acrylonitrile) (PAN), N,N-Dimethylformamide (DMF) and methanol is used as received from SASOL (class 3) (South Africa), in combination with acrylonitrile monomer (AN) received from Sigma-Aldrich at purity $\geq 99\%$ containing monomethyl ether hydroquinone inhibitor. Azobisisobutyronitrile (AIBN) is received from Plascon (South-Africa), but required recrystallization purification while AN needed to be rid of hydroquinone inhibitor by means of an inhibitor removal column (Sigma-Aldrich) prior to polymer synthesis. These steps of material purification are explained in section 3.2.

During the redox initiated synthesis of mono pyrene functional PAN by ceric ammonium nitrate (CAN) catalyzed reactions, the following materials are required: 1-pyrenemethanol (98%) and 1-pyrenebutanol (99%) functional species are used as received from Sigma-Aldrich, as well as a catalytic stock solution prepared from catalytic CAN ($\geq 98.5\%$, ACS), and nitric acid (HNO_3)(65%) both received from Sigma-Aldrich.

The mono pyrene functional PAN is prepared in addition by ATRP synthesis. This method required the purification of CuBr_2 (98%) catalyst, obtained from Sigma-Aldrich. During the purification step, glacial acetic acid (CH_3COOH , 100%), received from Merck Millipore, is used followed by ethanol (99.9%) from Kimix. The functional initiators are prepared from the hydroxyl pyrenes by the use of tetrahydrofurane (THF) and dichloromethane (DCM) solvents as obtained from Kimix. Active reagents include α -bromoisobutyryl bromide (98%, Sigma-Aldrich) reagent, and triethylamine (TEA) ($\geq 99\%$, Sigma-Aldrich) from which the hydrated product is dried over anhydrous MgSO_4 ($\geq 99.5\%$, Sigma-Aldrich). Polymerization from initiators are achieved through the use of HPLC grade CHROMASOLV PLUS[®] dimethyl sulfoxide (DMSO)($\geq 99.7\%$, Sigma-Aldrich) solvent, 2,2'-bipyridyl (bpy)($\geq 99\%$, Sigma-Aldrich) ligand and purified CuBr catalyst. DMF is used to carry product through an alumina

column consisting of a glass tube filled with neutral, activity grade Super1, aluminum oxide (Al_2O_3), as received from (Sigma-Aldrich) and precipitated in methanol during the recovery step.

Preceding the copolymerization, (1-pyrene)methyl-2-methyl-2-propenoate (PyMMP) macromonomer is synthesized using TEA and methacryloyl chloride (97%, Sigma-Aldrich) in DMF/THF solvent. ACS grade hydrochloric acid (HCl) (37%, Sigma-Aldrich) and anhydrous sodium carbonate (Na_2CO_3) ($\geq 99.5\%$, Sigma-Aldrich) is used as washing reagents and MgSO_4 for product drying purposes. Copolymerization is achieved using similar chemicals as used in PAN synthesis. These include HPLC grade DMSO solvent, AIBN initiator, AN monomer and methanol precipitation matrix.

Chloroform-d (CDCl_3) (100%, 99.96 atom%) and dimethyl-sulfoxide-d₆ (DMSO-d_6) (100%, 99.96 atom%) from Sigma-Aldrich is used as solvents for liquid $^1\text{H-NMR}$ analysis and N,N-dimethylacetamide (DMac) HPLC grade CHROMASOLV PLUS[®] ($\geq 99.9\%$, Sigma-Aldrich) for SEC analysis.

3.2 Material Purification

All experimental chemicals used are of high quality, however, some required further treatment prior to use. Such procedures include the removal of hydroquinone inhibitor from AN monomer, crystallization of AIBN initiator as well as the reduction of copper based catalyst to the active CuBr state.

3.2.1 Inhibitor removal from AN monomer

AN monomer is stored with 35 ppm to 45 ppm monomethyl ether hydroquinone inhibitor. As AN is light sensitive, this inhibitor is essential by acting as an antioxidant in the prevention of any spontaneous radical induced polymerization. Prior to polymerization, the inhibitor is removed by passing the monomer through a glass column filled with hydroquinone inhibitor remover as received from Sigma-Aldrich.

3.2.2 AIBN Recrystallization

In an effort to remove any impurities from the AIBN initiator prior to use, a general procedure of recrystallization is used. AIBN (5 mg) is added to a 100 ml beaker containing 80 ml of methanol. The solution is magnetically stirred and heated to a temperature of 45°C . After stirring at the predetermined temperature of 45°C for approximately 10 minutes the solution

is filtered by means of a buchner funnel, through a filter paper pre-wetted by methanol. In order to achieve recrystallization, the beaker containing methanol solvated AIBN is sealed by parafilm and placed in the freezer. The solution is left for a period of approximately 2 hours after which the AIBN crystals are removed by filtration. The crystals are washed by cooled methanol (stored in the fridge prior to recrystallization) several times before drying under vacuum for approximately 5 hours. The dried crystals are placed into a sealed container and stored in the fridge until use.

3.2.3 Copper bromide (CuBr) purification

The purification of the copper based ATRP catalyst is done from the commercially available CuBr_2 as obtained from Sigma-Aldrich. A general procedure is followed as initially presented by Keller *et al.*¹ The catalyst is initially dispersed in glacial acetic acid and left to stir in a sealed round bottom flask overnight. The dispersion is then filtered with a glass funnel leaving the reduced Cu(I)Br on the filter paper. Following filtration, the product is washed several times with ethanol (100 ml) and placed under reduced pressure by means of a shlenk system in effort to dry the product, after which an over pressure of argon gas is applied to the sealed vessel and stored in the fridge until use. By this method any oxidized Cu(II) should be reduced to active Cu(I) state to be used as CuBr ATRP catalyst.

3.3 Preparation of oxidized MWCNTs

The following procedure is based on the synthetic method as presented by Hummers *et al.*² Pristine MWCNTs (4 g) together with NaNO_3 is added to a 500 ml beaker to produce a relative ratio of 2:1 (MWCNTs: NaNO_3). After the addition of a stirrer bar, the beaker is placed in an ice bath before slowly adding 92 ml of H_2SO_4 (30% in H_2O). The solution is left to stir for 10 minutes after which 3 g of KMNO_4 is added slowly under vigorous stirring, not allowing the reaction temperature to exceed 20 °C. Stirring continues for a further 10 minutes, followed by the reaction being heated to 98 °C in an oil bath. After the solution turns dark brown, and effervescence is ceased, 184 ml of distilled water is slowly added. The temperature is maintained for a further 15 minutes under stirring. A 3 wt% solution of H_2O_2 is added to the solution to achieve a final reaction volume of 400 ml, and left to stir for 20 minutes. Ultimately the MWCNTs are neutralized by numerous cycles of centrifuging, decanting of the H_2O , and addition of additional distilled H_2O . Cycles are halted once the solution presents a neutral pH (approximately 7) MWCNTs are dried by use of a Christ Alpha 2-4 LD freeze drier to produce the oxidized MWCNTs.

3.4 Synthesis of homo PAN

DMF (30 ml) is added to a 500 ml, single neck, round bottom flask as the reaction medium. The sealed reaction is degassed with argon gas for 10 minutes, while under vigorous stirring using a magnetic stirrer. Distilled acrylonitrile monomer (5.5 g) is added via a syringe to produce a monomer content of approximately 18 wt%. The reaction is left to stir for a further 15 minutes before adding the recrystallized AIBN initiator (5.5 mg) quantitatively amounting to 0.1 wt% regarding the amount of acrylonitrile added to the solution. The reaction vessel is then placed in an oil bath, preheated to 70 °C and left to stir for 48 hours. The obtained polymer is precipitated in excess amounts of methanol and filtered off using a Buchner funnel. The off-white product is left to dry under vacuum at room temperature until a constant weight is observed. Drying is achieved by means of a Shel Lab vacuum oven.

3.5 Synthesis of pyrene functional PAN

3.5.1 Ce⁺⁴ mediated synthesis of mono pyrene functional PAN

The CAN redox system is investigated as a viable method for the preparation of mono pyrene chain end functional PAN, with attributes lying in reaction speed, low cost and mild reaction conditions. Polymerization procedures are obtained in literature^{3,4} from which a general synthetic method is constructed.

The appropriate hydroxy pyrene initiator, AN monomer and the desired reaction medium (i.e. H₂O, DMF, DMSO, THF, methanol and mixtures thereof) are added to the appropriate sized (100 ml to 500 ml) single neck round bottom flask.

The solutions are stirred vigorously during concurrent degassing by inert argon gas for approximately 15 minutes. Following the degassing step, the reaction vessels are preheated to the desired reaction temperature (20 °C to 55 °C) preceding the addition of the catalytic ceric ammonium nitrate (CAN) solution. These solutions consisted of the predetermined amount of CAN in a 1M nitric acid (HNO₃) solution which is added to the stirring mixture over 10 to 20 minutes using a flow pump. The reactions are left to polymerize for the required amount of time (1 to 24 hours) after which the product is recovered by precipitation in water (stored in fridge prior to recovery step). The precipitated product is quantitatively extracted via centrifuging (Digicen 21 Orto Alresa centrifuge) and washed several times with distilled water, to isolate the solid product by decanting the unwanted liquid in an effort to remove impurities and water soluble catalyst. Decanting cycles are done until the diluent became clear, indicating the removal of the ceric catalyst. Finally the product is placed under

vacuum at 40 °C and dried until constant weight in an effort to remove solvent traces by use of a Heidolph Laborota 4000 rotor evaporator connected with a Vacuubrand pump unit.

Due to various case studies being investigated, such as temperature, solvent, time and catalyst dependence, a universal quantitative method regarding reagents is not possible, however general guidelines are followed. Such general reaction specifications include an AN monomer content amounting to approximately 10 wt% to 20 wt% of the reaction medium being used. A CAN catalytic solution of Ce(IV) concentration of 0.1 M to 3 M in nitric acid (1 M) is introduced into the reaction amounting to 1 wt% to 4 wt% of reaction medium. The catalytic CAN solution is incorporated dropwise at a flow rate of 0.25 ml/min incorporation of 2.5 ml to 5 ml for the individual reactions.

3.5.2 ATRP synthesis of mono pyrene functional PAN

3.5.2.1 Synthesis of ATRP initiator

For the synthesis of the pyrene functional ATRP initiator, two methods found in literature were reviewed and used to produce the method that follows.^{5,6} A 10 ml solution of THF solvating 2-bromoisobutyryl-bromide (1.2 mmol or 1.8 ml) is added to a 50 ml THF solution containing pyrene-methanol (6.0 mmol or 1.4 g), TEA (1.8 mmol or 2.4 ml). The addition of the 10 ml 2-bromoisobutyryl-bromide containing solution is done dropwise at 0 °C and over 1 hour via a flow pump operating at a flowrate of 0.15 ml/min. After this addition, the reaction is left to stir over night at room temperature allowing the esterification reaction to commence. Following esterification, the solvent is removed by rotary evaporation using a Heidolph Laborota 4000 rotor evaporator connected with a vacuubrand pump unit. Distilled water is added to the dried product in order to dissolve the amine salt byproduct, followed by the extraction of the ATRP initiator using 100 ml of DCM. The DCM solution is then washed using 400 ml saturated sodium bicarbonate solution followed by 400 ml of distilled water. This organic DCM solution is removed and dried over MgSO₄ by stirring at room temperature overnight. The hydrated MgSO₄ is removed by filtration using a stinted glass filter and a general bench top vacuum pump (KNF Neuberger Laboport unit). Finally the DCM is removed under vacuum using a vacuum oven set at 40 °C to produce the desired pyrene functional ATRP initiator.

NMR analysis of 1-pyrenemethyl-2-bromoisobutyrate shows a spectrum summarized as follows. ¹H NMR (CDCl₃): 8.05 ppm to 8.38 ppm (m, 9H, aromatic H), 5.92 ppm (s, 2H, -CH₂-), 1.89 ppm (s, 6H, -CH₃). The spectra representing that of the 1-pyrenebutyl-2-

bromoisobutyrate initiator is presented by the following: ^1H NMR (CDCl_3): 7.87 ppm to 8.32 ppm (m, 9H, aromatic H), 4.29 ppm (t, 2H, $-\text{CH}_2-$), 3.41 ppm (t, 2H, $-\text{CH}_2-$), 2.01 ppm (quint, 2H, $-\text{CH}_2-$), 1.96 ppm (s, 6H, $-\text{CH}_3$). 1.90 ppm (quint, 2H, $-\text{CH}_2-$)

3.5.2.2 Synthesis of mono pyrene functional PAN by ATRP

The production of mono functional PAN polymer commences via the respective 1-pyrenemethyl 2-bromoisobutyrate and 1-pyrenebutyl 2-bromoisobutyrate presynthesized ATRP initiators. The hydroxyl terminated macroinitiator (3.05×10^{-4} mol) is added together with bpy ligand (9.15×10^{-4} mol) to a clean shlenk reaction vessel containing AN monomer solvated in HPLC grade DMSO to produce a approximately 30 wt% solution (8.56 M AN). The monomer and solvent content therefore varied with the variation in the targeted molecular weight, however, maintaining a constant molar ratio of the remaining reagents of initiator/catalyst/ligand being at 1/1/3. To this vessel, a clean magnetic stirrer is added and the flask is sealed by a rubber septum preceding 4 cycles of freeze pump thaw. During the final frozen state of the reagents, the seal is carefully removed followed by the addition of CuBr catalyst, while maintaining a steady flow of argon over the reaction. The vessel is sealed and left under a slight overpressure of argon atmosphere after which the reaction containing the solid reagents is placed in an oil bath, preheated at 60 °C, where it is left to thaw under stirring for 15.5 hours. The produced polymer solution is then diluted with DMF and passed through a 3 inch alumina column for catalyst removal followed by precipitation in excess amounts of methanol. The precipitated polymer is collected via filtration and methanol washing for the removal of both ligand and unreacted initiating species. The final product is dried under reduced pressure, using a vacuum oven, until constant weight is observed.

3.5.3 Synthesis of multi pyrene functional PAN

3.5.3.1 Synthesis of PyMMP macromonomer

Preceding the synthesis of multi pyrene functional PAN the appropriate macromonomer, (1-pyrene)methyl-2-methyl-2-propenoate (PyMMP), is produced by the method to follow. This synthesis is based on the presented method by Lou *et al.*⁷ The reaction solution is prepared in a 100 ml single neck round bottom flask consisting of 1 ml TEA (7.2×10^{-3} mol) and 25 ml THF. To this solution 0.5 grams of 1-pyrenemethanol (2.2×10^{-3} mol) is added after which the reaction vessel is sealed by the use of a rubber septum and submerged in an ice bath. Under magnetic stirring the reactants is left to stir for approximately 5 minutes

followed by the drop wise addition of 0.63 ml methacryloyl chloride (6.5×10^{-3} mol) using a 1 ml plastic syringe with fitted needle. After the addition of methacryloyl chloride, the reaction is left to stir over night at room temperature (approximately 25°C). Following the removal of the produced salt by filtration, the THF is removed under reduced pressure by use of a rotary evaporator. The product is then dissolved again in 30 ml of DCM followed by washing with a 1.0 M of HCl solution. The organic solution is further treated by washing with an aqueous Na_2CO_3 solution and finally by distilled water. The organic layer is isolated by the use of a separation funnel and left to dry over MgSO_4 until the following morning. Filtration of the solution is followed by removal of the solvent under reduced pressure. The produced yellow salt is solvated from the addition of 1ml THF to be precipitated by adding excess volumes of methanol (approximately 10 ml) and left over night in the fridge. The final product is collected by filtration from THF/methanol solution followed by purification of the macromonomer in the same way. Gravimetric analysis shows yields of 77% attainable and an NMR spectrum summarized as follows: $^1\text{H-NMR}$ (DMSO-d_6): 8.05 ppm to 8.38 ppm (m, 9H, aromatic H), 6.05 ppm (dq, 1H, $\text{C}=\text{CH}_2$), 5.90 ppm (s, 2H, $\text{CH}_2\text{-O}$), 5.67 ppm (quint, 1H, $\text{C}=\text{CH}_2$), 1.89 ppm (dd, 3H, CH_3)

3.5.3.2 Synthesis of multi pyrene functional PAN by CFR copolymerization

The copolymerization of acrylonitrile (AN) and (1-pyrene)methyl-2-methyl-2-propenoate (PyMMP) macromonomer is done by simple conventional free radical (CFR) polymerization. This is achieved by the addition of predetermined amounts of PyMMP macromonomer (dependent of target mol% PyMMP incorporation) together with 5 g of AN monomer (9.4×10^{-2} mol) and 5 mg AIBN to a clean round bottom flask containing 20 ml of HPLC grade DMSO. The AN composition therefore makes up approximately 18.5 wt% of the reaction matrix with 0.1 wt% AIBN relative to AN monomer content. The addition of a magnetic stirrer to the reaction is followed by sealing the vessel with a rubber septum and argon is utilized for degassing of the solution for 15 minutes whilst stirring at room temperature. The solution is left under a slight argon over pressure and placed in a preheated oil bath at 70 °C to stir for 48 hours. The produced polymer is precipitated in excess methanol and collected by use of a büchner funnel. The product is washed several times with methanol in an effort to remove unreacted products before drying at reduced pressures until constant weight.

3.6 Electrospinning

All PAN fibers are spun from DMF solutions containing 10 wt% of polymer and experimental spinning parameters of a 15 KW applied voltage, a tip to collector distance (TCD) of 15 cm and a flowrate of 0.03 ml/min. A consistent needle diameter of 0.9 mm is maintained as well as the use of a 1 ml B.Braun plastic syringe, operating at ambient parameters of approximately 25 °C and a relative humidity ranging from 35% to 40%, measured by an industrial CFZ-20-S dehumidifier.

3.7 Carbonization

Precursor nanocomposite nanofibers are carbonized during subjection to a general stepwise heating pattern as presented in literature.⁸ The fibrous mats are placed into a tubular GHC 12/450 carbide furnace connected to a Eurotherm 2160 controller. The temperature is raised from room temperature at a heating rate of 5 °C/min to 300 °C and kept at this temperature under an oxygen environment for 2 hours in an effort to achieve cyclization and oxidation of the fibers. The samples are then subjected to an inert atmosphere by purging the chamber with argon gas. In a second heating step the temperature is raised again at a heating rate of 5 °C/min to a temperature of 700 °C in the process of pre-carbonization and stalled at this temperature for 1 hour. Still under the argon atmosphere, the temperature is raised at a 5 °C/min heating rate to a final temperature of 1100 °C and left at this temperature for 2 hours. This final step is known as the carbonization step.

3.8 Characterization (analytical techniques)

3.8.1 ¹H-NMR spectroscopy

In order to analyze the product obtained, based on hypothesized molecular structure as well as purity thereof, ¹H-NMR spectroscopy is used. The specific instrument used is a Varian^{Unity} Inova 400MHz spectrometer run on VnmrJ 2.1 B software using a 5mm PFG dual broadband probe. Samples are run at a preset temperature of 20 °C in a solution matrix of both deuterated dimethyl sulfoxide (DMSO-*d*₆) as well as deuterated chloroform (CDCl₃) dependent on product solubility as well as solvent peak overlapping. Final spectral analysis is done by means of MestReNova software.

3.8.2 SEC

SEC analysis is done in a DMAc solvent to obtain data such as relative molecular weights, dispersities as well as functionality incorporation by means of a RI/UV dual detector system. All SEC analysis are done on a system, consisting of a Waters 717 plus auto-sampler, a Shimadzu LC-10AD pump and a column setup as follows: a 50 mm × 80 mm guard column, a PSS GRAM precolumn (100 Å, 10 µm, 8.0 mm × 300 mm) followed by two PSS GRAM columns (3000 Å, 10 µm, 8.0 mm × 300 mm). The detector setup consisted of a Waters 2487 dual wavelength UV detector in series with a Walters 410 differential refractometer and run on Breeze Version 3.30 SPA software. The system is calibrated with poly(methyl methacrylate) standards, thus producing relative molecular weight data. All samples were made up to a concentration of 1 mg/ml and run at a controlled temperature of 40°C.

3.8.3 UV-visible spectroscopy

For analyzing the removal of unreacted functional molecules, the presence of pyrene functionality could be tracked based on UV active character. For these types of procedures an Analytik Jena Specord 210 plus UV spectrometer is used. An absorbance screening in the ultraviolet-visible area of 200 nm to 400 nm by slit size 1 nm is investigated of DMF based solutions (and therefore referenced against DMF) in Perkin Elmer UV/Vis spectroscopy cell quartz cuvettes. WinASPECT PLUS operating software used is in order to process produced data.

3.8.4 UV-Fluorescence spectroscopy

The characteristic property of fluorescent emission activity associated with pyrene functionality is reported to be affected by π - π interactions. This phenomenon is used in analyzing the degree of association at CNT/compatibilizers interface by means of fluorescent emission signal quenching. This investigation is accomplished by use of a Chirascan-plus Circular Dicroism (CD) spectrometer. Instrumental specifications entail a 150 W air-cooled Xe lamp light source in combination with a F/7 split-Wollaston prism monochromator and a high performance UV-visible-IR avalanche photo diode detector. Spectral data is obtained by scanning for emission signals over the range of 385 nm to 500 nm following excitation at wavelength 345 nm and comparable absorbance spectra is presented by running excitation scanning over the wavelength range 200 nm to 380 nm utilizing maximum emission wavelength of 394 nm. Produced data is analyzed by Pro-Data Control and Pro-Data Viewer software. Samples are analyzed at sample holder temperature set at 20°C.

3.8.5 TGA

An indirect determination of the compatibilizer association with MWCNTs is gravimetric analysis of the extracted MWCNT/Pyrene-functional-PAN complex by thermal gravimetric analysis (TGA). This is achieved by using a Perkin Elmer TGA 7. Samples of approximately 3 mg are exposed to a heating cycle of 10°C/min from ambient temperature to a final heat environment of 600 °C. Gravimetric analysis of samples are done over the desired temperature range in an inert nitrogen atmosphere introduced at a flow rate of 20 ml/min. Final curve plotting and analysis is done on “TA universal analysis” software.

3.8.6 SEM

For the analysis of produced fibrous nanocomposites, SEM is used to present imaging data. Composites spun onto aluminum foil are cut into segments of approximately 1 cm × 1 cm surface area to be presented to metal stubs by means of double sided carbon tape. The prepared samples are gold coated by sputtering for 6 minutes before being presented for analysis by a Leo 1430VP SEM equipped with a 133 eV resolution Centaurus detector operated at a 5.9 keV and a 10 mm² detection area. Imaging of magnification of 7 × 10³ is obtained at 7 KV and analyzed by Axiovision LE Release 4.4 software for the acquirement of data such as fiber diameter and data point distribution.

3.8.7 TEM

As a method of investigating nanocomposite internal morphology, TEM analysis is selected as appropriate technique. Samples are imbedded in resin made up from an Agar 100 resin kit (from Agar Scientific) and left to crosslink at 60°C for 24 hours. The prepared samples are microtomed into individual sheets of 100 nm to 150 nm diameter by a Reichert Ultracut S ultramicrotoming instrument. The sample imbedded sheets are analyzed by a FEI Tecnai 20 transmission electron microscope equipped a Lab6 emitter operating at 200 kV and Tridiem energy filter used to produce imaging by a Gatan CCD camera.

3.9 References

- 1) R. Keller, H. Wrcoff and L. E. Marchi, *Inorg. Synth.*, 1946, **2**, 1-4.
- 2) W. S. Hummers Jr and R. E. Offeman, *J. Am. Chem. Soc.*, 1958, **80**, 1339-1339.
- 3) M. Degirmenci, E. Taskesen, S. Hicri and H. Yilmaz, *J. Polym. Sci. Part A*, 2008, **46**, 5404-5413.
- 4) L. Ma, X. Yang, L. Gao, M. Lu, C. Guo, Y. Li, Y. Tu and X. Zhu, *Carbon*, 2013, **53**, 269-276.
- 5) M. A. Semsarzadeh and M. Abdollahi, *J. Appl. Polym. Sci.*, 2012, **123**, 2423-2430.
- 6) J. K. Oh and K. Matyjaszewski, *J. Polym. Sci. A Polym. Chem.*, 2006, **44**, 3787-3796.
- 7) X. Lou, R. Daussin, S. Cuenot, A. -. Duwez, C. Pagnouille, C. Detrembleur, C. Bailly and R. Jérôme, *Chem. Mater.*, 2004, **16**, 4005-4011.
- 8) M. Aviles, J. Gines, J. Del Rio, J. Pascual, J. Perez-Rodriguez and P. Sanchez-Soto, *J. Therm. Anal. Calorim.*, 2002, **67**, 177-188.

Chapter 4

Results and discussion

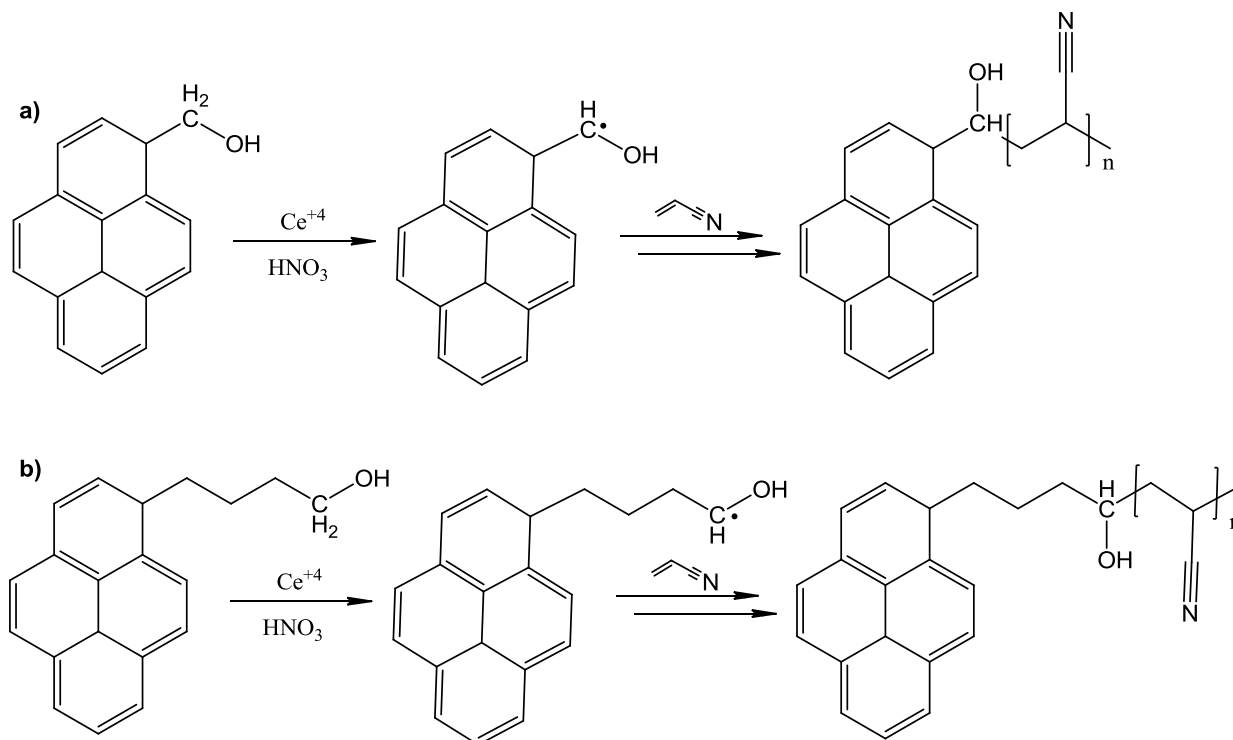
This chapter reports on the synthesis of both mono α -chain-end functional PAN and multi-functional PAN based copolymers of pyrene functionality. The extent of the association between MWCNTs and the pyrene functional polymers is investigated regarding the noncovalent π - π stacking interaction between the MWCNT surfaces and the pyrene moieties. Interactions are investigated by TGA, $^1\text{H-NMR}$, and UV-fluorescence analysis after which the functional polymers are used as a dispersing agent for MWCNTs in a PAN matrix. MWCNT/PAN fibrous nanocomposites are finally produced by electrospinning from the PAN solution with noncovalently functionalized pristine MWCNTs and an investigation of nanocomposite nonofibers is achieved by SEM and TEM imaging. Preliminary results on graphene nanofiber composites are given as well as preliminary results on the carbonization of the nanofiber precursors to produce carbon nanofibers, with pristine MWCNTs.

4.1 Synthesis of py-PAN via a cerium initiated redox system

The use of an oxidizing agent such as ceric ammonium nitrate (CAN) in a redox activated polymerization system possesses various appealing attributes. Such properties include the high solubility in organic solvents, allowing for the use of low cost, easily obtainable and environmentally friendly reaction mediums. The fast reaction rate of these redox systems also allows for short reaction times desired in cases of tedious polymer synthesis. Undemanding reaction conditions allow for polymerization at moderate temperatures resulting in low synthetic costs, additionally reducing the probability of undesired side reactions. An advantage of the simplistic nature of the redox activated system allows for initiation from readily available molecules, acting as reducing agents and includes alcohols, ketones, aldehydes, amides, thiols and acids.^{1,2}

The characteristic properties of the aforementioned synthesis make a compelling argument for the use of this technique in the polymerization of the desired polymer. This technique was accordingly chosen as the initial method to produce the pyrene chain-end functional polyacrylonitrile (PAN).

The method of Köken *et al.*² as well as Ma *et al.*³ was consulted and served as a guide-line to the systematic study that was conducted in an effort to produce a viable synthetic procedure for the production of pyrene α -chain-end functional PAN. The effect of the reaction matrix, temperature, catalytic concentration, reducing agent (initiating specie) as well as acidic concentration of the stock solution, containing the Ce(IV)/HNO₃ redox couple, was investigated. A schematic representation of the general reaction is presented below.



Scheme 4.1: The synthesis of py-PAN polymers by the redox initiated, Ce(IV) catalyzed polymerization from (a) 1-pyrenemethanol and (b) 1-pyrenebutanol initiators respectively.

Due to a variation in solvent preference for the reagents present in the reaction, a solvent study was undertaken in order to find a reaction medium suitable for the complete system. The produced yields were observed using various solvents, tested under similar reaction conditions regarding reaction time, temperature, monomer quantity, and catalytic solution. Systems of water, methanol, DMF, DMSO, THF and chloroform were tested and individually presented in Table 4.1. The indicated dilutions were made up with water.

Table 4.1: Solvent dependent study on yields produced by redox system.

| Reaction number | Initiator | Solution matrix | Yield obtained | Temperature of reaction (°C) | Reaction time (h) | Molar ratio of initiator to ceric ion | Molar ratio of initiator to monomer |
|-----------------|-----------------|------------------|----------------|------------------------------|-------------------|---------------------------------------|-------------------------------------|
| 1 | Pyrene methanol | THF | 0.84% | 45 | 1 | 1:1 | 1:305 |
| 2 | Pyrene methanol | DMSO | 0.90% | 45 | 1 | 1:1 | 1:305 |
| 3 | Pyrene methanol | Chloroform | 0.95% | 45 | 1 | 1:1 | 1:305 |
| 4 | Pyrene methanol | Methanol | 0.64% | 45 | 1 | 1:1 | 1:305 |
| 5 | Pyrene methanol | 25% Methanol | 1.22% | 45 | 1 | 1:1 | 1:305 |
| 6 | Pyrene methanol | 50% Methanol | 1.06% | 45 | 1 | 1:1 | 1:305 |
| 7 | Pyrene methanol | 75% Methanol | 1.22% | 45 | 1 | 1:1 | 1:305 |
| 8 | Pyrene methanol | DMF | 1.48% | 45 | 1 | 1:1 | 1:305 |
| 9 | Pyrene methanol | 10% DMF | 1.15% | 45 | 1 | 1:1 | 1:305 |
| 10 | Pyrene methanol | 25% DMF | 1.20% | 45 | 1 | 1:1 | 1:305 |
| 11 | Pyrene methanol | 50% DMF | 1.19% | 45 | 1 | 1:1 | 1:305 |
| 12 | Pyrene methanol | H ₂ O | 1.29% | 45 | 1 | 1:1 | 1:305 |
| 13 | Pyrene methanol | H ₂ O | 2.04 % | 45 | 1 | 1:1 | 1: 157 |
| 14 | Pyrene methanol | DMF | 1.43% | 55 | 1 | 1:1 | 1:305 |
| 15 | Pyrene methanol | H ₂ O | 2.03% | 55 | 1 | 1:1 | 1:305 |

The low yields obtained indicate that no system would support the solvation of the entire range of reagents simultaneously. The solvation of the catalytic CAN is lost with the change

in matrix from water to solvents supporting initiator solvation, such as methanol, chloroform and DMF. Solvents producing the greatest yields were found to be a 100% H₂O or DMF matrix respectively. A water matrix supports the catalytic solvation, but is not a suitable solvent for the initiator, leading to an in-homogeneous dispersion of the initiator species. Using a DMF solvent on the other hand leads to the homogeneous dispersion of the initiator specie but not the catalytic ceric(IV) ions to initiate polymerization by the single electron redox system. Two reactions at a slightly higher temperature (55 °C) were run in parallel and comprised of a water and DMF matrix respectively (reactions 18 & 19). At this elevated temperature water proved the superior matrix and this precipitation reaction method was undertaken in further optimization of the method. When comparing similar reactions but altering the monomer composition (reactions 12 & 13), it is observed that at lower monomer composition a higher yield was evident, indicating incomplete monomer conversion, at slightly lower yields than produced by Köken *et al.*² in the synthesis of acrylonitrile-block-poly(dimethylsiloxane) copolymers at a runtime of 1.5 hours. Following the solvent dependent study, an investigation into the temperature dependence of the reaction was undertaken and results thereof are presented in Table 4.2.

Table 4.2: Temperature dependent study on yields produced by redox system.

| Reaction number | Initiator | Solution matrix | Yield obtained | Temperature of reaction (°C) | Reaction time (h) | Molar ratio of initiator to ceric ion | Molar ratio of initiator to monomer |
|-----------------|-----------------|------------------|----------------|------------------------------|-------------------|---------------------------------------|-------------------------------------|
| 16 ^a | Pyrene methanol | H ₂ O | 12.15% | 20 | 24 | 1:7.5 | 1:305 |
| 17 | Pyrene methanol | H ₂ O | 6.09% | 45 | 24 | 1:7.5 | 1:305 |
| 18 | Pyrene methanol | H ₂ O | 4,96% | 55 | 24 | 1:7.5 | 1:305 |
| 19 | Pyrene methanol | H ₂ O | 7.24% | 65 | 24 | 1:7.5 | 1:305 |

^a 32 300 g/mol, \bar{M}_n 1.40 (as obtained from SEC analysis)

At an increased catalyst concentration to a monomer ratio of 1:7.5 (initiator to ceric ion) an overall increased yield is observed under similar reaction conditions. At these conditions and a runtime of 24 hours the temperature dependent study indicates optimum yield at mild reaction temperatures of 20°C as supported in literature.¹⁻³ The relative molecular weight produced from this reaction is estimated by SEC, calibrated to PMMA standards, to be

32 400 g/mol with a polymer dispersity of 1.40. In accordance to the study an investigation into the reaction time was undertaken and presented in Table 4.3.

Table 4.3: Time dependent study on yields produced by redox system.

| Reaction number | Initiator | Solution matrix | Yield obtained | Temperature of reaction (°C) | Reaction time (h) | Molar ratio of initiator to ceric ion | Molar ratio of initiator to monomer |
|-----------------|-----------------|------------------|----------------|------------------------------|-------------------|---------------------------------------|-------------------------------------|
| 20 | Pyrene methanol | H ₂ O | 5.82% | 20 | 1 | 1:20 | 1:279 |
| 21 | Pyrene methanol | H ₂ O | 8.01% | 20 | 4 | 1:20 | 1:279 |
| 22 ^a | Pyrene methanol | H ₂ O | 20.84% | 20 | 6 | 1:20 | 1:279 |

^a 43 800 g/mol, \bar{D} 1.63 (as obtained from SEC analysis)

An increased yield is observed as the CAN concentration is further increased to a 1:20 molar ratio of initiator to ceric ion. The time dependent study portrayed in Table 4.3 indicates full conversion not being attainable even after 6 hours of runtime. These results presented are in contrast to those reported by Köken *et al.*² who stated yields of 60 % being achievable under similar conditions when producing high molecular weight PAN-block-PDMS copolymers. The molecular weight obtained from the highest yielding reaction is seen to have a greater molecular weight than mentioned in the temperature study. At an increased catalytic concentration, an increased molecular weight as well as polymer dispersity is seen at a quarter of the reaction time. Further investigation into the effect of the concentration of the catalytic solution is represented in Table 4.4.

Table 4.4: Quantitative catalyst dependent study on yields produced by redox system.

| Reaction number | Initiator | Solution matrix | Yield obtained | Temperature of reaction (°C) | Reaction time | Molar ratio of initiator to ceric ion | Molar ratio of initiator to monomer |
|-----------------|-----------------|------------------|----------------|------------------------------|---------------|---------------------------------------|-------------------------------------|
| 23 | Pyrene methanol | H ₂ O | 0.49 % | 25 | 1 | 1:1 | 1:279 |
| 24 | Pyrene methanol | H ₂ O | 3.49 % | 25 | 1 | 1:7.5 | 1:279 |
| 25 | Pyrene methanol | H ₂ O | 4.71 % | 25 | 1 | 1:20 | 1:279 |
| 26 | Pyrene methanol | H ₂ O | 5.94 % | 25 | 1 | 1:30 | 1:279 |
| 27 | Pyrene methanol | H ₂ O | 2.04 % | 45 | 1 | 1:1 | 1: 157 |
| 28 ^a | Pyrene methanol | H ₂ O | 12.15 % | 20 | 24 | 1:7.5 | 1:305 |
| 29 ^b | Pyrene methanol | H ₂ O | 20.84 % | 20 | 6 | 1:20 | 1:279 |
| 30 ^c | Pyrene methanol | H ₂ O | 43.33 % | 20 | 24 | 1:25 | 1:35 |
| 31 ^d | Pyrene methanol | H ₂ O | 46.52 % | 20 | 24 | 1:30 | 1:42 |
| 32 ^e | Pyrene methanol | H ₂ O | 82.25 % | 25 | 24 | 1:25 | 1:42 |

^a Same as reaction 16 (32 300 g/mol, \bar{M}_n 1.40), ^b same as reaction 22 (43 800 g/mol, \bar{M}_n 1.63),
^c 1 600 g/mol, \bar{M}_n 1.07, ^d 1 500 g/mol, \bar{M}_n 1.08, ^e 1 500 g/mol, \bar{M}_n 1.08

An increase in yield is observed in comparison to similar reactions of mild reaction temperatures and reaction time of 1 hour, when the initiator: Ce(IV) molar ratio is increased from 1:1 to 1:7.5 and further increased to 1:20, 1:25 and finally 1:30. When comparing reactions 31 and 32 it seems at mild reaction conditions of 20°C to 25°C high yields are achievable at high concentrations of catalytic solutions (1:25 to 1:30). At the low initiator:monomer ratios of reactions 30 to 32, low molecular weights are obtained at low polymer dispersities, although high yields are obtained. Finally an investigation is undertaken to establish if the further isolation of the pyrene moiety might lead to a greater yield. This is achieved by using an alternate initiating specie of which the pyrene

functionality is shifted further from the active polymerization site by three carbon atoms. The resulting data is presented in Table 4.5.

Table 4.5: Initiator study using pyrene butanol initiator.

| Reaction number | Initiator | Solution matrix | Yield obtained | Temperature of reaction (°C) | Reaction time (h) | Molar ratio of initiator to ceric ion | Molar ratio of initiator to monomer |
|-----------------|----------------|------------------|----------------|------------------------------|-------------------|---------------------------------------|-------------------------------------|
| 33 | Pyrene butanol | H ₂ O | 1.50% | 45 | 24 | 1:1 | 1:359 |
| 34 | Pyrene butanol | H ₂ O | 0.97% | 45 | 1 | 1:1 | 1:359 |
| 35 | Pyrene butanol | H ₂ O | 0.35% | 20 | 1 | 1:1 | 1:279 |
| 36 | Pyrene butanol | H ₂ O | 1.82% | 20 | 1 | 1:7.5 | 1:279 |
| 37 | Pyrene butanol | H ₂ O | 4.80% | 20 | 1 | 1:20 | 1:279 |

In order to investigate the possible influence that the pyrene functionality might have on the initiator reactivity, an increased molecular spacing was effectively incorporated, separating the reactive hydroxyl group from the functional group. This was done by making use of an alternate 1-pyrenebutanol initiator. The molecule differs from 1-pyrenemethanol based on an extension of a 3 carbon atom spacing separating the reactive site from the functional moiety.

The study, however, showed very similar results as that presented by the pyrene methanol initiated reactions. Reactions 33 and 34 indicate the incomplete conversion at 1 hour and reactions 35 to 37 show an increase in yield being observed at increased CAN concentrations. Overall, however, yields do not seem to vary considerably when comparing the results presented by the pyrene methanol to butanol based initiators. These results suggests that the reactivity may not be the problem, but rather the insolubility of the initiator being the major contributing factor which results in inhomogeneously dispersed reactants in the solvent matrix.

Following the unsatisfactory yields produced from ample variations in reaction conditions, proving the reliability of such a cerium initiated redox system felt necessary. In doing so, the quality of the data produced regarding the yields obtained from each experimental run is assured. For this reason the CAN catalyzed, redox initiated polymerization from a simple

linear alcohol was undertaken. The success of these polymerizations is based on the yields obtained from similar experimental variations as presented during the study into the polymerization system to this point.

Table 4.6: Study of general catalytic system study, using simple linear aliphatic alcohol initiator.^a

| Reaction number | Initiator | Yield obtained | Molecular weight (g/mol) | Polymer dispersity (\bar{D}) | Temperature of reaction (°C) | Molar ratio of initiator to ceric ion | Molar ratio of initiator to monomer |
|-----------------|-----------|----------------|--------------------------|----------------------------------|------------------------------|---------------------------------------|-------------------------------------|
| 38 | Hexanol | 21.97% | 191 300 | 1.61 | 20 | 1:1 | 1:279 |
| 39 | Hexanol | 38.26% | 155 900 | 1.87 | 20 | 1:7.5 | 1:279 |
| 40 | Hexanol | 53.39% | 176 600 | 1.70 | 20 | 1:20 | 1:279 |
| 41 | Hexanol | 65.83% | 127 700 | 1.88 | 35 | 1:7.5 | 1:279 |
| 42 | Hexanol | 84.09% | 190 700 | 1.57 | 55 | 1:7.5 | 1:279 |

^a All reactions are run at a 1 hour reaction time in H₂O reaction medium

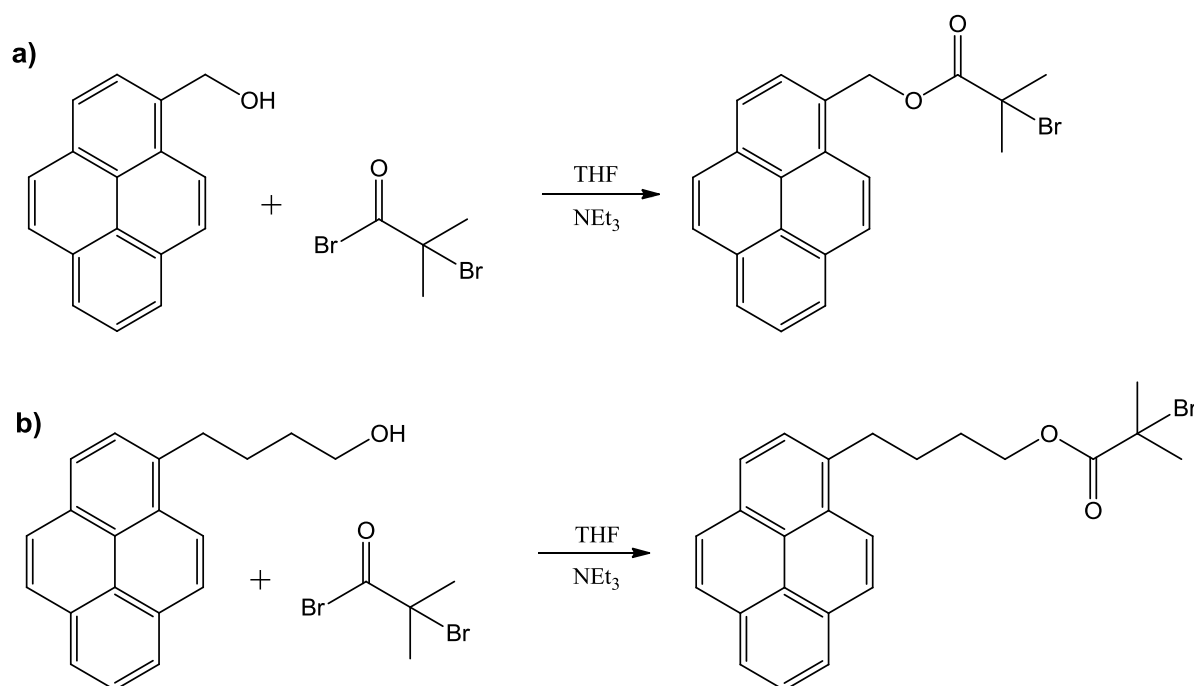
Reaction runs using simple linear aliphatic hydroxyl terminal hydrocarbons show satisfactory conversions at 1 hour, however, it indicated similar trends as observed by the pyrene based initiators. The yields obtained seem to increase with increasing catalytic CAN concentration and increasing temperature. High molecular weights are obtained for all the presented reactions, with no clear specific trend in the Mn or \bar{D} values. The results support the reliability of the previous data as the lower yields obtained by the hydroxyl functional pyrene initiator cannot be the result of improper methodology. This, however, renders the use of this method of redox initiated polymerization redundant for the synthesis of pyrene chain-end functional PAN in large yields. The major appealing features of this technique are the radical production occurring at reasonable rates, allowing for polymerization at mild temperatures achievable in a short period of time. However, this is not the case with the use of the 1-pyrenemethanol and 1-pyrenebutanol initiators. Further investigation into the production of chain-end functional PAN by the redox system was halted and alternate methods were explored to produce the pyrene functional polymer.

4.2 Synthesis of mono pyrene chain-end functional PAN via ATRP synthesis

The previously discussed redox initiated system might be theoretically superior regarding aspects such as reaction runtime, required input energy or heat and ease of reaction based on a simplistic one-step method. The redox system was, however, abandoned as sufficient amounts of polymer production proved problematic. ATRP is an extensively documented method of controlled polymer synthesis and widely used in the production of homopolymers as well as several variations of copolymers including multiple architectures thereof.⁴ Even though ATRP synthesis mostly requires the initial preparation of the appropriate initiator, the produced polymer is of high quality and low polymer dispersity is produced by this well-documented synthetic method.

4.2.1 Synthesis of 1-pyrenemethyl-2-bromoisobutyrate and 1-pyrenebutyl-2-bromoisobutyrate ATRP initiators

The synthesis of pyrene functional initiators is achieved using an altered method of that presented by Oh and Matyjaszewski⁵ as well as Semsarzadeh and Abdollahi.⁶ A yield of 94% was achieved for the 1-pyrenemethyl-2-bromoisobutyrate and 96% for the 1-pyrenebutyl-2-bromoisobutyrate individual initiators. An illustration of these reactions to produce the ATRP initiators is presented in Scheme 4.2 below.



Scheme 4.2: Synthesis of (a) 1-pyrenemethyl-2-bromoisobutyrate and (b) 1-pyrenebutyl-2-bromoisobutyrate ATRP initiators from 1-pyrenemethanol and 1-pyrenebutanol reagents respectively.

Formation of the appropriate products is verified by $^1\text{H-NMR}$ spectroscopy of both the 1-pyrenemethanol and 1-pyrenebutanol reagents as well as the resultant products. The $^1\text{H-NMR}$ spectra of both 1-pyrenemethanol and the resulting 1-pyrenemethyl-2-bromoisobutyrate are presented in Figure 4.1. A spectrum of the alternate 1-pyrenebutanol and produced 1-pyrenebutyl-2-bromoisobutyrate is presented in Figure 4.2.

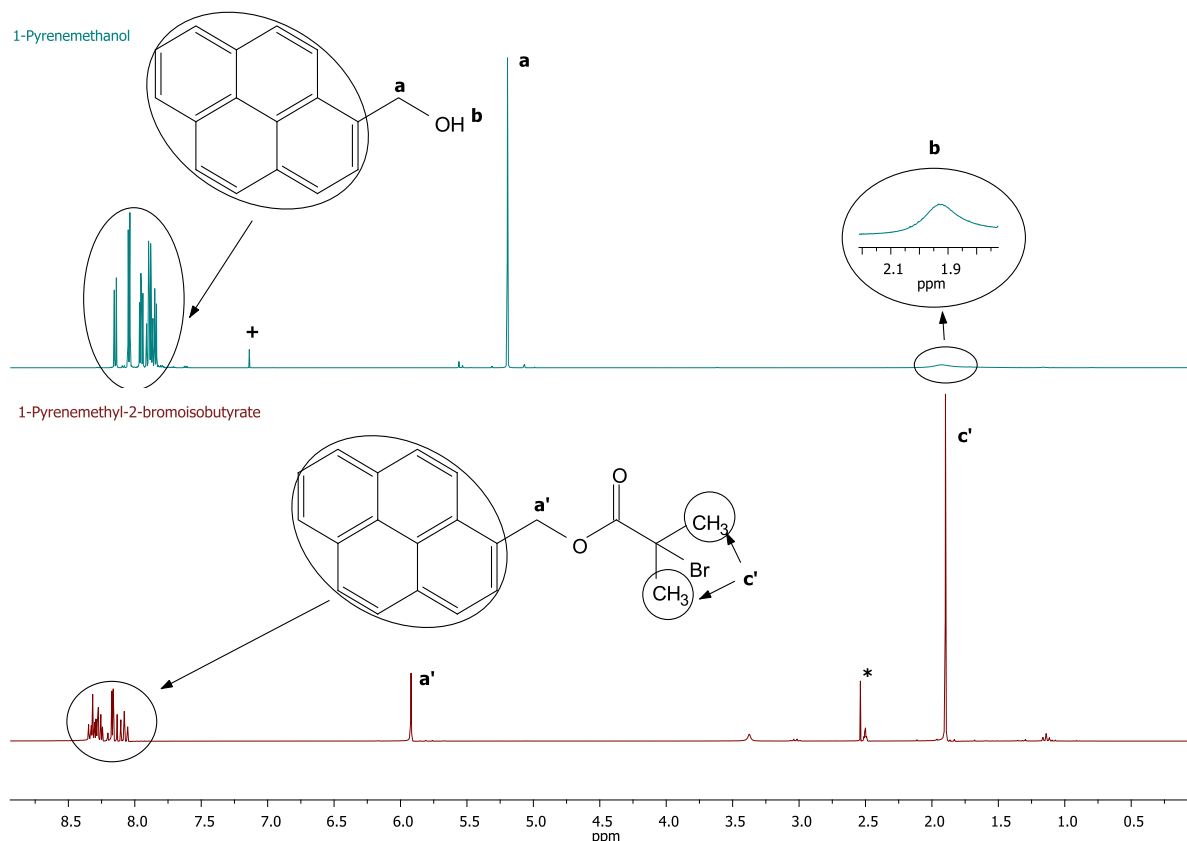


Figure 4.1: $^1\text{H-NMR}$ spectra of 1-pyrenemethanol (in CDCl_3 , "+"") and resultant 1-pyrenemethyl-2-bromoisobutyrate (in DMSO-d_6 , "*"") after esterification to form the ATRP macroinitiator.

In the $^1\text{H-NMR}$ for the commercially obtained 1-pyrenemethanol, a multiplet representing the pyrene moiety can be seen at a chemical shift of 7.83 ppm to 8.16 ppm. Moving upfield, a singlet can be observed at a chemical shift of 5.20 ppm representing the two alkane protons ($-\text{CH}_2-$) and further up at 2.93 ppm a broad peak is shown, which is indicative of an exchangeable hydroxyl proton.

When analyzing the $^1\text{H-NMR}$ spectra of the bromoisobutyrate end-capped ATRP initiator, the presence of the pyrene representing multiplet is carried over to a slightly downfield shifted chemical shift of 8.04 ppm to 8.36 ppm. The $-\text{CH}_2-$ protons are, compared to that of the 1-pyrenemethanol, shifted to a more deshielded chemical shift of 5.92 ppm resulting from the neighboring oxygen becoming less electron rich upon esterification. Further downfield, another singlet is observed, consistent to what is to be expected from the introduced terminal methyl protons at a chemical shift of 1.90 ppm. The exchangeable peak

at 1.93 ppm is seen to disappear upon esterification, indicating the extraction of all unreacted reagents and a high purity of the obtained product. Peak integration confirm signal intensity to be consistent with proton quantity by presenting the ratio of peak intensities of pyrene moiety/-CH₂-CH₃ to be approximately 9/2/6.

The effect of the increased atomic spacing of three additional carbons between the initiating site and the functional pyrene moiety is investigated, as was done for the mono-functional PAN synthesis by the initially investigated redox system. This investigation requires the synthesis of a butane spaced ATRP initiator by esterification from the 1-pyrenebutanol reagent. Using an identical synthetic route as that explained to form 1-pyrenemethyl-2-bromoisobutyrate, the 1-pyrenebutyl-2-bromoisobutyrate alternate was formed at similar yields of 96%. Formation of the required product is similarly confirmed from the analysis by ¹H-NMR spectroscopy.

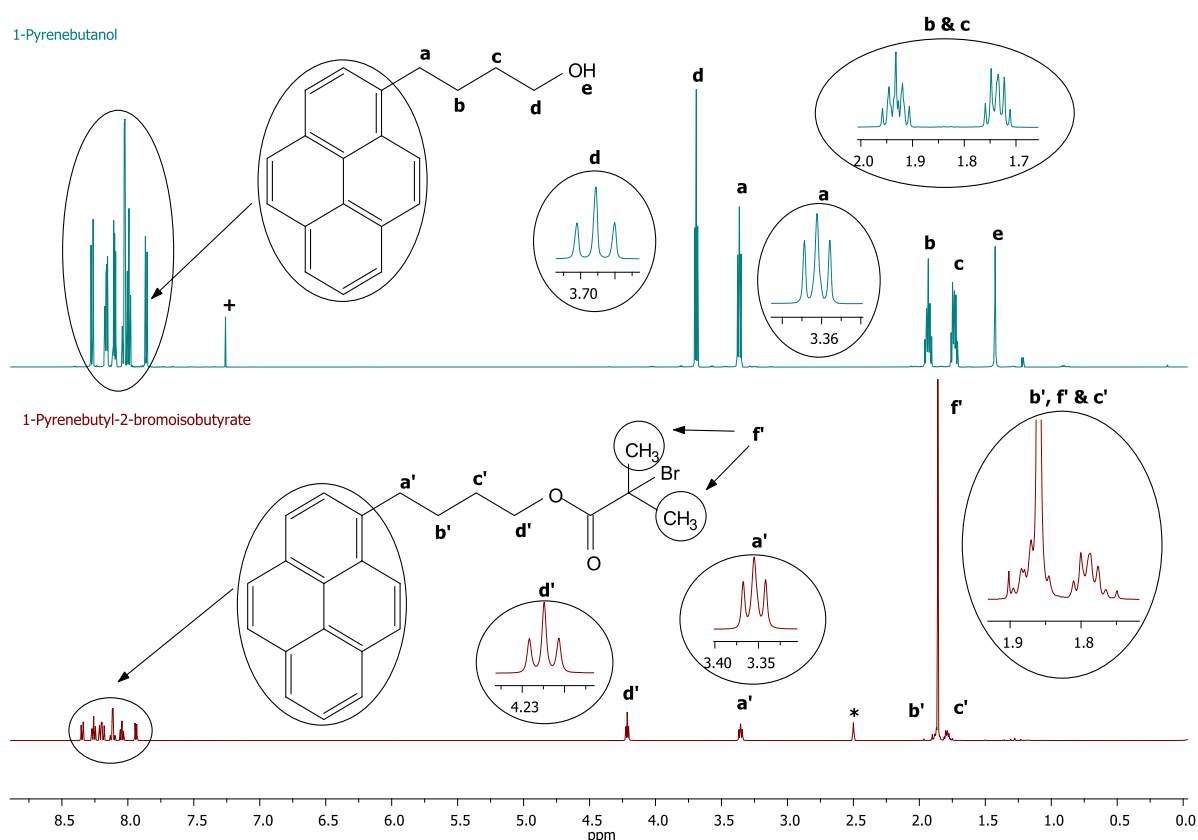


Figure 4.2: ¹H-NMR spectra of both 1-pyrenebutanol (in CDCl₃, "+") and resultant 1-pyrenebutyl-2-bromoisobutyrate (in DMSO-d₆, "**") after esterification to form the ATRP macroinitiator.

Similarly to the initially synthesized 1-pyrenemethyl-2-bromoisobutyrate initiator, the commercially available precursor, in this case 1-pyrenebutanol, was analyzed concurrently with the 1-pyrenebutyl-2-bromoisobutyrate product for comparative purposes. The ¹H-NMR spectrum of 1-pyrenebutanol indicates the presence of the pyrene moiety by the appearance of the multiplet peaks at a chemical shift of 7.84 ppm to 8.30 ppm. The alkane

protons (-CH₂-) labeled “d” and “a” are represented by respective triplets present at chemical shifts of 3.69 ppm and 3.37 ppm. Alkane protons (-CH₂-) labeled “b” and “c” are represented by slightly distorted quintets at positions 1.91 ppm and 1.71 ppm respectively. Signals “a” and “c” appear in a slightly shielded position relative to similar protons “d” and “b” due to a longer range coupling to the electronegative oxygen moiety. At a chemical shift of 1.43 ppm a final signal is present indicating the hydroxyl bearing proton. Integrational analysis confirms peak assignment by presenting a quantitative signal ratio of aromatic-multiplet/(-CH₂-)/-OH being approximately 9/2/1.

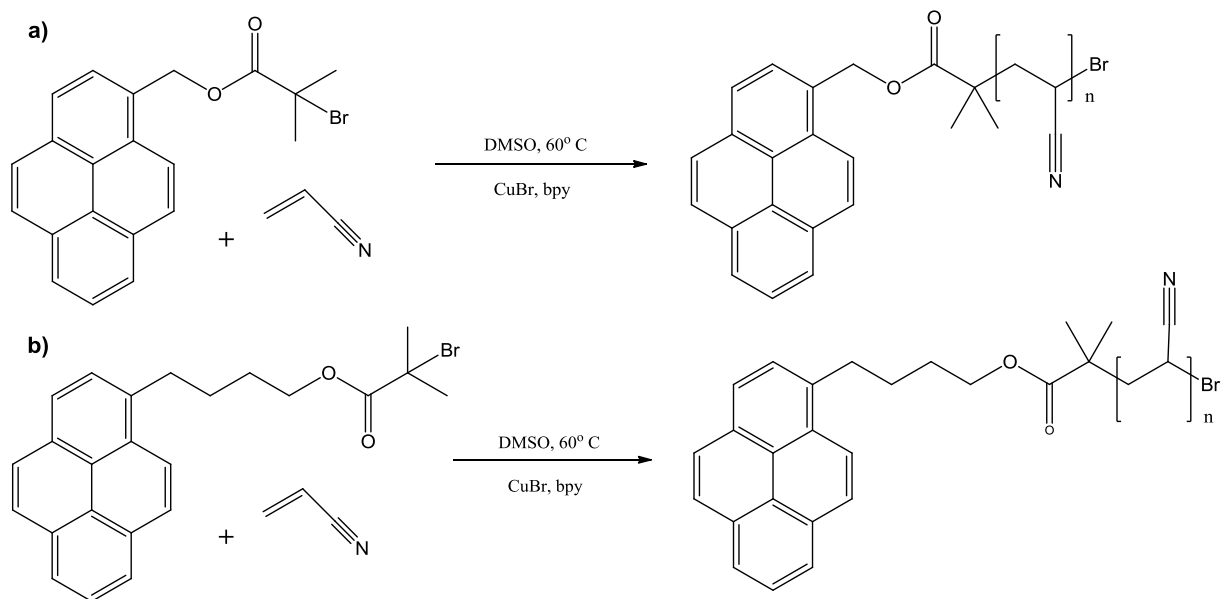
¹H-NMR analysis on the produced ATRP initiator indicates that the pyrene moiety is carried over from the 1-pyrenebutanol precursor and is presented at a chemical shift of 7.92 ppm to 8.36 ppm. Compared to the precursor peaks the multiplet is barely altered resulting from long range coupling of the introduced halogenated functionality having very little magnetic influence on the conjugated system, in contrast to what is observed for the methanol based initiator. The shift in the pyrene representing multiplets are seen to be shifted downfield by approximately 0.20 ppm in the case of the methyl spaced ATRP initiator compared to a shift by approximately 0.01 ppm observed for the butyl spaced initiator. Alkene protons labeled “d’ ” and “ a’ ” are represented as triplet peaks at 4.21 ppm and 3.36 ppm respectively The peak configuration is a result of direct influences from the two neighboring protons “ c’ ” and “ b’ ” across two bonds (by ²J splitting). The protons represented by label “ d’ ” are in a more desheilded state than “ a’ “, resulting from being bonded to an oxygen group. The two protons represented by “ d’ ” are therefore even more shifted downfield from its chemical shift in the precursor state, resulting from the highly electronegative ester incorporation. At chemical shifts of 1.87 ppm and 1.80 ppm the alkane protons labeled “ b’ ” and “ c’ ” are represented by slightly distorted quintets, resulting from primary (²J) coupling of 4 protons and the slight influence of long range (³J) coupling. The peak representing protons “ c’ ” is presented at the more desheilded position (compared to “c”) as a result of the ester based end-group. Positioned in between these quintets presenting slight overlapping with the signal representing protons “ b’ ” at a chemical shift of 1.86 ppm, an intense singlet is observed representing all 6 protons present on the terminal methyl groups. The hydroxyl peak is seen to disappear from the spectrum representing the formation of the produced initiator as esterification commences via the removal of this proton, indicating good conversion. Peak assignments are once again confirmed by integrational analysis presenting relative peak intensities of pyrene-multiplet/-CH₂-/-CH₃ showing an expected ratio of approximately 9/2/6.

In short, the synthesis of both initiators progressed without complications with both producing high yields of clean product. These macroinitiators can be used as suitable ATRP initiators to form the required mono pyrene chain-end (α) functional PAN polymer.

4.2.2 Synthesis of py-PAN

The controlled method of ATRP polymer synthesis was applied from the presynthesized ATRP pyrene macroinitiators to produce α -chain-end functional PAN of various molecular weights and low degrees of polymer dispersity (\mathcal{D}). The initiators were derived from both 1-pyrenemethanol and 1-pyrenebutanol starting reagents respectively (see Scheme 4.2). Esterification of both reagents with α -bromoisobutyryl bromide resulted in the formation of two appropriate ATRP macroinitiators. These being 1-pyrenemethyl-2-bromoisobutyrate and 1-pyrenebutyl-2-bromoisobutyrate respectively. The polymerization efficiency of the synthesized initiators were compared in order to estimate the possible influence of the pyrene moiety on the reactivity by methods such as delocalization by the conjugated ring structure.

Simple ATRP was used targeting three variations in molecular weight of 5 300 g/mol, 3 000 g/mol and 12 000 g/mol respectively. The variations in molecular weights were achieved by variation of solvent and AN monomer composition whilst maintaining a monomer to solvent concentration of 8.56 M and Initiator/CuBr/Bpy molar ratio of 1/1/3. A schematic representation of the polymerization mechanism is presented in Scheme 4.3 below.



Scheme 4.3: Synthesis of py-PAN polymers from (a) 1-pyrenemethyl-2-bromoisobutyrate and (b) 1-pyrenebutyl-2-bromoisobutyrate ATRP initiators.

$^1\text{H-NMR}$ spectroscopy was used to analyze all of the polymers as synthesized from the two variations in ATRP initiators. The analysis was done to confirm the formation of the mono-functional polymer as well as estimate the average mol% functionality of the chains based on the pyrene moiety incorporated relative to the monomeric units of a single chain. From this data the molecular weights could also be estimated. Spectra of both the 1-pyrenemethyl-2-bromoisobutyrate and 1-pyrenebutyl-2-bromoisobutyrate initiated PAN polymers are presented in Figures 4.3 and 4.4 respectively.

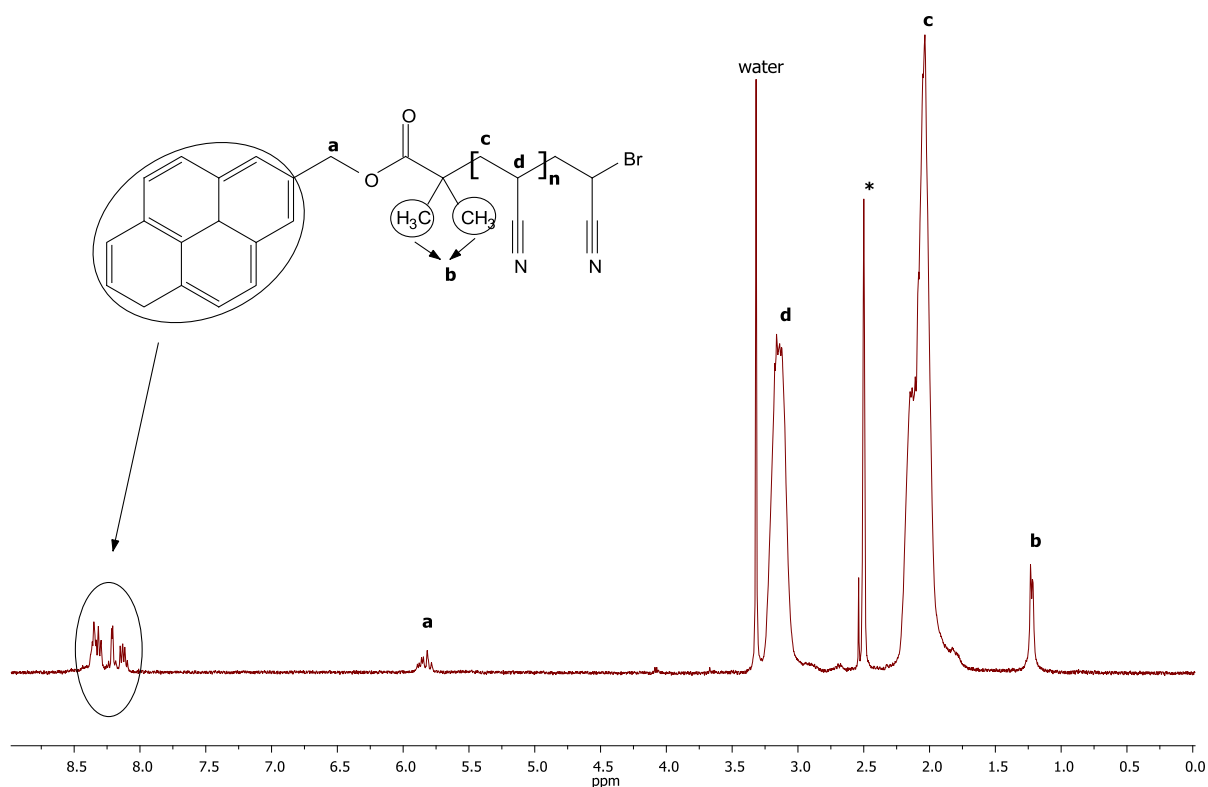


Figure 4.3: $^1\text{H-NMR}$ spectra of py-PAN'2 (1.09 mol% functionality) as synthesized from 1-pyrenemethyl-2-bromoisobutyrate ATRP macroinitiator.

$^1\text{H-NMR}$ analysis of the produced mono pyrene functional PAN indicates the maintenance of peaks associated with the 1-pyrenemethyl-2-bromoisobutyrate initiator (Figure 4.3), such as a slightly broadened pyrene representing multiplet (8.06 ppm to 8.46 ppm), aliphatic $-\text{CH}_2-$ protons ('a') moderately shifted by 0.11 ppm to a more shielded position of 5.81 ppm, with great alteration of methyl positioned protons ($-\text{CH}_3$) being shifted by 0.67 ppm to a more shielded position of 1.23 ppm. This is of course as a result of the relocation of the electronegative Br specie during polymerization. The presence of the broad peaks at positions 3.16 ppm and 2.04 ppm represents the two chemically and magnetically inequivalent proton positions along the AN polymeric chain as presented in Figure 4.3. Water signals in $^1\text{H-NMR}$ spectra (seen at 3.30 ppm)⁷ produced for DMSO solvated samples are commonly seen due to the hygroscopic nature of DMSO.^{8,9} The $^1\text{H-NMR}$ spectra in effect confirms the formation of the hypothesized functional polymer. Similar conformational analysis by $^1\text{H-NMR}$ was done on the functional polymer produced from the 1-pyrenebutyl-2-bromoisobutyrate initiator (Figure 4.4). As in the aforementioned analysis, signals representing the functional initiator are carried over to the spectra representing the produced functional polymer. Slightly broadened proton signals are observed for both the pyrene functionality (7.91 ppm to 8.38 ppm) as well as the aliphatic ($-\text{CH}_2-$) protons, "d" (4.10 ppm slightly more deshielded from 4.21) and "a" (3.36 ppm). The aliphatic protons labeled "b"

and “c” appear to be completely overwhelmed by the aliphatic polymeric proton signal labeled “f” at a chemical shift of 2.92 ppm. The aliphatic protons labeled “b” and “c” seem to experience minimal alteration of magnetic environment from the initiator species, as opposed to the methyl associated proton peaks being shifted by 0.36 ppm to a more shielded position of 1.5 ppm, post polymerization. This is, similar to the previously discussed situation for the alternate mono-functional polymer and is as a result of the replacement of the electronegative halogen with the less electronegative AN segments represented by the broad proton signals at 2.01 ppm and 3.16 ppm.

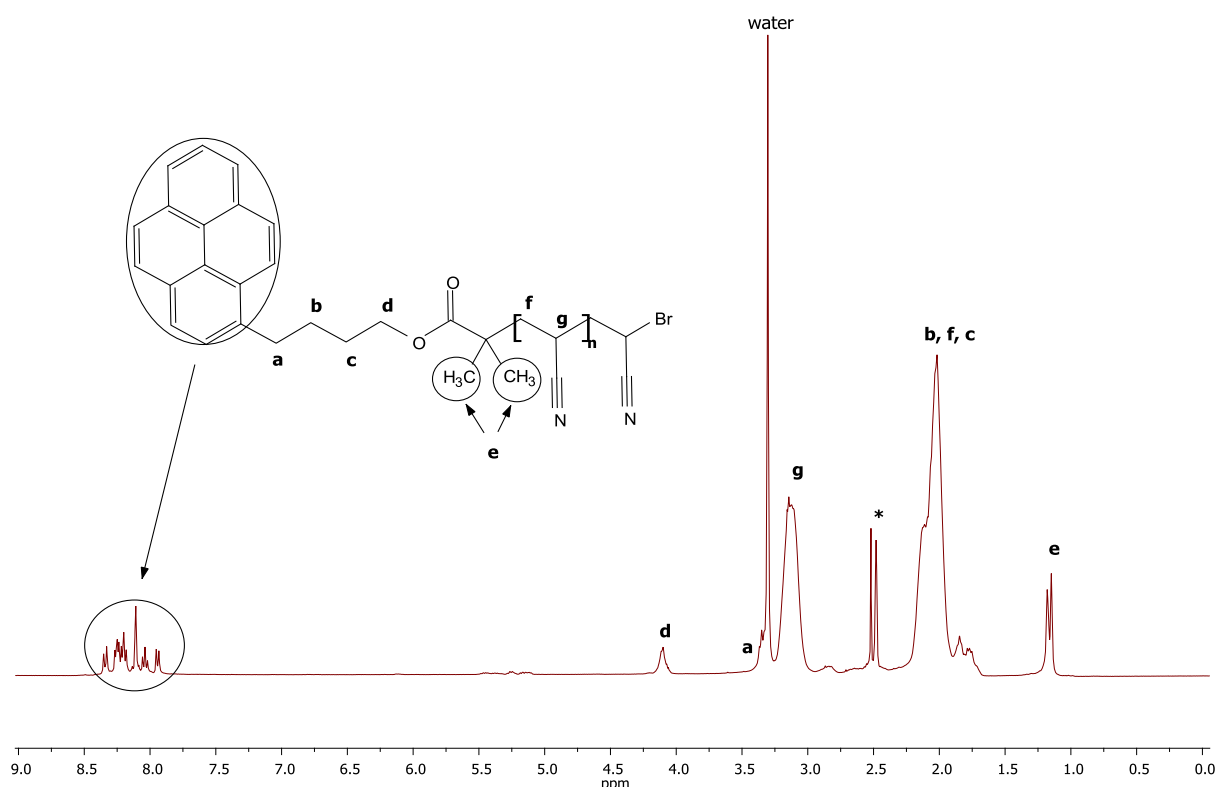


Figure 4.4: ¹H-NMR spectra of py-PAN-5 (3.03 mol% functionality) as synthesized from 1-pyrenebutyl-2-bromoisobutyrate ATRP macroinitiator.

From the ¹H-NMR analysis the average molecular weight can be estimated by the integration of signals produced by protons in the pyrene moiety (observed in the chemical shift region of 7.87 ppm to 8.38 ppm) relative to that of signals representative of protons attached to monomeric substituents of the polymer backbone represented by broad signals at 2.0 ppm for secondary (-CH₂-) and/or at 3.1 ppm for tertiary (>CH-) bonded protons respectively.

To determine the molecular weights of the mono pyrene functional polymers, the integration relative to the tertiary proton was used based on the isolation of this peak in both cases of

mono-functional PAN as produced from both variations of initiator. The molecular weights can be determined by using the following equation:

$$M_n^{NMR} = \frac{(\int \text{Polymeric proton signal})}{(\int \text{Chain end proton signal})/9} \times M_n^{M_0} + M_n^{Initiator} \quad \text{Equation 4.1}$$

M_n^{NMR} represents the molecular weight of the polymer as determined by NMR analysis, $M_n^{M_0}$ the molecular weight of the AN monomer (53.06 g/mol) and $M_n^{Initiator}$ the molecular weight of appropriate ATRP initiators (381.26 g/mol and 423.34 g/mol respectively). $^1\text{H-NMR}$ analysis also allows for the determination of the pyrene functionality based on the quantitative incorporation of pyrene to the PAN polymer. This is expressed as the mol% pyrene functionality of the py-PAN polymers based on the macroinitiator incorporation (bearing a pyrene moiety) relative to the conventional AN monomer present in the produced mono-functional polymers. The mol% pyrene functionality is calculated by equation 4.2 and presented together with the molecular weights, polymer dispersity and obtained yields in Table 4.7

Mol% pyrene functionality

$$= \frac{(\int \text{Chain end proton signal})/9}{[(\int \text{Chain end proton signal})/9 + (\int \text{Polymeric proton signal})]} \times 100$$

Equation 4.2

Table 4.7: Specifications of py- PAN polymers as prepared from 1-pyrenemethyl-2-bromoisobutyrate and 1-pyrenebutyl-2-bromoisobutyrate ATRP macroinitiators.

| | M_n^{Target} | Yield | SEC | | $^1\text{H-NMR}$ | Mol% pyrene functionality |
|-----------------|-----------------------|---------|--------------------|---------------|--------------------|---------------------------------|
| | | | M_n^{SEC} | \mathcal{D} | M_n^{NMR} | |
| Py-PAN·1 | 3 000 g/mol | 14.55% | 2 800 g/mol | 1.32 | 3 000 g/mol | 1.97 |
| Py-PAN·2 | 5 300 g/mol | 36.68% | 26 500 g/mol | 1.27 | 5 200 g/mol | 1.09 |
| Py-PAN·3 | 12 000 g/mol | 28.05% | 29 700 g/mol | 1.48 | 12 800 g/mol | 0.43 |
| Py-PAN·4 | 3 000 g/mol | 18.17% | 2 100 g/mol | 1.13 | 1 100 g/mol | 7.14 |
| Py-PAN·5 | 5 300 g/mol | 19.91 % | 6 200 g/mol | 1.08 | 2 198 g/mol | 2.86 |
| Py-PAN·6 | 12 000 g/mol | 8.88 % | 6 800 g/mol | 1.11 | 2 280 g/mol | 2.78 |

Py-PAN (1 to 3) is synthesized from 1-pyrenemethyl-2-bromoisobutyrate ATRP initiators.

Py-PAN (4 to 6) is synthesized from 1-pyrenebutyl-2-bromoisobutyrate ATRP initiators.

The ATRP synthesis of mono pyrene functional PAN (py-PAN) from 1-pyrenebutyl-2-bromoisobutyrate initiator was a replication of the synthesis from the 1-pyrenemethyl-2-bromoisobutyrate initiator, however, results indicate less than satisfactory molecular weights. The low molecular weight production seems to point to premature termination

reactions. As the sole variable between these two methods of polymerization is the initiator unit, the probability lays in the pyrenebutyl based ATRP initiator leading to the abundance in termination reactions. This initiator carries a pyrene moiety at a position 3 carbon atoms further from the initiating site than that of the pyrenemethyl based initiator. A possible explanation is that the loss in radical stabilization character could result in the termination step accruing more readily for the same reaction conditions that are favored by ATRP from the 1-pyrenemethyl-2-bromoisobutyrate initiator.

SEC in N,N-dimethylacetamide (DMAc) was used to indirectly determine the degree of control achieved by the \bar{D} values produced as well as in the confirmation of pyrene incorporation by the use of a dual detector system of RI and UV (365 nm). Pyrene possesses UV activity at a wavelength of 365 nm which is not the case for PAN. By detection of a UV signal overlapping with that of the RI signal in the produced chromatograms, the incorporation of the pyrene moiety to the polymer chain can be deduced. Figure 4.5 shows the SEC analysis and the detector signals of UV (365 nm) and RI.

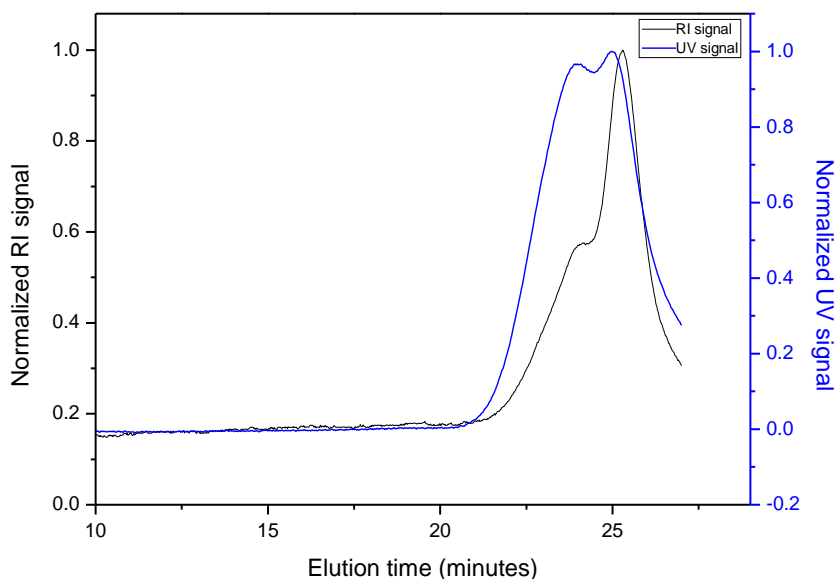


Figure 4.5: Elugram of SEC analysis on py-PAN-2 (1.09mol% functionality) with a dual detection system of RI and UV (365 nm).

From the RI and UV signals represented in the elugram, a clear overlapping is observed which is indicative of the presence of pyrene functionality in the polymer chain.¹⁰ The peaks observed for all of the obtained mono-functional PAN express the same bimodal type distribution (appendix, figures A1 to A5). This suggests a loss in control being experienced during the ATRP reactions when following this specific procedure. An expected loss in

control can be explained by the use of a protic solvent. These solvents have been reported to lead to fast polymerization reactions and results in a loss of control regarding the produced molecular weights.^{11,12} Tsarevsky et al.¹³ supports these reports by work in which the fast polymerization of ATRP in protic solvents are explained as resulting from reversible dissociation and substitution of the halide ligand leading to insufficient deactivation reactions.

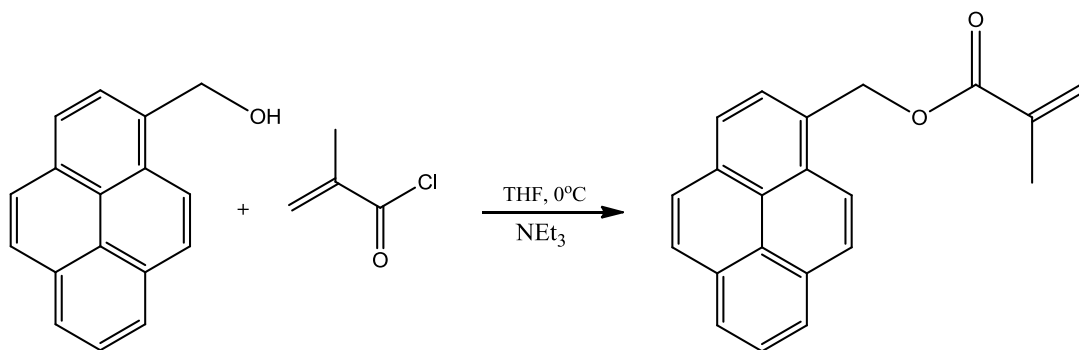
Nevertheless the preparation of mono pyrene functional PAN by functionalization at the α -chain-end proved successful, from presynthesized 1-pyrenemethyl-2-bromoisobutyrate ATRP initiator and to a lesser extent for the 1-pyrenebutyl-2-bromoisobutyrate initiator. Concern, however, has been raised regarding the bimodal distribution observed in elugrams for both signals of overlapping UV and RI detector responses which indicates that the polymers are produced with little control.

4.3 Synthesis of multi pyrene functional PAN via CFR copolymerization

The choice was made to incorporate pyrene functionality into the length of the PAN chain for a more comprehensive study involving multiple pedant groups protruding from the polymer chain. This would theoretically allow for a stacking association more closely to MWCNTs, representing a traditional polymer wrapping interaction when compared to the mono α -chain-end functional polymer counterpart. Conventional free radical (CFR) polymerization was used to synthesize the multi-functional polymers. The synthesis offers less polymerization control, as in the case of a controlled polymerization method such as ATRP, however, offers a robust method of producing high polymer yields at less stringent reaction parameters. The ease of CFR mediated copolymerization produced sufficient motivation for using this method for the production of the required multi pyrene functional PAN. Copolymers were produced from a combination of both conventional acrylonitrile (AN) monomer and a presynthesized, pyrene pendant macromonomer (PyMMP). As this technique progresses in the absence of a catalytic species, the contamination of the copolymer by metal residue is excluded,¹⁰ additionally simplifying the extraction and purification steps of the polymer product.

4.3.1 Synthesis of PyMMP macromonomer

(1-pyrene)methyl-2-methyl-2-propenoate (PyMMP) was successfully synthesized using a synthetic route based on that, presented by Lou *et al.*¹⁰ (Scheme 4.4).



Scheme 4.4: Synthesis of (1-pyrene)methyl-2-methyl-2-propenoate (PyMMP) macromonomer from 1-pyrenemethanol.

A produced yield of 77% was shown to be obtained by gravimetric analysis after the isolation of the macromonomer from the unreacted pyrenemethanol species. The product was analyzed by $^1\text{H-NMR}$ spectroscopy (Figure 4.6) as a means of proving the formation of the hypothesized macromonomer.

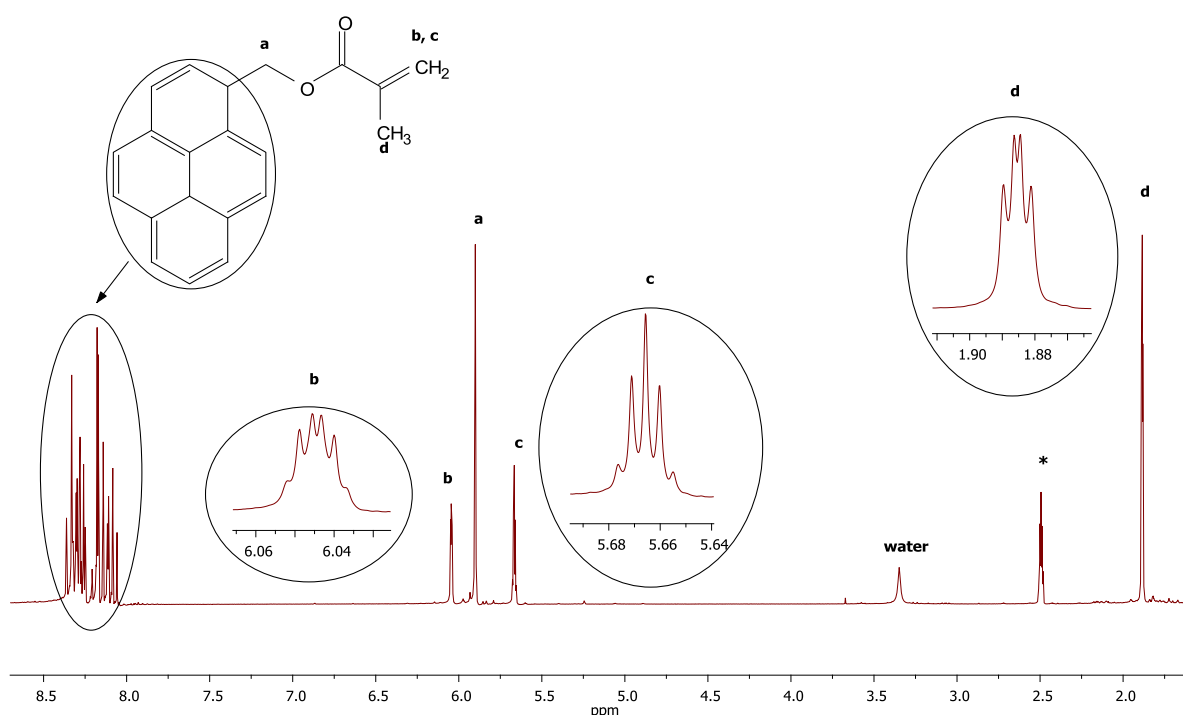


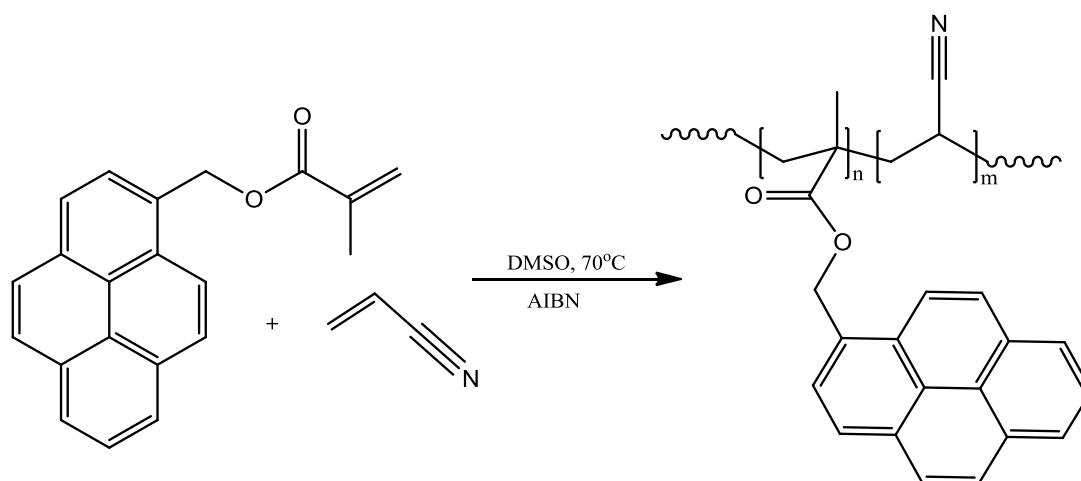
Figure 4.6: $^1\text{H-NMR}$ spectra of produced (1-pyrene)methyl-2-methyl-2-propenoate (PyMMP) to be used as macromonomer in the production of PAN-co-PyMMP polymers.

From the $^1\text{H-NMR}$ spectra it is clear that the expected macromonomer has been successfully synthesized. A multiplet is observed in the chemical shift region of 8.05 ppm to 8.38 ppm which is characteristic of the pyrene functional group. A singlet is observed for the chemically equivalent alkane protons ($-\text{CH}_2-$), represented by label "a" in the $^1\text{H-NMR}$

spectra. The alkene protons ($=\text{CH}_2$) labeled “b” and “c” are immobilized by the π -system of the double bond and is therefore fixed in magnetically inequivalent spaces, producing two different chemical shifts as indicated. The germinal protons, gave rise to separate signals split by influences of protons across two bonds (by ^2J splitting) as well as across 3 bonds (by ^3J splitting). At the chemical shift of 6.05 ppm an overlapping doublet of quartets is observed appearing as a multiplet representing proton ‘b’ and at 5.67 ppm proton ‘c’ is represented by a quintet signal. At the chemical shift of 1.89 ppm the protons labeled “d” is represented by a doublet of doublets resulting from nuclear magnetic proton influences presented by magnetically inequivalent protons “b” and “c”.

4.3.2 Synthesis of PAN-co-PyMMP

Copolymerization was achieved through the simple CFR polymerization of conventional acrylonitrile (AN) monomer and (1-pyrene)methyl-2-methyl-2-propenoate (PyMMP) macromonomer (Scheme 4.5). The production of copolymer bearing pyrene functionality of three compositions was targeted. This was achieved by altering the AN conventional monomer to presynthesized PyMMP macromonomer feed composition to amount to a 0.1 mol%, 1.0 mol% and 2.0 mol% composition of PyMMP macromonomer relative to the total monomer incorporation. The schematic representation of the polymerization is presented below.



Scheme 4.5: Synthesis of PAN-co-PyMMP polymers by copolymerization of acrylonitrile (AN) and (1-pyrene)methyl-2-methyl-2-propenoate (PyMMP) macromonomers using CFR polymerization.

$^1\text{H-NMR}$ analysis was utilized in order to not only confirm the incorporation of the pyrene into the produced copolymer but also to determine the quantity of pyrene incorporated into the copolymer chain. A representation of the spectra produced for the pyrene functional copolymers (PAN-co-PyMMP) is shown in Figure 4.7 below.

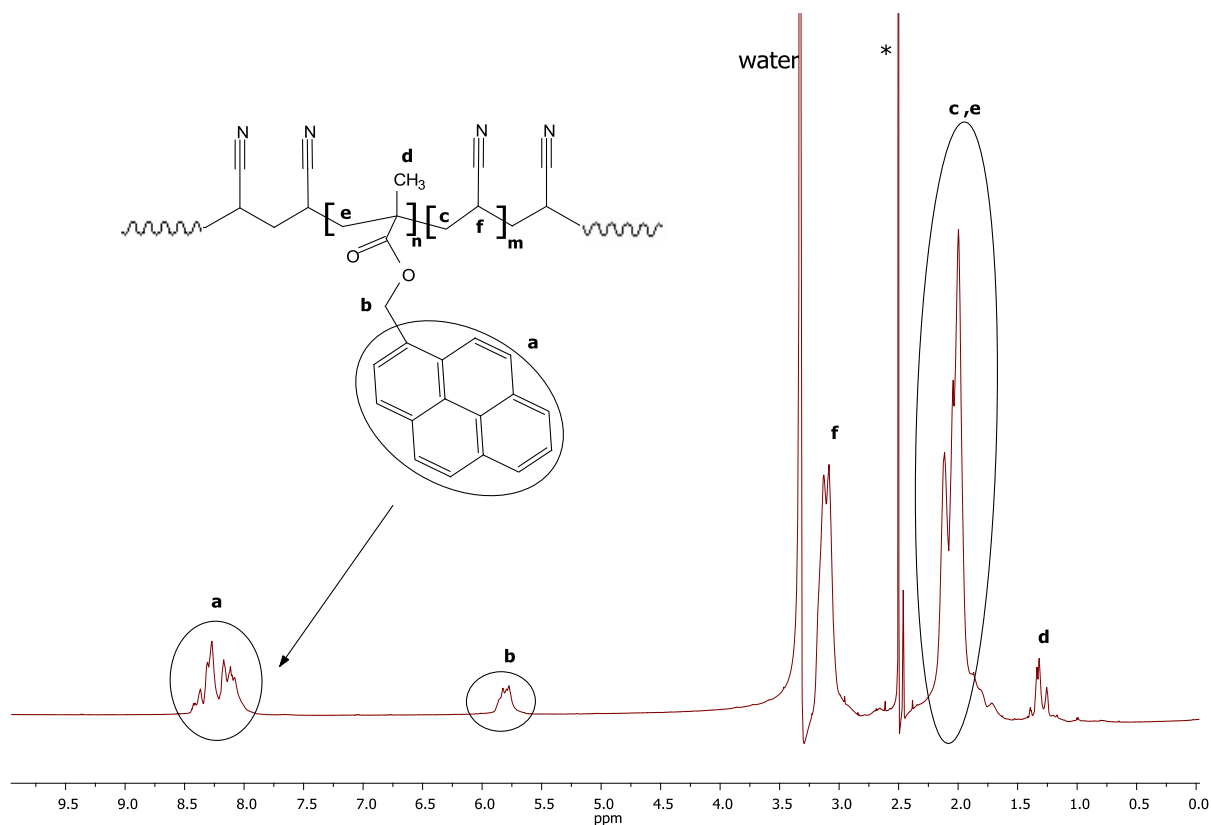


Figure 4.7: $^1\text{H-NMR}$ spectra of PAN-co-PyMMP-3 (2.02 mol% functionality) as polymerized from conventional AN monomer and PyMMP macromonomer.

The $^1\text{H-NMR}$ analysis on the produced copolymer presents a spectrum containing signals indicative of both PyMMP and AN monomer presence. Signals introduced from the PyMMP macromonomer incorporation include the pyrene representing multiplets at a range of chemical shift 7.94 ppm to 8.47 ppm (slightly broadened when referring to PyMMP representing spectra), an aliphatic ($-\text{CH}_2-$) proton signal at 5.78 ppm (0.12 ppm upfield from original shift), and methyl ($-\text{CH}_3$) peaks appearing at a chemical shift of 1.32 ppm (shifted 0.57 ppm upfield from original shift). The expected disappearance of signals representing alkene protons at 5.67 ppm and 6.05 ppm is observed as the electronegative π -bond is utilized during polymerization. The aliphatic protons ($-\text{CH}_2-$) labeled “e” appears at a chemical shift similar to the unassociated PyMMP macromonomer which overlaps with one of the broad peaks generally seen for a PAN polymer. This overlapping peak appears at chemical shifts of approximately 2.04 ppm also represents the tertiary associated proton and the secondary associated proton signal appears at a chemical shift of approximately 3.15 ppm.

From the spectra on the individual copolymers, proton signal integration can be applied to the pyrene representing multiplets (7.84 ppm to 8.56 ppm) relative to either of the two chemically inequivalent protons along the polymer chain (1.92 ppm to 2.25 ppm or 3.01 ppm to 3.28 ppm). Taking into account the proton quantity represented by each signal, the

relative quantity (represented in mol%) of one monomer unit to the other can be calculated as incorporated into the copolymer chain. Integration relative to the tertiary bonded proton on the PAN chain segments is used to determine the degree on PyMMP incorporation because of the signal showing no overlapping with other proton signals and can be calculated from equation 4.3 to follow.

$$\text{Mol\% PyMMP composition} = \frac{(\int \text{Pyrene proton signal})/9}{(\int \text{PAN segment proton signal})} \times 100 \quad \text{Equation 4.3}$$

Calculated PyMMP macromonomer composition together with relative molecular weight and polymer dispersities are presented in Table 4.8.

Table 4.8: Specifications of PAN-co-PyMMP copolymers.

| | Target PyMMP composition | NMR | SEC | |
|-----------------------|--------------------------|-------------------|---------------|-----------|
| | | PyMMP composition | M_n^{SEC} | \bar{D} |
| PAN-co-PyMMP·1 | 0.1 mol % Py-MMP | 0.45 mol% | 284 200 g/mol | 2.03 |
| PAN-co-PyMMP·2 | 1.0 mol % Py-MMP | 1.22 mol % | 225 700 g/mol | 2.11 |
| PAN-co-PyMMP·3 | 2.0 mol % Py-MMP | 2.02 mol% | 69 600 g/mol | 2.65 |

The molecular weights of the multi-functional copolymers are obtained from SEC analysis on a system calibrated to PMMA standards. The molecular weights presented are, therefore, merely relative to these standards but can be used in the comparison of copolymers to one another. During the comparative analysis of copolymers against the mono-functional PAN, however, a comparison is struck based on mol% pyrene functionality. The values as explained are both obtained from $^1\text{H-NMR}$ analysis and based on accurate proton signal integration. Because of the pyrene functionality being quantitatively determined by the same analytical method, mono and multi-functional polymers can be compared based on similarly determined pyrene functionality. This proves helpful during the investigation into the noncovalent interaction character of all produced polymers with MWCNT surfaces, as investigated in section 4.4.

When comparing the copolymer dispersities to that of the py-PAN polymers obtained by ATRP synthesis, an expected decrease in control is observed for the copolymer series as an increase in \bar{D} values are seen for the uncontrolled CFR polymerizations. High dispersities are inherent to CFR polymerization reactions, accompanied by irregular fluctuations in the molecular weights. Upon further observation of the data represented in Table 4.8, an inverse correlation is observed as an increased PyMMP macromonomer incorporation results in broadening of the dispersities, accompanied by a decrease in the molecular weight. The

pyrene incorporation to PAN-co-PyMMP polymers is seen to increase with an increase of the PyMMP macromonomer incorporation feed. When considering the drop in M_n^{SEC} it is observed that the final molecular weight of 69 600 g/mol for the 2.02 mol% PyMMP incorporation is approximately 4 times smaller than the initial molar mass of 284 200 g/mol as observed for the 0.45 mol% PyMMP sample. Interestingly, the value of PyMMP content in itself is increased approximately 4 times from initial 0.45 mol% to a final 2.02 mol%. This indicates some degree of an inverse relationship between PyMMP incorporation and the produced molecular weight.

Copolymers were analyzed, as in the case of the mono pyrene functional PAN, by SEC using a dual RI/UV detection system in an effort to prove universal pyrene incorporation. Figure 4.8 shows a high correlation between RI and UV signals observed for the multi pyrene copolymer series. This proves the universal incorporation of pyrene functionality into the copolymer chain.

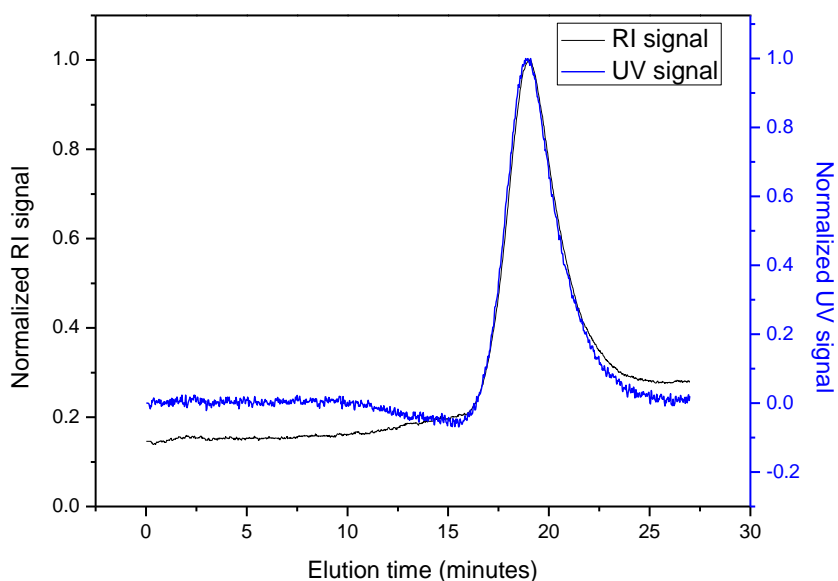


Figure 4.8: Elugram of SEC on PAN-co-PyMMP-1 (0.45 mol% functionality) using a dual detection system of RI and UV (365 nm).

This concludes the synthetic section of the project regarding the production of the various pyrene functional PAN based polymers. The following section focuses on the use of these polymers as interfacial compatibilizers for MWCNT filler incorporation into PAN matrix by noncovalent interaction.

4.4 Pyrene-functional-PAN/MWCNT nanocomposites by noncovalent interaction

Noncovalent interactions between pyrene functional PAN and MWCNTs are visually represented by preparing three vessels containing 25ml of DMF solvent and 5mg pristine MWCNTs. To two of the identical vessels 32mg of pyrene functional PAN was added (py-PAN:2 and PAN-co-PyMMP:2 polymers respectively) after which all three vessels were left under magnetic stirring overnight. The vessels containing the pitch black liquids were taken of the stirring plate and left to stand for several hours. In the vessel containing only MWCNTs in DMF, a dark layer formed at the bottom of the vessel beneath a clear liquid, presenting the expected precipitation of MWCNTs. The vessels containing the additional functional polymer, shows the liquid maintaining the deep black colour, indicating the suspension of the MWCNTs. This can be explained by the properties of the pyrene functional PAN being able to noncovalently associate with MWCNT surfaces, yet simultaneously be solubilized in a medium known as a good solvent for the PAN moiety. No visual distinctions could be made between the two samples containing the functional polymers as both solutions present a homogeneous black colour. This visual observation is photographically represented in the image below.

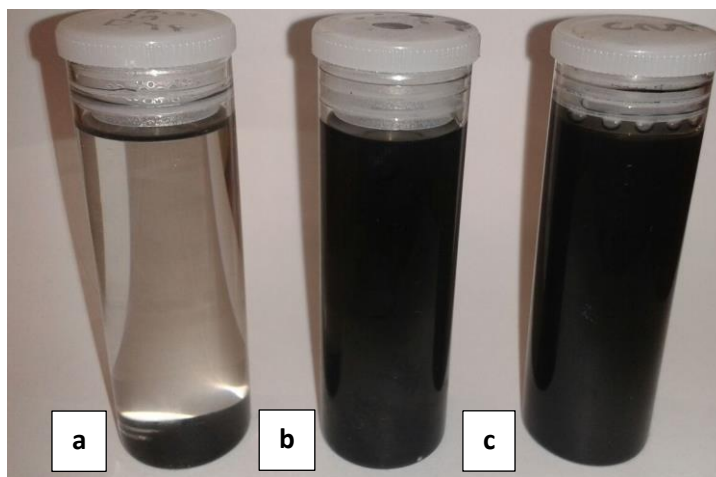


Figure 4.9: MWCNT dispersion ability of functional polymer by comparative representation of a (a) polymer deprived solution, a (b) PAN-co-PyMMP:2 polymer (1.22 mol% functionality) and (c) py-PAN :2 polymer (1.09 mol% functionality) containing solution.

4.4.1 TGA analysis

Thermal gravimetric analysis (TGA) was run on the hybrid composites of MWCNTs and the aforementioned mono and multi pyrene functional variations of PAN in order to support the

results of the solution dispersion and prove the integrity of the noncovalent association. Samples were prepared in a manner similar to that explained above in the visual representation (5 mg of pristine MWCNTs, 32 mg pyrene functional polymer in 25 ml DMF) to make up a functional polymer to MWCNT weighted ratio of 1:6.4 for both the mono- and multi-functional PAN. Samples used were a mono pyrene functional PAN polymer of average molecular weight approximately 5 200 g/mol and a multi-functional pyrene containing PAN copolymer of 1.22 mol% PyMMP composition with an average molecular weight of approximately 225 700 g/mol. As indicated in the synthetic part of this document (section 4.2 to 4.3 specifically) $^1\text{H-NMR}$ was used to determine the pyrene quantity or mol% functionality of both the mono- and multi-functional polymers. This analysis allows for the determination of the average incorporation of pyrene functionality for a certain polymeric chain length. This correlates to 4 400 g/mol (approximately 83 AN units) average chain length of PAN per PyMMP unit, and a 5 200 g/mol (approximately 91 AN units) average PAN chain length for the mono-functional polymer containing the pyrene functional end-group. The two samples were sonicated for a minute each to ensure the disruption of MWCNT aggregates and allow for association with the functional polymer. Samples are then subjected to centrifugation at 15 000 rpm for 2 minute cycles in an effort to remove any MWCNT and MWCNT/pyrene functional PAN complexes. The collected black matter was washed several times to ensure removal of any unassociated polymer and left to dry prior to TGA analysis. Removal of the functional polymers from the DMF washing solutions is supported by the UV analysis of the diluent. UV analysis was done on the diluent of the samples showing the complete removal of unassociated functional polymer from the extracted complexes. A representation of the successful removal of the unassociated polymer after 4 washes is evident by the disappearance of UV signals (Figure 4.10) produced by the pyrene moiety in the characteristic pyrene absorption region of wavelengths 300 nm to 400 nm.¹⁴

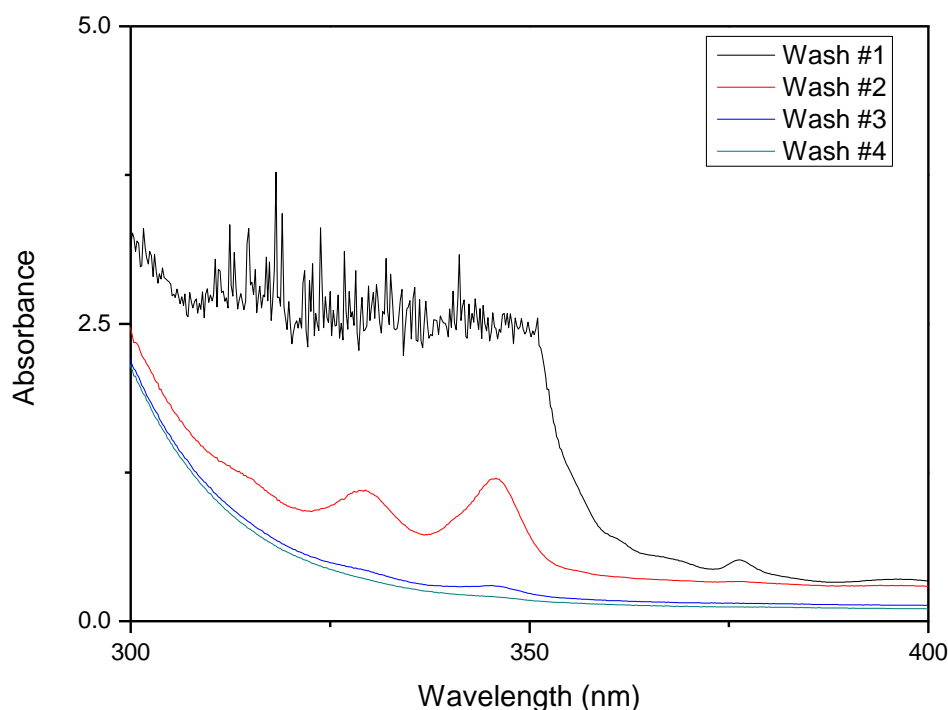


Figure 4.10: Illustration of unassociated functional polymer removal during TGA sample preparation by UV analysis of diluent from consecutive washes of (b) PAN-co-PAN-2/MWCNT composites by DMF solvent.

TGA thermograms were analyzed of the extracted materials as well as for homo PAN and pristine MWCNTs. All the curves presented the individual weight loss (%) obtained as the temperature is increased from 25°C to 600°C at a heating rate of 10°C/min under an inert N₂ atmosphere (Figure 4.11). The MWCNTs and PAN components make up the vast majority of the extracted composite materials and their resulting TGA curves can be used to better understand the convoluted data obtained for the various composites. The pristine character of the MWCNTs is confirmed by showing negligible weight loss of 0.38 wt% over the analyzed temperature range. Data obtained for pure PAN shows a single distinctive drop in weight over the temperature range 250°C to 450°C. This can be seen as an initial sharp drop in weight to 257°C followed by a lesser intense drop to a final weight, 39.17% that of the initial sample. This drop is evident for both of the extracted complexes indicating the presence of both mono- and multi-functional polymer in the respective complexes.

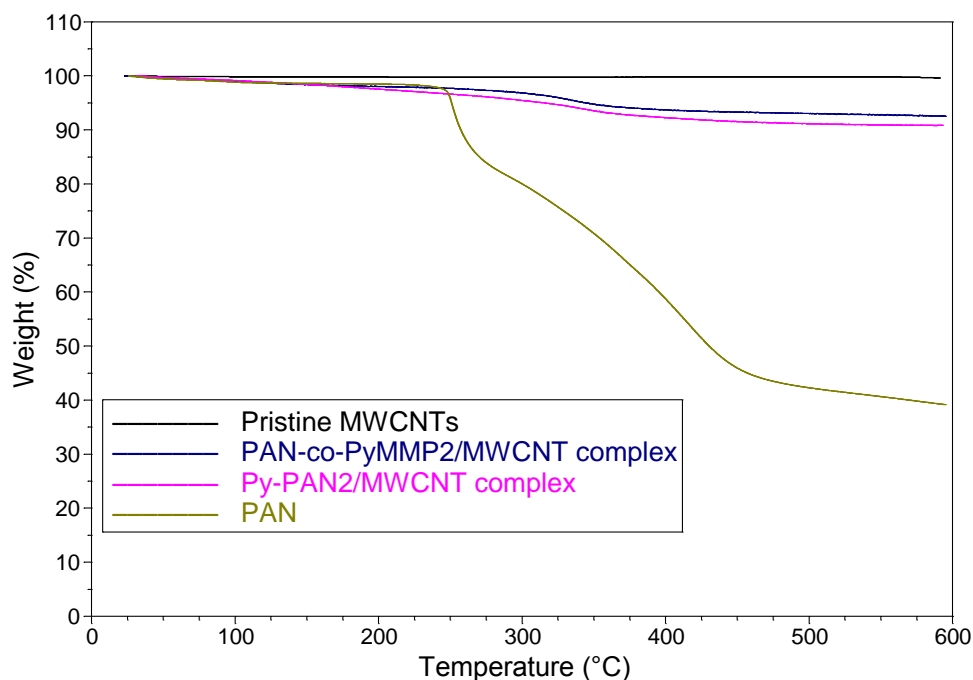


Figure 4.11: TGA thermogram representing % weight loss associated with pristine MWCNTs, py-PAN:2 (1.09 mol% functionality), PAN-co-PyMMP:2 (1.22 mol% functionality) copolymer and homo PAN polymer under inert N_2 environment.

The convoluted curves are indicative of the presence of functional polymer in both variations of functionality and therefore, prove the integrity of noncovalent association between MWCNT surfaces and pyrene moieties observed in the presented polymers. This preliminary data is representative of the relative functional polymer composition of each extracted complex, however, the true wt% composition is somewhat underestimated. The functional polymer will not show a weight loss consistent with the overall polymer because of the incomplete thermal decomposition of PAN to carbon matter in an inert atmosphere. TGA thermograms of the extracted complexes was compared to that of the specific, pristine, functional PAN in order to determine the true weight of polymer represented by the presented weight loss. Equation 4.4 is used together with appropriate weight losses, as obtained from TGA graphs (appendix, figures A9 to A12), to determine the true wt% composition of functional PAN in each complex and presented in Table 4.9 below.

$$\text{True wt\% composition of functional PAN} = \text{Weight loss of extracted complex (\%)} \times \left(1 + \left(\frac{\text{Weight left of functional PAN (\%)}}{100} \right) \right)$$

Equation 4.4

Table 4.9: Weight loss data as presented by TGA analysis.

| | Weight loss of extracted complex (%) | Weight loss of functional PAN (%) | True wt% of functional PAN |
|-----------------------------|--|---|-------------------------------|
| Multi-functional PAN | | | |
| 0.45 mol% PyMMP | 5.86 % | 49.58 % | 8.82 % |
| 1.22 mol% PyMMP | 7.46 % | 44.23 % | 11.61 % |
| 2.02 mol% PyMMP | 9.26 % | 41.36 % | 14.68 % |
| Mono functional PAN | | | |
| 1.09 mol% functionality | 9.16 % | 41.33 % | 14.54 % |

Different sizes of the multi- and mono-functional polymers may allow different mechanical influences to arise during extraction of the polymer from the solvent. These include encapsulation of smaller molecules (as in the case of Py-PAN·2) within MWCNT agglomerates or the variation in polymer entanglements arising from the different degrees of polymerization or steric hindrance (as in the case of PAN-co-PyMMP·2). For these reasons, in combination with the need to estimate the true polymer compositions of the extracted materials, the analysis into the complex compositions is simply a representation of the integrity of the interactions between the MWCNT surfaces and the functional polymers in immobilizing the polymers onto the MWCNTs. A comparison between the different molecular structures of the mono- and multi-functional configuration seems a bit ambitious. However, when comparing the estimated polymer composition of complexes prepared from the various multi-functional polymers, it does seem to indicate the increasing interaction strength as the pyrene quantity is increased along the multifunctional copolymer chain. The statement is supported by the greater pyrene quantity seemingly resulting in an elevated polymer extraction efficiency of the MWCNTs that leads to an increased polymer composition in the extracted complexes. An increase in functionality of 0.77 mol% PyMMP content (0.45 mol% to 1.22 mol%) results in an increase of extracted polymer of 2.79 wt% with an increase in functionality of 0.80 mol% PyMMP content (1.22 mol% to 2.02 mol%) resulting in a further increase in extracted polymer of 3.07 wt%. Based on these findings indicating the integrity of the MWCNT/pyrene-functional-PAN complex interactions, both functional polymers seem like viable options to be used as compatibilizers in the construction of the MWCNT/polymer composites.

4.4.2 $^1\text{H-NMR}$ analysis

It has been reported to see an alteration of peaks in a $^1\text{H-NMR}$ spectra by broadening, quenching and/or shifting after presenting MWCNTs to samples which are capable of associating with MWCNT surfaces via a π - π stacking interaction.¹⁵⁻¹⁸ In order to further investigate the potential π - π interaction, identical $^1\text{H-NMR}$ samples were prepared of both a mono (of sample code "py-PAN·3") as well as a multi (of sample code "PAN-co-PyMMP·2") pyrene functional PAN copolymer in DMSO-d_6 together with TMS internal standard. A reference spectrum was acquired on both of the samples, after which MWCNTs were added to the solutions, achieving a final composition of 20 wt%, 33 wt% and 50 wt% MWCNTs relative to the functional polymers. After the addition of each of the three desired MWCNT quantities, the solution is sonicated for 1 minute to achieve dismantling of MWCNT conjugates and universal dispersion of exfoliated nanotubes. Each of the desired MWCNT compositions were analyzed by $^1\text{H-NMR}$ spectroscopy and the resulting spectra overlaid, using the universally present TMS reference peak positioned at a chemical shift of 0 ppm. Spectral analysis shows, by comparative integration relative to the TMS reference, a definite signal quenching as well as peak broadening, not only of signals representative of pyrene functionality but interestingly to a lesser extent of peaks representing protons in the polymeric PAN backbone (Figure 4.12) potentially also showing association of the PAN with the MWCNT surface.

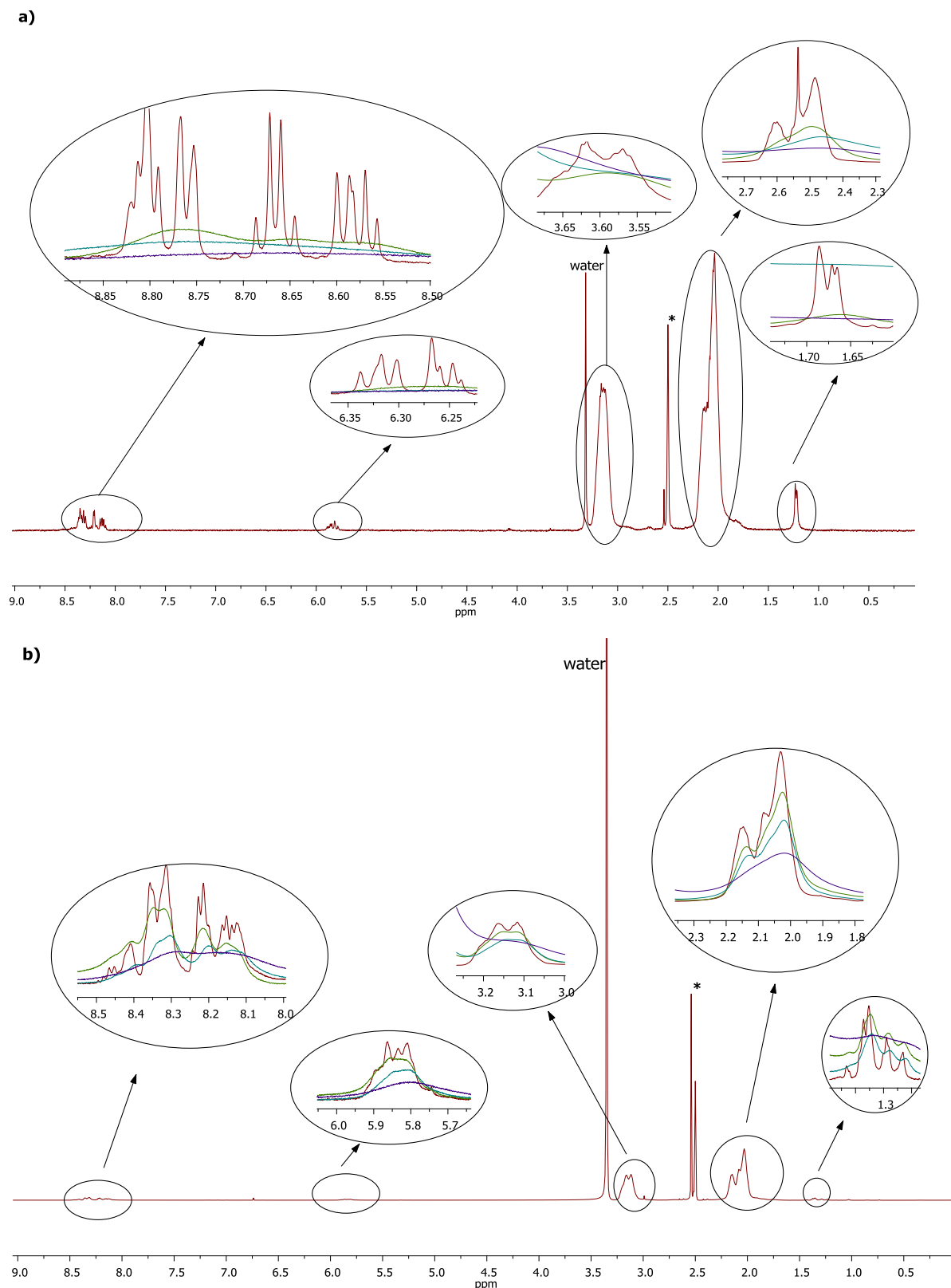


Figure 4.12: Overlaid $^1\text{H-NMR}$ spectra of a) py-PAN-3 (0.43 mol% functionality) and b) PAN-co-PyMMP-2 (2.02 mol% functionality) polymers with each spectra representing a 0 wt% (red), 20 wt% (green), 33 wt% (blue) and 50 wt% (purple) MWCNT loading fraction relative to functional sample.

An increasing quenching strength is represented by a weaker peak signal, and is observed to a greater extent as the MWCNT quantity is increased by integration against relevant proton peaks. This phenomenon is evident, indicating a clear signal quenching and/or broadening of peaks. The true quenching extent can, however, be investigated by integrational analysis of the proton presenting peaks. As signal quenching is supposedly resultant of π - π stacking, the degree of the signal depletion is investigated for the pyrene moiety, capable of such π - π interactions. Integration of pyrene representing multiplets (8 ppm to 9 ppm) against TMS reference (0 ppm) for the mono chain-end functional PAN shows an initial quenching of 17% of for 20 wt% MWCNT composition, a further quench to 49% is observed for 33 wt% MWCNT and finally a 70% quenching magnitude is evident for a 50 wt% MWCNT comprising nano hybrid (Table 4.10). For the multi pyrene functional PAN a quench of 13% is seen at 20 wt% MWCNT composition, a further quench to 22% is observed at 33 wt% MWCNTs and final quench of 31% is evident at 50 wt% MWCNTs.

Table 4.10: Quenching of pyrene multiplet signals for py-PAN-3 (0.43 mol% functional) and PAN-co-PyMMP-2 (1.22 mol% functional) polymers as obtained by $^1\text{H-NMR}$ analysis.

| MWCNT composition | Mono pyrene functional PAN | Multi pyrene functional PAN |
|--------------------------|-----------------------------------|------------------------------------|
| 0 wt% | 0% | 0% |
| 20 wt% | 17% | 13% |
| 33 wt% | 49% | 22% |
| 50 wt% | 70% | 31% |

The data presented in Table 4.10 shows the quenching of the peaks representing the multi pyrene functional PAN sample to be significantly less than represented in the case of the mono pyrene functional sample. The final signal quenching at 50 wt% MWCNT composition is seen to be more than twice as severe in the case of the mono functional sample when compared to the multi-functional polymer. The 1.22 mol% multi pyrene functional representative PAN-co-PyMMP polymer is calculated to contain approximately 240 AN monomeric units per PyMMP macro unit. This equates to each pyrene moiety being alternated by a PAN segment of approximately 12 700 g/mol average chain length. As the overall mass of both samples were identical, the calculated estimation is made that the pyrene content for the multi-functional PAN is approximately 1.95 times that of the mono functional PAN. This estimation clarifies the data indicating an apparent decrease in quenching ability of MWCNTs on the multi-functional sample, as the ratio of MWCNTs to pyrene functional unit is substantially less.

From the data presented in Table 4.10, the trends involving π - π stacking interactions, represented by signal quenching of the pyrene functionality is graphically represented for both mono and multi-functional polymers (Figure 4.13).

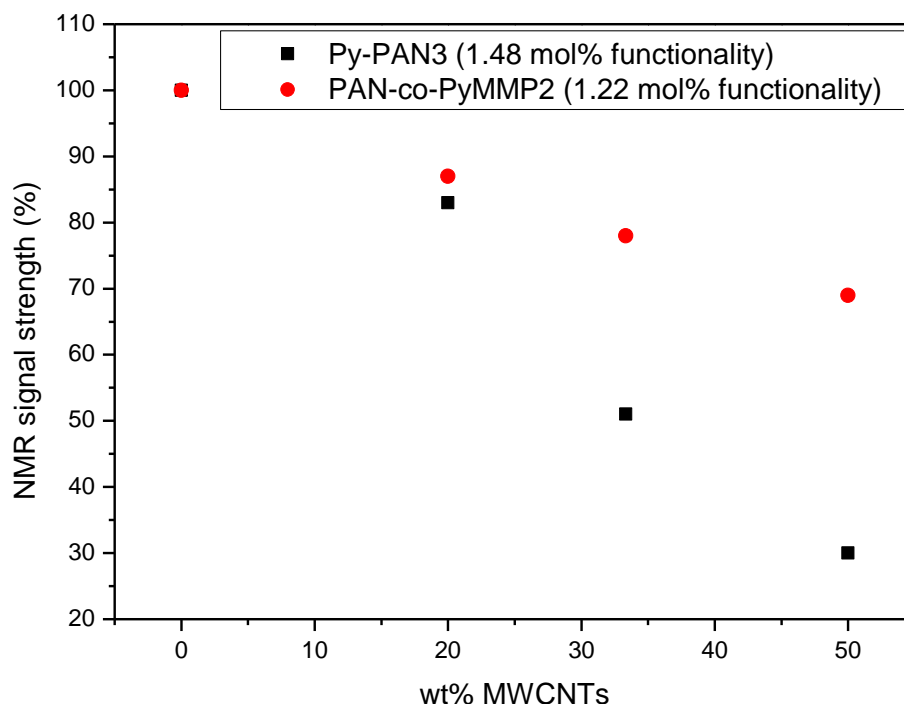


Figure 4.13: $^1\text{H-NMR}$ quenching trends of pyrene representing multiplets graphically represented in comparison of py-PAN-3 (0.43 mol% functionality) and PAN-co-PyMMP-2 (1.22 mol% functionality) polymers.

The reason for the multi-functional PAN showing a non-linear type association with the MWCNTs can be explained by a variation in apparent MWCNT/pyrene-moiety ratio relative to that of the mono-functional PAN. The fact that a greater initial quenching is seen at lower MWCNT loadings could be explained by the fact that the bulky nature of the copolymer may inhibit the association of multiple interaction sites within the same polymer. Thus at higher amounts of MWCNTs, the pyrene moieties remain inaccessible to the nanotubes and therefore do not partake in the noncovalent π - π stacking interaction. This exclusion of some pyrene moieties would mimic the characteristic of a higher MWCNT/polymer ratio, presenting the illusion of a retarded quenching ability at these high MWCNT compositions. Another explanation is that the multiple attachment sites in the multi-functional polymer simply allows for a stronger association which is more evident at lower MWCNT loadings. Nevertheless, despite the potential overall lower interaction, it is expected that each of the individual polymer chains are more firmly anchored to the MWCNT surface due to the

multiple interactions and the summation of the individual interactions along the polymer chain.

The phenomenon of signal quenching seems not to be reserved exclusively to the functional moiety as some degree of signal quenching appears to be evident for protons representing peaks of the polymeric backbone. The severity of this second degree interactions was further analyzed in much the same way as for the π - π stacking of pyrene moiety. Analysis into the extent of association of the polymeric back bone to the MWCNT surface was attempted by analytically integrating signals of the polymeric protons of non-conjugated character against the TMS singlets for both the mono as well as multi-functional polymer (Table 4.11). The cluttered positioning of signals associated with these protons proved problematic, as peak broadening results in multiple overlapping of signals in this region. The isolated shift associated with TMS reference assured no interference of such overlapping and the choice was made to present ratios of these isolated signals relative to the entire shift of the 1 ppm to 5 ppm region bearing a convoluted representation of polymeric protons. This region bears the presence of solvent peaks, which were excluded from the obtained regional integration. Signals to be integrated across the shift 1 ppm to 5 ppm are slightly enhanced by solvent peaks, however, dominated by polymer signals.

Table 4.11: Quenching of polymeric proton signals for py-PAN:3 (0.43 mol% functional) and PAN-co-PyMMP:2 (1.22 mol% functional) polymers as obtained by $^1\text{H-NMR}$ analysis.

| MWCNT composition | Mono pyrene functional PAN | Multi pyrene functional PAN |
|--------------------------|-----------------------------------|------------------------------------|
| 0 wt% | 0% | 0% |
| 20 wt% | 5% | 18% |
| 33 wt% | 11% | 19% |
| 50 wt% | 31% | 20% |

The data suggests not only the occurrence of the π - π interaction between pyrene and the MWCNT surface but an additional interaction to be evident at a fraction of the magnitude regarding polymeric protons. This relative interaction of pristine PAN with the surface of MWCNTs has been reported in literature,¹⁹ however, at a lesser severe interaction strength when compared to the π - π interactions. This would indicate the mechanistic association of noncovalent polymer wrapping to some extent. An interesting observation is that the trend in the quenching is quite similar to what is seen for the pyrene quenching. The mono-functional polymer again shows a linear type tendency. This is compared to the multi-functional polymer indicating an intense initial quenching magnitude of 18% at a 20 wt% MWCNT composition followed by only a slight seemingly linear increase in quenching magnitude observed by further incremental increases in quenching of 2% to the 50 wt% MWCNT

composition. The mono functional polymer, however, presents a larger final quenching magnitude of 31% when compared to the final signal quenching magnitude of 20% evident for multi-functional polymer. If in fact a polymer wrapping type mechanism is in play, the bulky pyrene functionalities protruding from the copolymer could in effect prevent to a great extent the close association of the polymeric backbone with MWCNT surfaces. This is seemingly evident from data presented for higher MWCNT compositions. This data, however, suggests inferior association by these “second degree” interactions when referring to the extent of quenching visible for the pyrene functional moiety capable of conjugated π -stacking type associations.

4.4.3 UV-fluorescence analysis

$^1\text{H-NMR}$ analysis indicated a near quantitative trend in signal quenching relative to MWCNT composition. Following this observation, UV-fluorescence (being a well-documented technique for observing emission energy quenching)^{14,20,21} was used to confirm and further investigate the quenching properties of the multi and mono pyrene functional PAN respectively as well as comparatively when exposed to variable MWCNT quantities.

A substantial advantage of the pyrene moiety is the characteristic fluorescent property it possesses. This fluorophore proves to be a considerable and sensitive marker in the investigation of inter-nanohybrid interactions.^{14,20,21} For this reason, fluorescent emission spectroscopy was used to present supporting data on the π - π stacking interaction of pyrene functionality and MWCNT surfaces.

The excited pyrene fluorescence signal has been shown to be effectively quenched by the noncovalent inter-pyrene/MWCNT interactions, brought about by strong van der Waals forces present between respective π -systems.²⁰ This evident quenching phenomenon has been widely reported^{22,23} and has been explained as being as a result of efficient electron or energy transfer in the intra molecular hybrid consisting of pyrene moiety and MWCNTs.^{14,24} This intermolecular energy transduction by immobilization of polymer onto pristine MWCNTs via pyrene functionality is analyzed by fluorescent spectroscopy when exposed to various MWCNT amounts. The deactivation of the excited state from the high energy pyrene emission seems dependent on the presented MWCNT content.

Multiple dilute samples of identical weights from respectively mono as well as multi-functional PAN in DMF were prepared and mixed with identical volumes (diluted from stock solution) of pristine MWCNTs in DMF. Samples were prepared to contain approximately

0.028 mg/ml of either mono or multi-functional PAN as well as a series of 0 wt%, 10 wt%, 20 wt%, 33 wt% and 50 wt% of MWCNTs relative to functional PAN for each of the two functionalities. Fluorescent emission spectra are collected by exciting at the maximum absorption wavelength of 345 nm and collecting emissions at wavelengths 380 nm to 450 nm. Normalized emission spectra of the complete series of MWCNT compositions were overlaid and are presented with the appropriate absorption spectra (collected from maximum emission of 380 nm). To exclude discrepancies brought about by variations in functionality, as expressed in $^1\text{H-NMR}$ analysis, mono and multi-functional PAN of similar pyrene quantity/functionality was analyzed. Samples of py-PAN·1 and PAN-co-PyMMP·3 were subjected to the aforementioned quenching analysis. These samples represent a mono pyrene functional PAN amounting to 1.97 mol% functionality and a multi pyrene functional copolymer of 2.02 mol% functionality (PyMMP composition). The resulting systematic fluorescent quenching data is graphically represented by Figure 4.14.

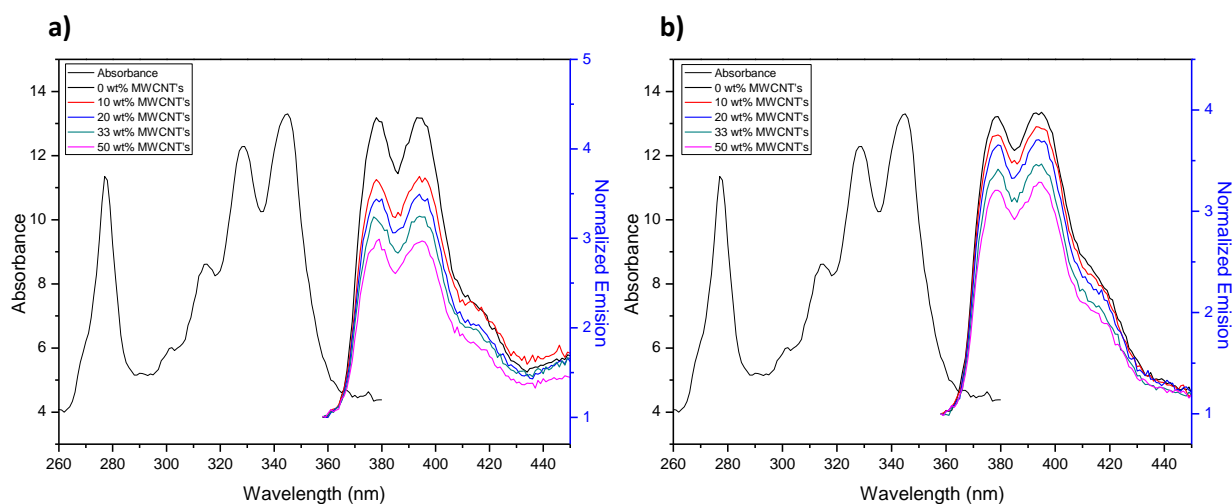


Figure 4.14: Representation of florescent quenching character observed for a) PAN-co-PyMMP·3 (2.02 mol% functionality) and b) py-PAN·1 (1.97 mol% functionality) polymers when exposed to various quantities of MWCNTs.

At first glance a clear superior quenching character is evident for the multi pyrene functional polymer when compared to the intense emission peaks observed for the mono pyrene functional PAN. When comparing the visual trends, it seems a gradual quench is observed for the mono-functional sample, correlating well with what was seen in the $^1\text{H-NMR}$ quenching analysis. The multi-functional polymer, however, seems to indicate an initial quench to a 10 wt% MWCNT composition superior in magnitude to what seems to be a more uniform quenching character for MWCNT incorporations 20 wt%, 33 wt% and 50 wt% compositions. The observed trends are numerically expressed in Table 4.12, for a more comprehensive investigation.

Table 4.12: Quenching trends of pyrene emission of py-PAN 1 (1.97 mol% functionality) and PAN-co-PyMMP 3 (2.02 mol% functionality) polymers as presented by UV-fluorescent analysis.

| Wt% CNT composition | Mono pyrene functional PAN | Multi pyrene functional PAN |
|---------------------|----------------------------|-----------------------------|
| 0 | 100% | 100% |
| 10 | 95% | 84% |
| 20 | 93% | 79% |
| 33 | 87% | 75% |
| 50 | 82% | 69% |

The tabulated quenching data presents a systematic quenching character observed for the mono-functional sample. Data presented for the multi-functional sample, however, seems to indicate an initial quenching of a large magnitude to the first loading fraction of 10 wt% MWCNT content. As the MWCNT content is systematically increased from 10 wt%, a more gradual trend in quenching magnitude is presented. A graphical representation of the data (Figure 4.15) was constructed up from data presented in Table 4.12.

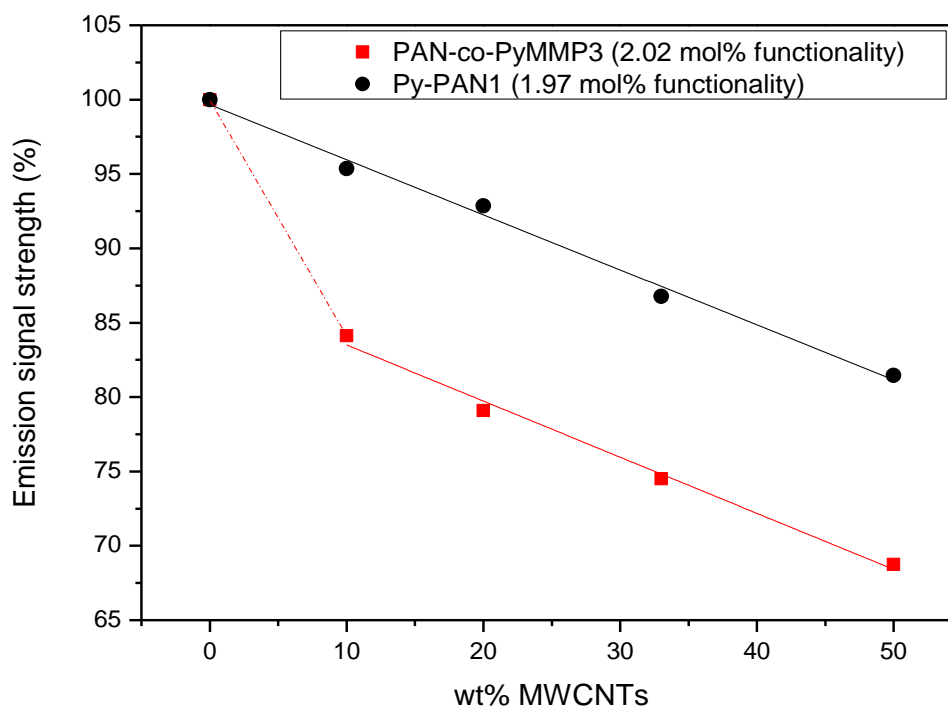
**Figure 4.15:** Fluorescent quenching trends graphically represented (with trends represented by guide lines) in comparison of PAN-co-PyMMP 3 (2.02 mol% functionality) and py-PAN 1 (1.97 mol% functionality) polymers.

Figure 4.15 presents clear trends in the fluorescent quenching characteristics of the mono and multi-functional polymers when exposed to increasing amounts of MWCNTs. The

mono-functional polymer presents a linear quenching character expressed by the linear fitted line at a slope of -0.371. The curve resulting from the multi-functional polymer presents a great degree of initial quenching measured at a 10 wt% MWCNT composition followed by an inflection point, after which a linear trend is followed at a less pronounced quenching magnitude. This linear trend is represented by a fitted line of a slope -0.377.

Additional UV-fluorescent quenching analysis was done on the py-PAN:3 and PAN-co-PAN:2 polymers that were investigated in the $^1\text{H-NMR}$ quenching analysis section (section 4.4.2). This was done in order to support the reliability of the data produced from NMR analysis by comparison of the quenching trends of both polymers to the fluorescent quenching trends.

The 1.22 mol% PyMMP containing copolymer and mono-functional PAN of 0.43 mol% functionality were analyzed by the same fluorescent procedure as for the previous fluorescent analysis. From the similarly presented fluorescent signals (Figure A13) data was extracted and presented in Table 4.13.

Table 4.13: Quenching trends of pyrene emission of py-PAN:3 (0.43 mol% functional) and PAN-co-PyMMP:2 (1.22 mol% functional) polymers as presented by UV-fluorescent analysis.

| Wt% CNT composition | Mono pyrene functional PAN | Multi pyrene functional PAN |
|----------------------------|-----------------------------------|------------------------------------|
| 0 | 100% | 100% |
| 10 | 94% | 91% |
| 20 | 90% | 85% |
| 33 | 80% | 81% |
| 50 | 68% | 76% |

The tabulated data is similarly to the previous data, extracted to a graphical representation in order to better establish the trends produced from the quenching analysis. This representation is expressed in Figure 4.16. The quenching trend observed from $^1\text{H-NMR}$ spectroscopy seems to be supported by the fluorescent emission analysis by indicating similar trends, but at somewhat elevated quenching values.

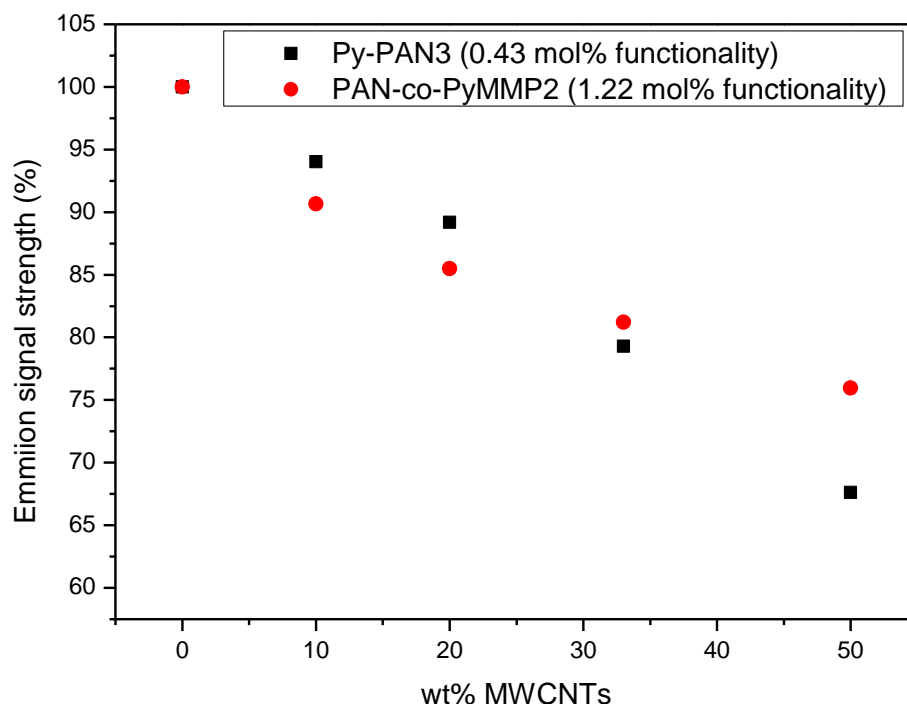


Figure 4.16: Fluorescent quenching trends observed for PAN-co-PyMMP2 (1.22 mol% functional) and py-PAN3 (0.43 mol% functional) polymers.

When comparing the same samples as used in $^1\text{H-NMR}$ analysis (Figure 4.16), the quenching trend are comparable in terms of the multi pyrene functional PAN exhibiting greater initial quenching at lower MWCNT compositions becoming increasingly weaker as a linear trend seems to present itself at increased amounts of MWCNTs. These trends are seemingly corresponding to molecular geometry as explained in the NMR section. This is concluded as all of the analyzed mono-functional samples seem to produce a linear type quenching trend against MWCNT filler compositions. The same is true for the multi-functional variation of PAN compatibilizers showing a deviation from linear trend at a lower MWCNT composition.

From both $^1\text{H-NMR}$ and UV-fluorescent analysis it seems clear that the multi-functional PAN polymer is the most efficient compatibilizing species for the dispersion of MWCNTs. The observation is especially evident at lower MWCNT loadings regarding superior interaction strength and assuming similar pyrene functionality.

4.5 Production of MWCNT/PAN nanocomposites by electrospinning

Electrospinning is used as the processing method to produce fibrous nanocomposites. The incorporations of fillers such as CNTs present difficulty as alteration of the molecular structure during integration to the matrix is sure to influence the filler's characteristic properties. One of the most popular methods used for the incorporation of inert carbon fillers into an organic solvents or polymer matrix is by means of chemical modification. In the current study, the well-established technique of using surface oxidized MWCNTs²⁵ was implemented to prepare PAN/MWCNT nanocomposite nanofibers by the electrospinning technique. This traditional method of preparing the nanocomposite nanofibers was compared to the method developed in this study to include the pristine MWCNTs into PAN nanofibers using the novel pyrene functional PAN polymers.

Compared to the method of covalent oxidative functionalization, pristine MWCNTs were introduced in the same loading fractions to the PAN matrix as a nondestructive, noncovalent method of MWCNT functionalization. The method does, however, require the additional incorporation of presynthesized pyrene functional PAN compatibilizer to be studied as a possible interface between MWCNT surface and the PAN matrix. The role of this interfacial compatibilizer is to allow for the dispersion of the pristine MWCNTs as in the case of surface oxidation. The noncovalent functionalization of the filler should in effect preserve the sp^2 hybridized molecular morphology on the surface of the MWCNTs and thereby the characteristic conductive as well as mechanical properties associated with these compounds.^{26,27,28} Spinning solutions were prepared of various sample series, each of which consisted of four variations of gradually increased filler loadings and each series representing a different compatibilizer to be spun into the fibrous nanocomposite.

A series of loading fractions of 0 wt%, 1.5 wt%, 3 wt%, and 5 wt% oxidized MWCNTs to PAN matrix were prepared for the production of the fibrous nanocomposites by the conventional covalent filler incorporation method, The series of prepared composites was replicated for the noncovalently functionalized filler composites by incorporating the pristine MWCNTs in the identical filler loading fractions. The 4 variations of filler loadings to polymer matrix were incorporated for each of the different variations of pyrene functional PAN.

To ensure the data is exclusively representative of molecular structure, weighted loadings of these compatibilizers were varied for each series to present similar pyrene quantity to each electrospun sample. By doing this, quantitative influences should be excluded as a factor in the analysis.

The mol% functionality is determined by the incorporation quantity of PyMMP macromonomer into the polymer chain during copolymerization of the PAN-co-PyMMP polymers. The values are determined from $^1\text{H-NMR}$ analysis, as explained in section 4.3. Similarly the pyrene quantity (mol% functionality) relative to the polymeric chain length or acrylonitrile (AN) repeat unit is investigated for the mono-functional py-PAN. This information is used to accurately calculate the average weighted compositions of the pyrene carrying monomer units in the functional PAN polymers (Table 4.14). In knowing what wt% of each polymer consists of the pyrene moiety, the required amount of each functional polymer can be determined to be incorporated to the electrospinning solution in order to achieve a similar pyrene quantity throughout all the spun composites.

Table 4.14: Data for mol% and resultant wt% of pyrene functionality, to be used in calculations for compatibilizer composition in spinning solutions.

| | Monomeric mol% of pyrene functionality | wt % of PyMMP composition |
|--|--|---------------------------|
| Multi Pyrene Functional PAN compatibilizers | | |
| PAN-co-PyMMP-1 | 0.45 | 2.50 |
| PAN-co-PyMMP-2 | 1.22 | 6.58 |
| PAN-co-PyMMP-3 | 2.02 | 10.51 |
| Mono Pyrene Functional PAN compatibilizer | | |
| Py-PAN-3 | 0.43 | 2.40 |








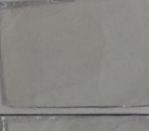





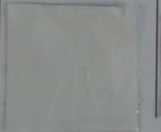






From the wt% of compatibilizer required for each electrospinning solution, a ratio of each compatibilizer to PAN matrix is determined by which a universal pyrene quantity is achieved for each spun composite. The spinning solutions consisting of the calculated ratio together with the various MWCNT compositions and DMF solvent is presented by in Table 4.15. The PAN matrix was incorporated into spinning solutions to make up a 10 wt% composition, using homo PAN of molecular weight 130 900 g/mol and dispersity of 1.87. The molecular specifications for PAN were obtained from SEC analysis in a dimethylacetamide (DMac) system, calibrated with PMMA standards.

Table 4.15: Tabulated representation of electrospinning solution compositions of each series prepared with loading fractions of 0 wt%, 1.5 wt%, 3 wt% and 5 wt% MWCNT compositions respectively.

| Compatibilizer | DMF solvent (ml) | Mol% functionality | Weight ratio of compatibiizer to PAN matrix |
|------------------------------------|------------------|--------------------|---|
| Multi Pyrene Functional PAN | | | |
| PAN-co-PyMMP·1 | 1 | 0.45 | 1: 25 |
| PAN-co-PyMMP·2 | 1 | 1.22 | 1: 66 |
| PAN-co-PyMMP·3 | 1 | 2.02 | 1: 105 |
| Mono Pyrene Functional PAN | | | |
| Py-PAN·3 | 1 | 0.43 | 1: 24 |

The spinning samples were all prepared in 1 ml of DMF containing the solvated PAN matrix (105.3 mg). The ratios account for a 4.2 mg, 1.6 mg and 1.0 mg composition of multi-functional PAN of respective increasing functionality and 4.5 mg of the mono-functional PAN. The universal molar value of pyrene moiety in this specific case is calculated at a 3.47×10^{-7} mol quantity for every sample of each series. MWCNTs were incorporated in increasing loading fractions to account for 0 wt%, 1.5 wt%, 3 wt% and 5 wt% of the final spun composite for each of the different compatibilizers as well as for oxidized MWCNTs in the absence of a compatibilizer. After the electrospinning solutions were prepared, the various composites of noncovalently incorporated MWCNTs as well as of the covalently functionalized MWCNTs were spun into fibrous state by means of single needle electrospinning. A physical comparison to each noncovalently compatibilized composite as well as to the composite of conventional covalent filler incorporation can be seen in Table 4.16.

Table 4.16: Electrospun nanofiber composite mats by various compatibilizing species in a series of 0 wt%, 1 wt%, 5 wt%, 3 wt% and 5 wt% MWCNT composition.

| Filler incorporation method | MWCNT loading fraction | | | |
|---|---|---|--|---|
| | 0 wt% | 1.5 wt% | 3 wt% | 5 wt% |
| Multi pyrene functional compatibilizer | | | | |
| PAN-co-PyMMP·1 |  |  |  |  |
| PAN-co-PyMMP·2 |  |  |  |  |
| PAN-co-PyMMP·3 |  |  |  |  |
| Mono pyrene functional compatibilizer | | | | |
| Py-PAN·3 |  |  |  |  |
| Compatibilization by covalent filler functionalization | | | | |
| Oxidized MWCNTs |  |  |  |  |

From the images of spun composites (Table 4.16), the incorporation of MWCNT filler is indicated by simply observing the hue of each series becoming darker as the loading fractions of MWCNTs are increased. The MWCNT series for 0.45 mol% PyMMP compatibilizer is seen to show a greater variation in hue, as a result of a thicker spun fibrous mat, compared to the thinner spun series using the 1.22 mol% PyMMP containing (1.22 mol% functional) compatibilizer.

SEM was used to determine the differences in the fiber morphology. Measurements from the images allow for the determination of the fiber diameters. The images and the corresponding fiber diameter distributions are presented in figures 4.17 to 4.19. The average fiber diameters as determined from the SEM images are shown in Table 4.17.

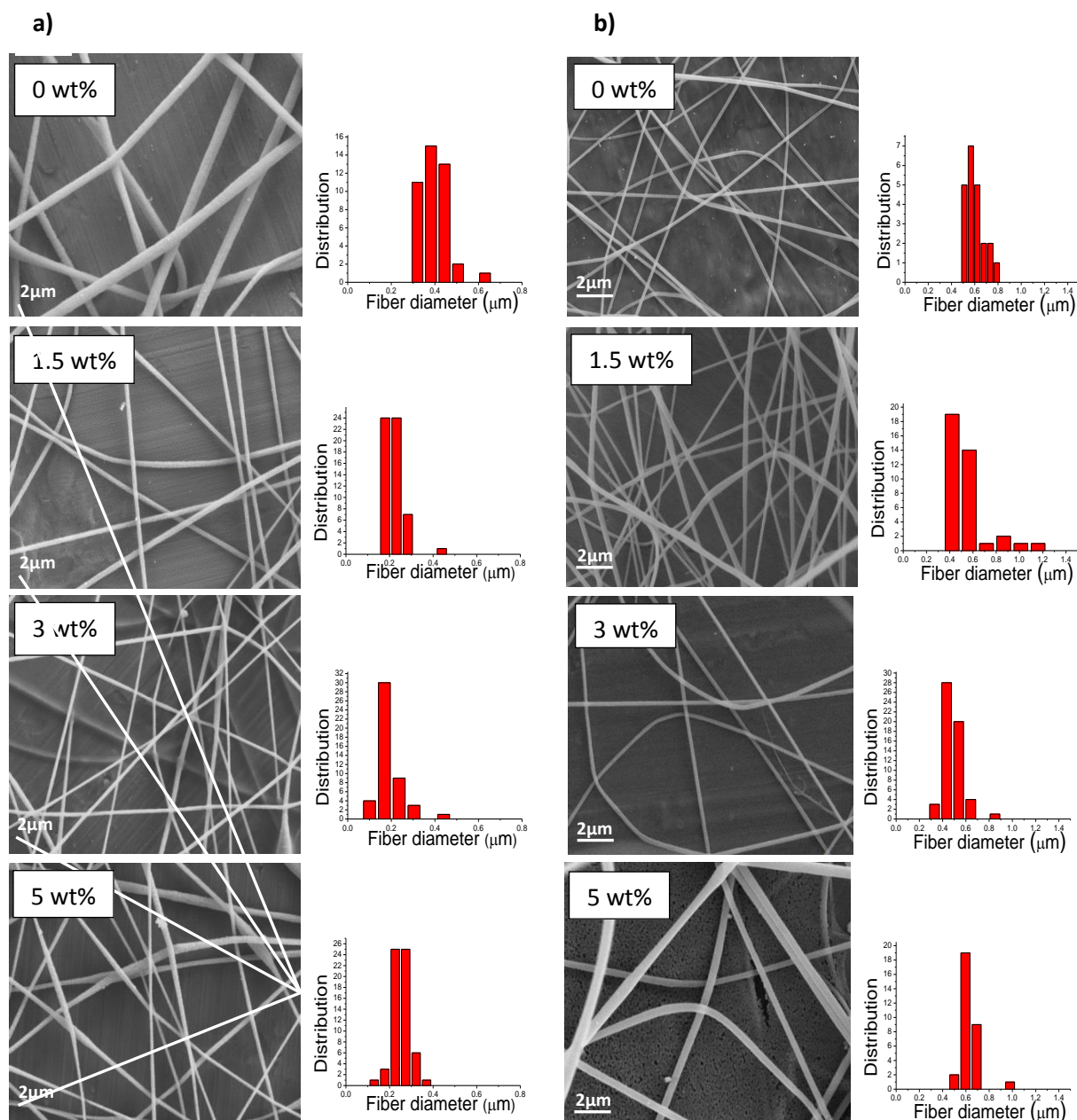


Figure 4.17: SEM images and corresponding average fiber diameter distributions of fibrous composites of 0 wt%, 1.5 wt%, 3 wt% and 5 wt% a) oxidized MWCNT composition and b) noncovalent incorporation of the same loadings of pristine MWCNTs by PAN-co-PyMMP-1 (0.45 mol% functionality) in a PAN matrix.

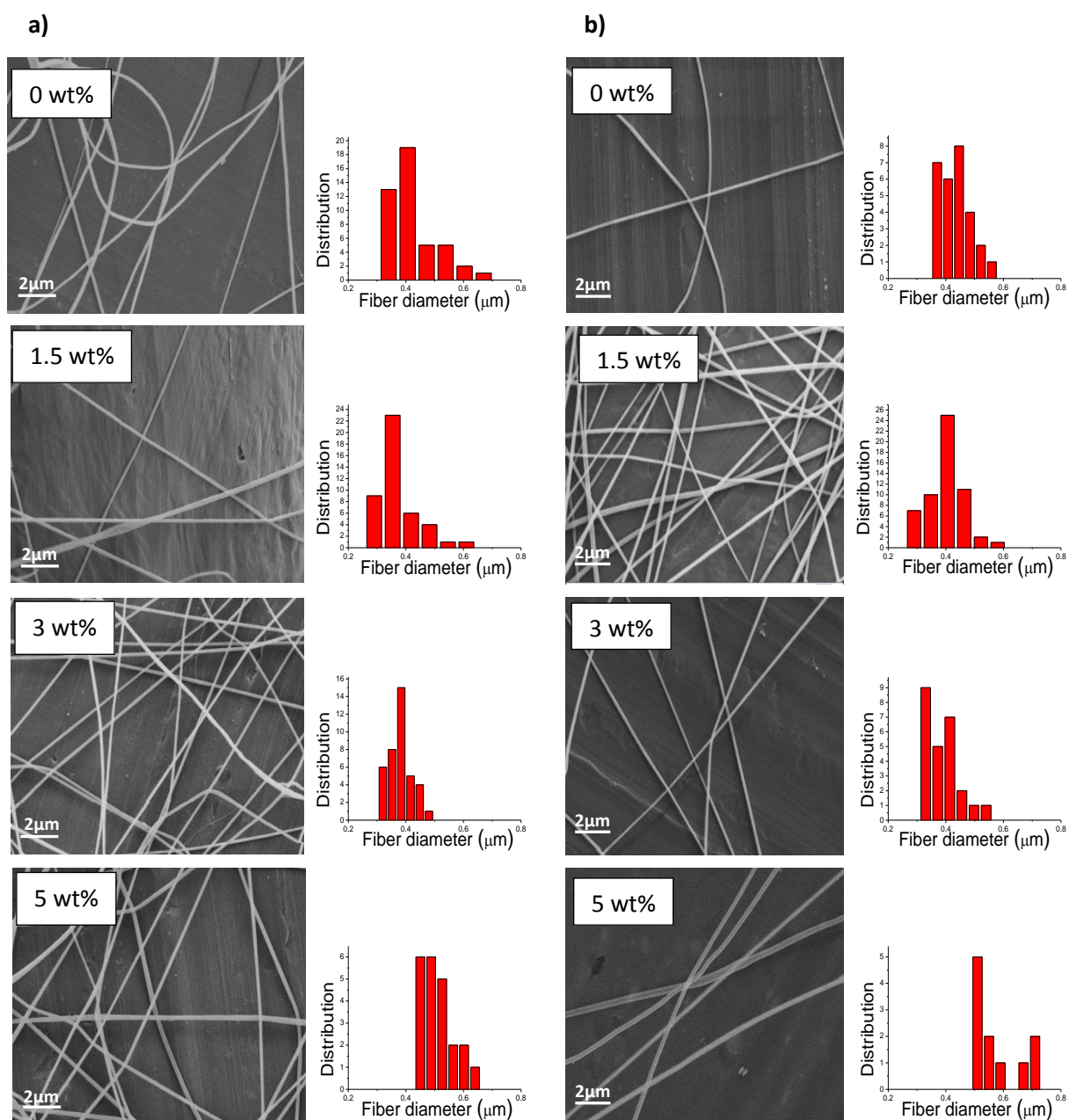


Figure 4.18: SEM images and corresponding average fiber diameter distributions of fibrous composites of 0 wt%, 1.5 wt%, 3 wt% and 5 wt% pristine MWCNT composition in PAN matrix by noncovalent incorporation using a) PAN-co-PyMMP-2 (1.22 mol% functionality) and PAN-co-PyMMP-3 (2.02 mol% functionality) respectively.

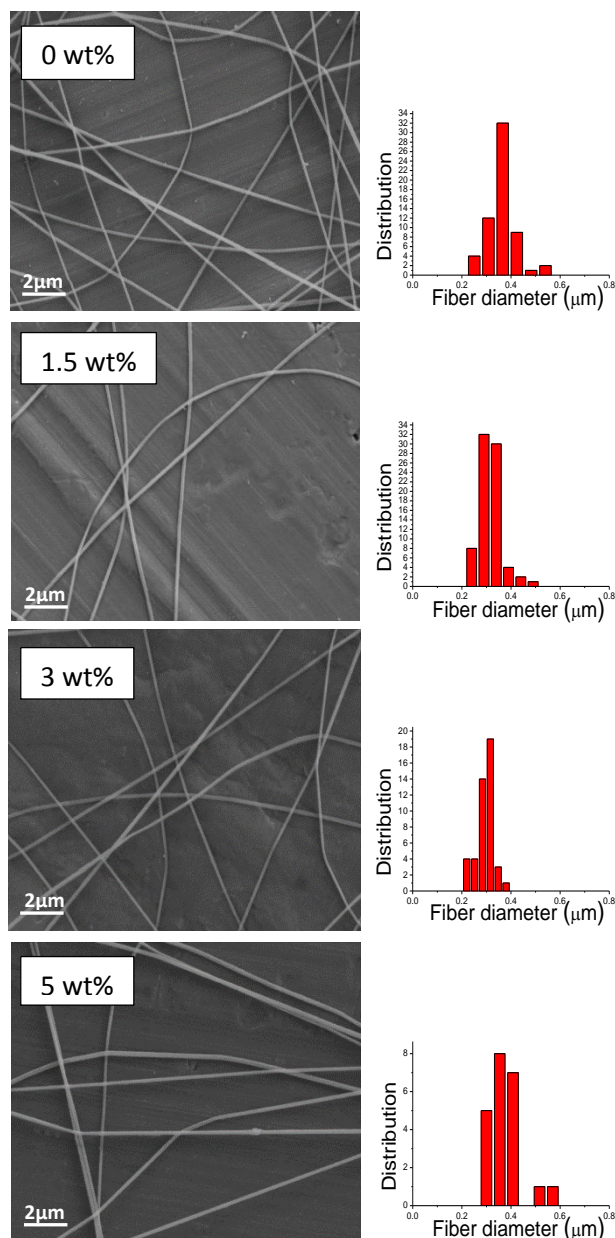


Figure 4.19: SEM images and corresponding average fiber diameter distributions of fibrous composites of 0 wt%, 1.5 wt%, 3 wt% and 5 wt% pristine MWCNT composition in PAN matrix by noncovalent incorporation using py-PAN-3 (0.43 mol% functionality).

Figure 4.20 shows the average fiber diameters for each series of both the covalent and the various noncovalently functionalized MWCNT filler nanofiber series. The error bars are emitted from this graph for the sake of simplicity.

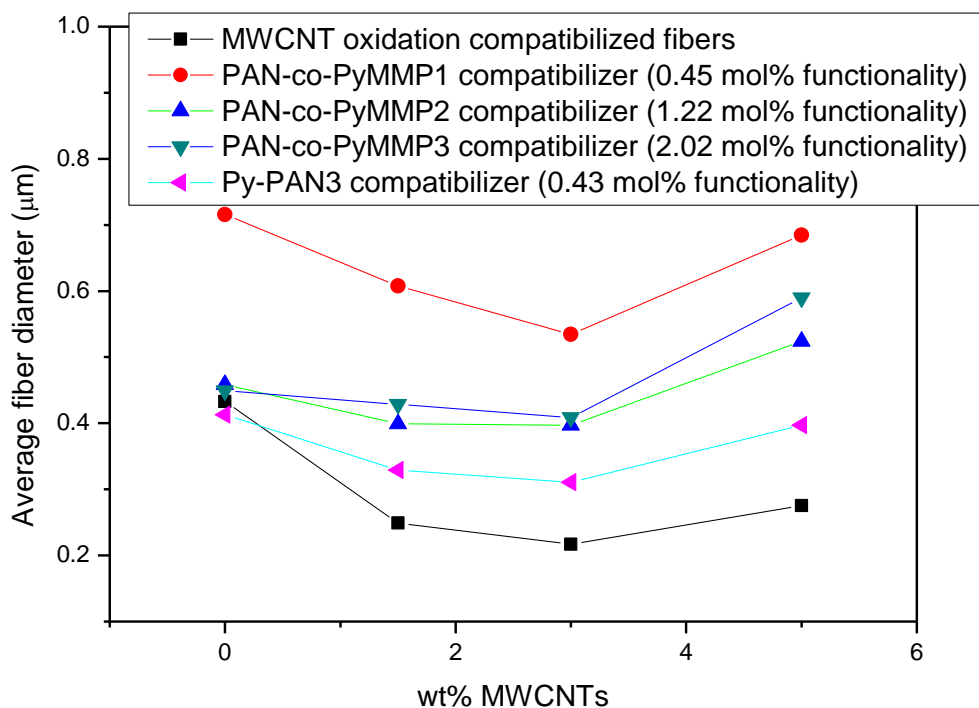


Figure 4.20: Average fiber diameters with increased MWCNT filler for the various compatibilizing methods. The methods being covalent oxidation of MWCNT filler as well as noncovalent functionalization by PAN-co-PyMMP-1 (0.45 mol% functional), PAN-co-PyMMP-2 (1.22 mol% functional), PAN-co-PyMMP-3 (2.02 mol% functional) and py-PAN-3 (0.43 mol% functional) compatibilizers.

From Figure 4.20 a clear and somewhat similar trend in fiber diameter is evident for each series spun at increasing filler loadings. All composites were spun at the reproduced specific electrospinning conditions of 15 kw applied voltage, tip to collector distance (TCD) of 15 cm, a flow rate of 0.03 ml/min and relative humidity of 35% to 40%. At these conditions an initial drop is observed in fiber diameters to 1.5 wt% MWCNT composition followed by a less intense drop or leveling to a minimum value in the range 1.5 wt% to 3 wt% after which a final, drastic increase in fiber diameter is observed to 5 wt% of filler content. As an investigation into the influence of MWCNT filler composition on fiber diameters, incremental analysis was done and is numerically presented in Table 4.17.

Table 4.17: Fiber diameter for composites of various filler functionalization species and incremental analysis thereof.

| | Fiber diameter (μm) at filler loading fractions | | | | Incremental analysis of fiber diameter (μm) | | | |
|-----------------------|--|---------|-------|-------|--|-----------|---------|---------|
| | 0 wt% | 1.5 wt% | 3 wt% | 5 wt% | 0-1.5 wt% | 1.5-3 wt% | 3-5 wt% | 0-5 wt% |
| | Oxidized MWCNT | 0.43 | 0.25 | 0.27 | 0.28 | -0.18 | -0.03 | 0.06 |
| PAN-co-PyMMP-1 | 0.72 | 0.61 | 0.54 | 0.69 | -0.11 | -0.07 | 0.15 | -0.03 |
| PAN-co-PyMMP-2 | 0.46 | 0.40 | 0.40 | 0.52 | -0.06 | 0.00 | 0.13 | 0.07 |
| PAN-co-PyMMP-3 | 0.45 | 0.43 | 0.41 | 0.59 | -0.02 | -0.02 | 0.18 | 0.14 |
| Py-PAN-3 | 0.41 | 0.33 | 0.31 | 0.40 | -0.08 | -0.02 | 0.09 | -0.02 |

During the incorporation to first loading fractions of 1.5 wt% MWNCTs, an overall decrease in fiber diameter is observed for all series. The magnitude of the fiber diameter decrease is observed to be much greater for the covalently functionalized MWCNTs when compared to the noncovalently functionalized samples. A fiber diameter decrease of 0.18 μm is observed for the oxidized MWCNT series compared to a 0.11 μm , 0.06 μm and 0.02 μm decrease observed for the 0.4 mol%, 1.22 mol% and 2.02 mol% multi-functional compatibilizer respectively. The mono pyrene functional (0.43 mol% functionality) compatibilizer produced a 0.08 μm decrease in fiber diameter falling in the range of the decreases observed for the multi-functional samples. Interestingly, a decrease in fiber diameter is less pronounced as the pyrene functionality is increased along the PAN-co-PyMMP backbone. This is evident for the samples of multi-functional character with a decrease of 0.05 μm seen compared to 0.45 mol% to 1.22 mol% pyrene composition and a further decrease of 0.04 μm to a 2.02 mol% PyMMP composition. As the composition of the filler is increased further to a 3 wt% composition for all the series, no drastic variations in fiber diameter is observed with a maximum decrease in diameter of 0.07 μm . The initial drop to 3 wt% filler composition therefore has a seemingly inverse relationship to relative pyrene functionality. From a filler composition of 3 wt%, a final increase in filler quantity to 5 wt% is seen to have a more significant influence on the fiber diameter. This final hike presents an increase in fiber diameter which is less prominent for the conventionally oxidized filler containing series followed by the mono-functional PAN compatibilized fibrous composites. The most significant increase, however, is seen at relatively similar magnitudes for the multi-functional

PAN compatibilized nanocomposite samples at the relative MWCNT compositions of 3 wt% to 5 wt%.

As an overall trend (0 wt% to 5 wt% MWCNTs), the oxidized filler series is seen to decrease in fiber diameter by 0.16 μm . A slight overall decrease in fiber diameter is observed at similar values of 0.02 μm and 0.03 μm for the 0.43 mol% mono pyrene functional and 0.45 mol% PyMMP comprising PAN compatibilizer respectively. At increased pyrene content of the multi-functional PAN, an increase in fiber diameter is observed as an overall 0.13 μm increase for the 1.22 mol% PyMMP and 0.18 μm increase for the 2.02 mol% PyMMP comonomer composition.

The results indicate some character of the viscoelastic fluid used to produce fibers of increased fiber diameter as relative pyrene functionality of compatibilizer is increased from the 0.43 mol% mono pyrene containing PAN to the 2.02 mol% PyMMP comonomer containing multi-functional PAN. The variable of filler induced viscosity can be neglected when comparing between MWCNT compatibilization methods, based on similar filler compositions. The relevant variable can be explained by the filler morphology and/or distribution thereof.

It seems two major influences results in the alteration of fiber diameter, where one phenomenon produces a decreased diameter as the other leads to an increase. The influences are seemingly counter active and dominate to different degrees comparing the different compatibilization methods. The noncovalent filler incorporation method is evidently affected to a greater extent by the phenomenon leading to the increased fiber diameter when compared to the general method of MWCNT functionalization, which is itself more affected by the phenomenon leading to a decreased fiber diameter. A trend is observed amongst the noncovalently produced composites, where an increased functionality is seen to result in a greater increase in fibrous composite diameter and a simultaneous retarding in effect of decreasing diameter magnitude. The decrease in fiber diameters can be seen as the MWCNT content is increased at low MWCNT loadings for all of the different compatibilization series. This is commonly explained as being a direct result of an increased whipping instability during the electrospinning process, resulting from the conductive MWCNT composition.^{29,30} The phenomenon associated with the increasing of fiber diameters appear in all of the series and is commonly explained as being as a result of the increased solution viscosity brought about by the increased filler composition.³¹ The effect of an increased fiber diameter as the MWCNTs are increased above 3 wt% composition is more dominant for the series making use of the compatibilizers of greater pyrene composition (or mol% pyrene functionality). The explanation for this could very likely be

because the interfacial compatibilizing polymers are acting as crosslinking materials between MWCNT's, therefore, leading to an increased solution viscosity and resultant fiber diameters. This is supported by the fact that the increase in viscosity is related to the degree in polymer functionality. The polymer of greatest pyrene quantity would have more possible association point with MWCNT surfaces and thus a greater degree of crosslinking probability leading to a an increased solution viscosity.

The physical distributions of nanotubes are, however, unknown and further analysis should be done in order to obtain such information. TEM analysis is of course the obvious choice in obtaining intra fibrous imaging, for filler distribution and alignment information.^{32,33} This, however, proved difficult for the low filler content use for the composite preparation.

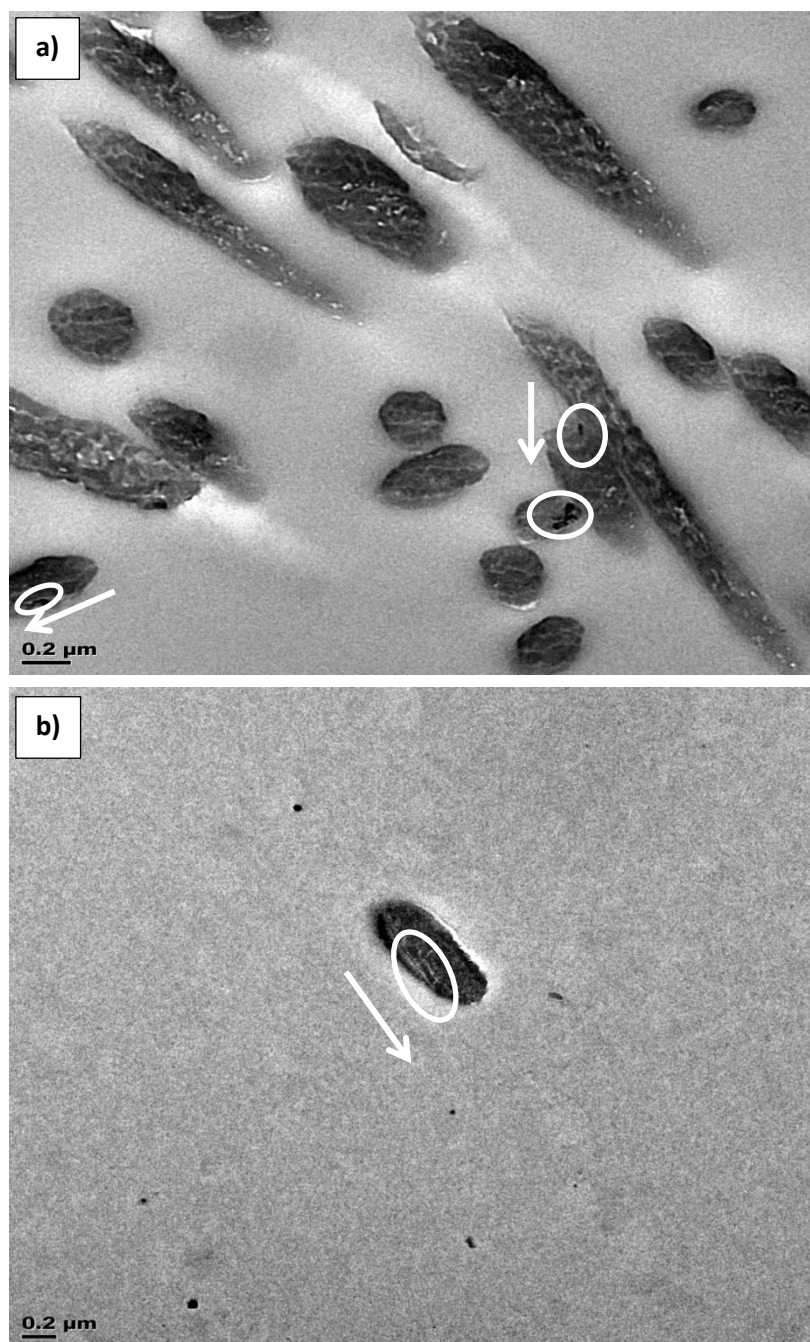


Figure 4.21: TEM imaging of nanofiber composites imbedded with 5 wt% of a) covalently oxidized MWCNTs and b) pristine MWCNTs by noncovalent compatibilization using PAN-co-PyMMP-3.

The TEM images of the composites containing 5 wt% covalently functionalized MWCNT (by surface oxidation) as well as the 5 wt% of noncovalently compatibilized MWCNT by PAN-co-PAN-3 indicate nanotube imbedding as well as alignment of the MWCNTs along the fiber axis. This can be seen in the cases where cross-sectional imaging of fibrous nanocomposites presented MWCNT fillers. Deep imbedding of MWCNTs is suggested by TEM imaging of oxidized and 2.02 mol% multi-functional PAN compatibilizers (Figure 4.21). Images of nanocomposites with noncovalent compatibilization of MWCNTs by polymers of

less functionality than the 2.02 mol% functional PAN-co-PAN-3 show MWCNT positioning nearer to the surface of the nanofibers (appendix, Figure A14).

4.6 Pyrene-functional-PAN/EG nanocomposites by noncovalent interaction

Curiosity led to the extension of this project into the investigation of using pristine graphene as filler in the same system as used with MWCNT filled composites. Expandable graphite (EG) was used as received from Graphit Kropfmühl and analyzed with regards to the investigation into the same noncovalent association between π -electrons in conjugated systems of pyrene functionality and graphitic surfaces. The variation between nanotube and graphite fillers lays in the absence of surface curvature for the graphene sheets. When referring to the literature an interesting discovery is made, in that studies indicate the increased noncovalent association of π - π stacking with a decrease in curvature of graphitic surface.³⁴⁻³⁶ This presents much promise into the further investigation to test the incorporation of these fillers by compatibilizers for the incorporation to PAN matrix.

Studies identical to that used for the analysis of noncovalent MWCNT/pyrene-functional-PAN association are employed to prepared graphene/pyrene-functional-PAN complexes. These studies entail the testing of interaction integrity by TGA, quenching analysis by $^1\text{H-NMR}$ spectroscopy, UV-fluorescence as well as the final production of fibrous composites and analysis thereof by SEM. As expressed in the section of noncovalent association with MWCNT fillers (section 4.4), interaction integrity is initially presented visually by means of simple solvation or gravimetric precipitation. Identical vessels to previous analysis were prepared of 25 ml DMF solution and 5 mg pristine filler (in this case expandable graphite). To one vessel a 32 mg of multi-functional copolymer was added as compatibilizer (1.22 mol% PyMMP containing PAN) and left to stir overnight. After the solutions were left to stand however, a clear deviation from previous results is seen (Figure 4.22). Both vessels present precipitation of the filler content as the expected interaction with the compatibilizer was not visually achieved. The vessel carrying the expected graphene/functional-PAN nano hybrid seems to present a slight darker hue, however, these initial results do not present a promising outlook to the final incorporation of this filler to the composite material.



Figure 4.22: Solvation analysis by visual representation of a) polymer deprived solution and b) multi-functional compatibilizing polymer containing solution with EG.

The integrity of noncovalent graphene/functional-PAN interactions are further tested by TGA analysis. The samples are again prepared as previously by the same vessel of polymer and filler containing DMF solution as in the visual representation above. The sample is sonicated for approximately 1 minute, followed by ultra-centrifugation at 15 000 rpm for 2 min cycles. This process removes any filler or composite and several washes by DMF ensure the removal of any functional polymer not immobilized on graphitic surface. After the extracted material was left to dry, it was analyzed by TGA over a temperature range of 20°C to 600°C and heating rate of 10°C/min, under inert N₂ atmosphere (Figure 4.23). This TGA spectra overlays curves of extracted complex together with pristine filler and virgin multi-functional polymer to be used as compatibilizer

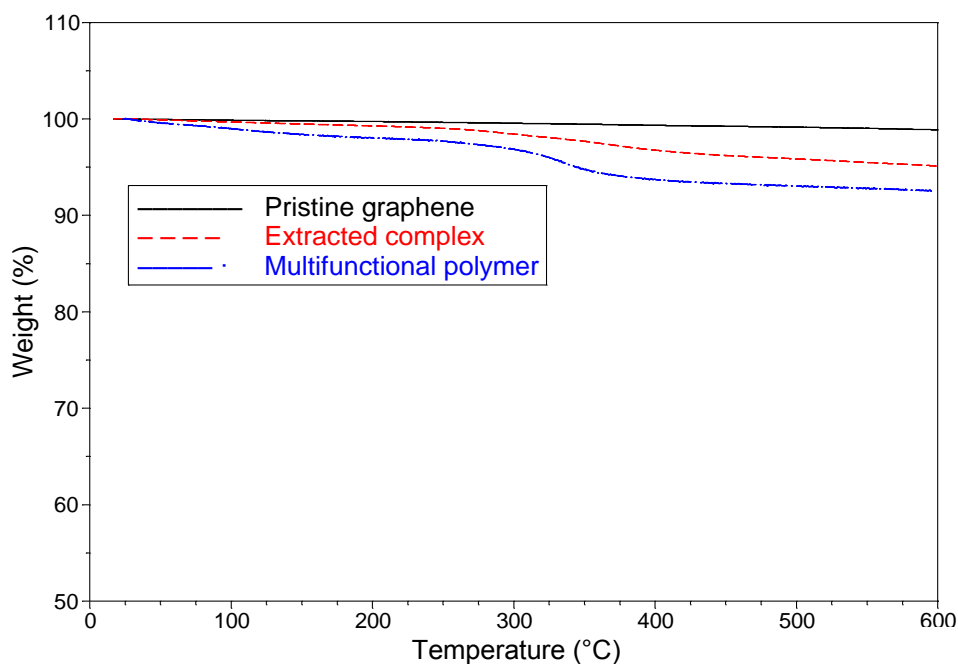


Figure 4.23: TGA curves representing % weight loss associated with pristine EG, extracted graphene/functional-PAN nano hybrid and virgin functional-PAN (of 1.22 mol% PyMMP content).

As would be expected, minimal alteration is seen for the curve representing graphite (1.23 wt%), due to pristine character, as well as the fact that the curve representing the multi-functional polymer closely resembles that of the extracted material. This suggests that there is in fact some degree of association between graphite material and functional polymer indicating composite formation. TGA presents an overall weight loss of 5.17% associated with the presented complex. This is of course not the true composition of graphene/functional-PAN nano hybrid as discussed in section 4.4.1. Due to the incomplete deterioration of PAN under presented conditions, the true weight loss is estimated via equation 4.4. This calculation presents a weight loss of 11.69%, comparing more to the polymer composition of lowest pyrene functionality (0.45 mol% PyMMP composition) referring to the MWCNT/functional-PAN extracted complexes in section 4.4.1. This would suggest a lesser degree of association of graphite filler with the copolymer compared to complexes of MWCNT filler and the same copolymer (1.22 mol% functionality) showing 16.86 wt% composition of functional PAN.

Quenching analysis via $^1\text{H-NMR}$ spectroscopy was attempted. Before any investigation was carried out, concern was presented during the preparation of the $^1\text{H-NMR}$ sample (Figure 4.24). Even after sonication for several minutes the filler seemed to stay agglomerated within deuterated solvent and settle to the bottom of the tube. Never the less, $^1\text{H-NMR}$ analysis was carried out.



Figure 4.24: Visual representation of ¹H-NMR sample prepared for noncovalent quenching analysis of EG/functional-PAN complex.

¹H-NMR analysis commenced, once again, in an identical fashion to that expressed in section 4.4.2, by the introduction of graphitic filler to the sample containing functional polymer (2.02 mol% functionality), amounting to 20 wt%, 33 wt%, and 50 wt% of filler relative to polymer matrix. Analysis was carried out in DMSO-d₆ solvent in the presence of a TMS standard (Figure 4.25).

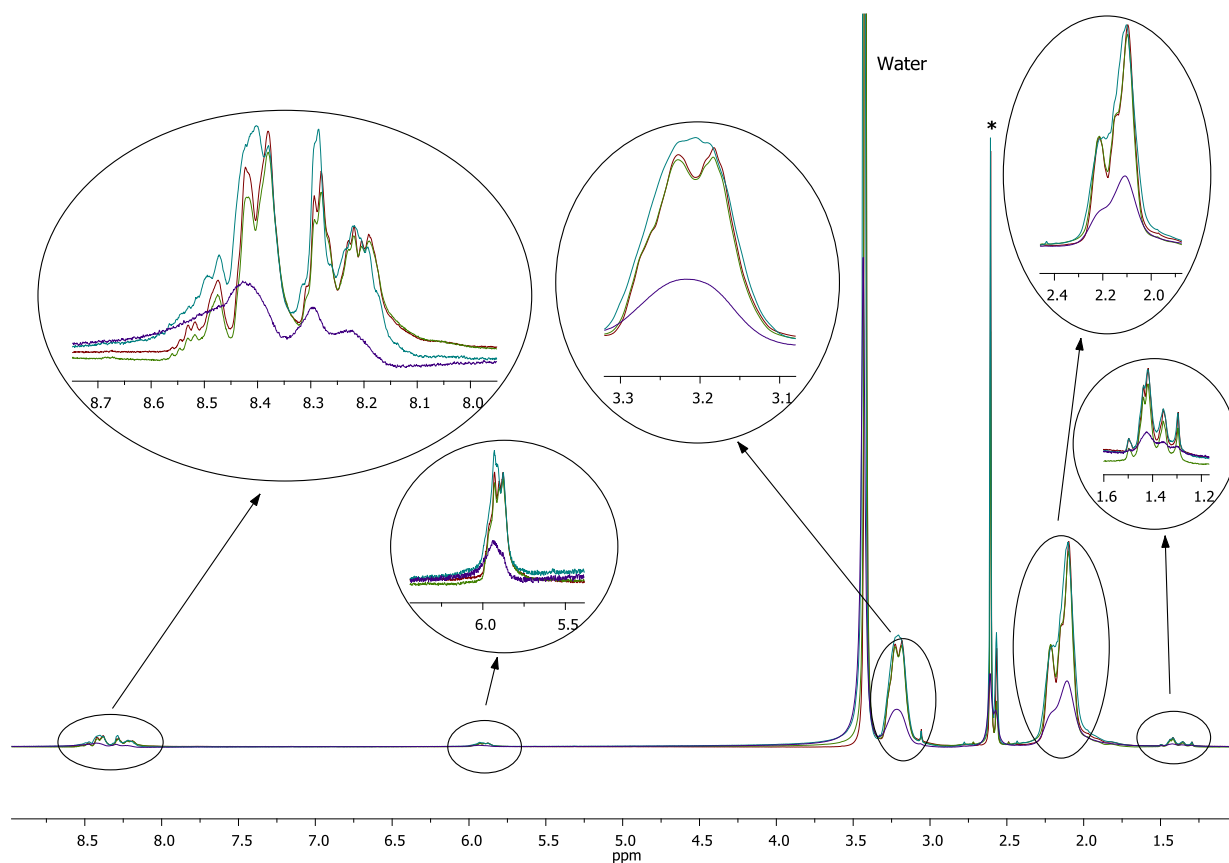


Figure 4.25: Overlaid $^1\text{H-NMR}$ spectra of multi-functional PAN each spectra representing a 0wt% (red), 20wt% (green), 33wt% (blue) and 50wt% (purple) respective EG loading fraction relative to functional sample.

The extent of filler quenching is estimated by integrational analysis against universally present TMS standard. Using MestReNova software on $^1\text{H-NMR}$ spectra, the filler induced quenching observations of the pyrene functionality is numerically extracted to construct a tabulated representation thereof (Table 4.18).

Table 4.18: Values obtained from quenching analysis of pyrene signals by $^1\text{H-NMR}$ on samples containing 0 wt%, 20 wt%, 33 wt% and 50 wt% EG relative to functional polymer.

| EG composition | Multi pyrene functional PAN |
|----------------|-----------------------------|
| 0 wt% | 0% |
| 20 wt% | 8% |
| 33 wt% | 10% |
| 50 wt% | 12% |

From this data a correlation is evident as in the case of MWCNT fillers, presenting a quenching in $^1\text{H-NMR}$ signal representing pyrene functionality relative to TMS standards. The weakening of pyrene representing multiplet is of increased magnitude as filler composition is increased.

The data is additionally represented graphically in effort to visualize trends of signal intensity against filler loading fractions (Figure 4.26).

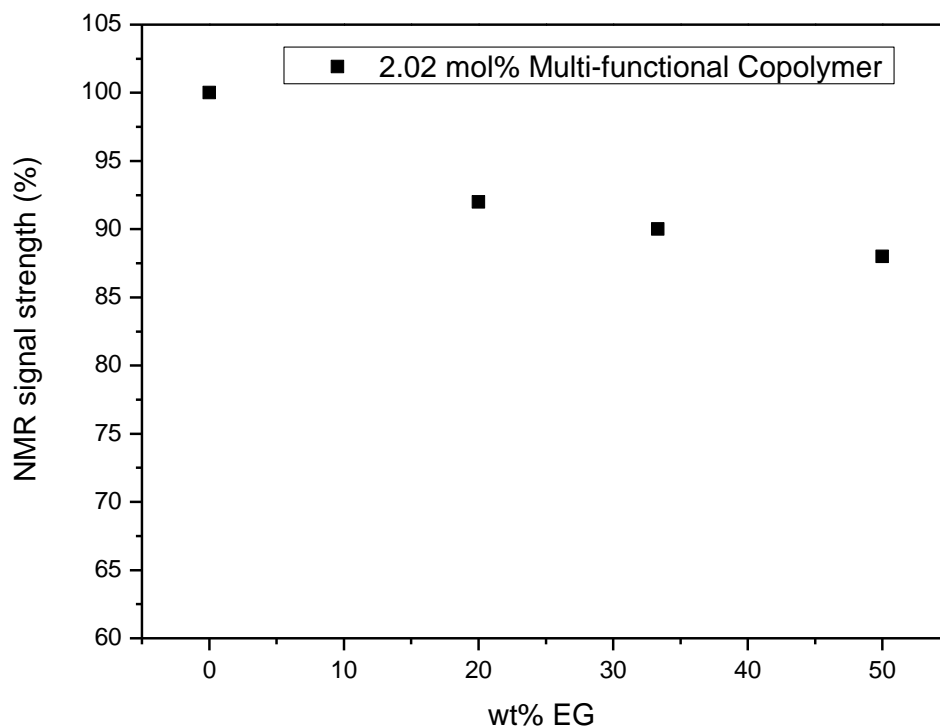


Figure 4.26: Representation of $^1\text{H-NMR}$ quenching character observed for 2.02 mol% multi-functional PAN when exposed to increasing loading fractions of EG filler.

The quenching trends as presented in Figure 4.26 seems to replicate the results obtained for the same multi pyrene functional copolymer then using the MWCNT fillers. This is deduced from the superior initial quench observed to the initial 20 wt% amounting to an average quenching magnitude of 0.4% per wt% filler content. This is followed by a gradual decreasing slope to the final filler composition of 50wt% amounting to an overall quenching magnitude of 0.13% per wt% filler content. This data, therefore, further supports that obtained by the analysis into noncovalent functionalization of MWCNT with the assumption of a decreased quenching magnitude resulting from the bulky nature or crosslinking ability of the compatibilizers. It is also observed that despite the similar trend resulting from molecular structure an overall quenching magnitude is very small indicating a weaker degree or extent of interaction.

Following $^1\text{H-NMR}$ analysis, the more credible fluorescent quenching was also investigated with increasing filler content. The analysis was replicated by using the same loadings of increasing weight fractions as investigated for the MWCNT fillers, by association extent to

the same pyrene functional copolymer (2.02 mol% PyMMP composition). This data is presented in Figure 4.27 below.

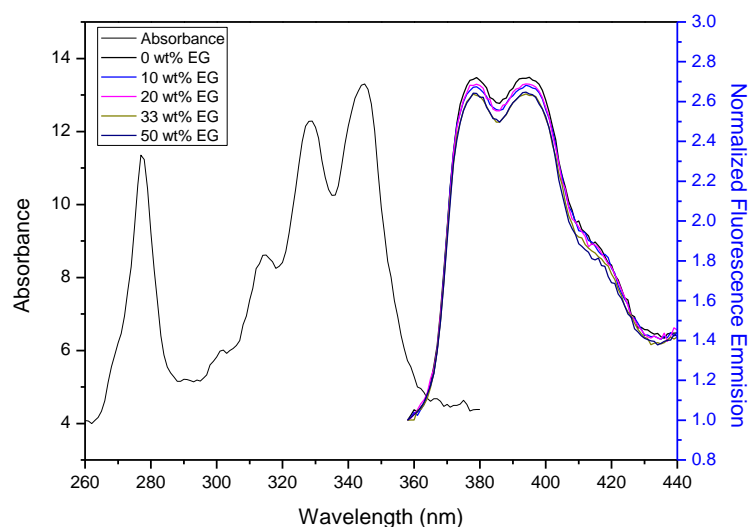


Figure 4.27: Representation of fluorescent quenching character observed for 2.02 mol% multi-functional PAN when exposed to increasing loading fractions of EG.

It is clear to see the inferior quenching presented by the copolymers exposed to the graphite when comparing exposed to MWCNTs (section 4.7, UV-fluorescent Analysis). The data is extracted to exact numerical values via OriginPro8.5 software and presented in the table below.

Table 4.19: Quenching trends of pyrene emission of PAN-co-PyMMP-3 (2.02 mol% functionality) polymers as presented by UV-fluorescent analysis.

| wt% EG composition | PAN-co-PyMMP-3 |
|---------------------------|-----------------------|
| 0 | 100% |
| 10 | 98.42% |
| 20 | 98.07% |
| 33 | 96.41% |
| 50 | 96.21% |

When comparing the fluorescent quenching data with that of $^1\text{H-NMR}$ quenching, the fluorescent data presents a quenching extent much less than presented in $^1\text{H-NMR}$ analysis even when analyzing similar filler loading fractions to the same multi-functional polymer. From the tabulated values a comprehensive comparison can be made between the π - π stacking interactions of pyrene functional PAN polymers and the graphite or MWCNT fillers respectively. Here it is clear to see the inferior degree or extent of association between filler

and functional copolymer when comparing the graphite fillers to the initially studied MWCNT fillers. The quenching of the fluorescent signal resulting from exposure to 50 wt% graphite filler is presented at approximately 4%. This presents a approximately 7.8 times weaker quenching (and thereby degree of association) when compared to the exposure of the same polymer to MWCNTs, presenting an overall quenching of the magnitude 31%. Although an increase in quenching magnitude is observed, the magnitude is far inferior to that expressed for the MWCNT complexes. The data is graphically presented in Figure 4.28 below.

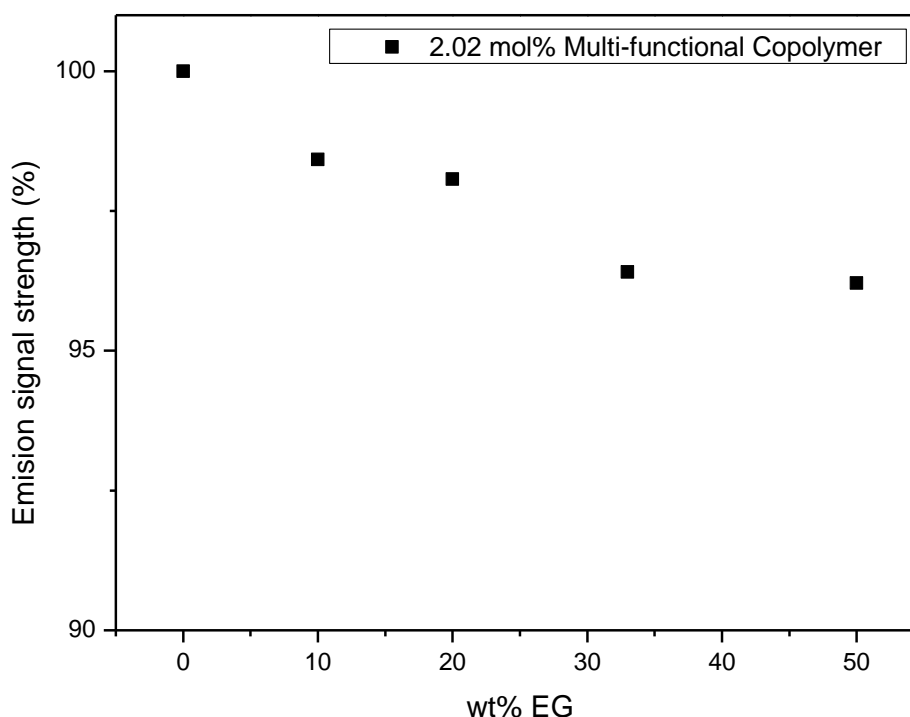



Figure 4.28: Fluorescent quenching trends graphically presented for 2.02 mol% multi-functional PAN when exposed to various loading fractions of EG filler.

Regarding the literature stating an increased noncovalent π - π stacking interaction to be expected for graphene sheets together with the visual representation of apparent agglomeration and data suggesting inferior degree of association, an assumption can be made. These results do not contradict literature, however, it is expected that because of the strong van der Waals π -stacking interactions the agglomeration prove far more difficult to dismantle than in the case of MWCNTs. Therefore the distribution of graphite filler into the composite matrix should prove difficult based on intensive competition for π - π interaction between the graphitic surface and the pyrene functionality opposed to exfoliation of the individual graphene sheets.

Following the investigation into non-covalent association extent the final step of composite processing is achieved by electrospinning under identical conditions as expressed previously in the production of fibrous composites (section 4.5). The composite preparation using the multi-functional compatibilizer of intermediate functionality (1.22 mol% PyMMP content) was utilized in the same ratios during preparation of viscoelastic solutions. These compositions are 1ml DMF, 105.3 mg PAN matrix polymer and 1.6 mg functional polymer, serving as compatibilizer. The solutions were loaded with 0 wt%, 1.5 wt%, 3 wt%, and 5 wt% filler composition relative to polymer before spinning. A visual representation of the spun fibrous mats is presented in Table 4.20 below.

Table 4.20: Physical representation of spun composites of various EG loading fractions.

| Filler incorporation method | EG loading composition | | | |
|---|---|---------|-------|-------|
| | 0 wt% | 1.5 wt% | 3 wt% | 5 wt% |
| Multi pyrene functional compatibilizer | | | | |
| 1.22 mol% PyMMP |  | | | |

This physical representation of fibrous composite mats indicates an expected change in hue with increasing graphite loading fractions, indicative of the increased filler content. However, it is expected that the graphene is extremely poorly dispersed in the nanofibers due to the very poor compatibilization resulting in un-exfoliated clusters as discussed previously. These mats were analyzed by SEM in order to obtain more insight to the morphology of the produced fibers. Imaging of each spun composite is presented in Figure 4.29 below.

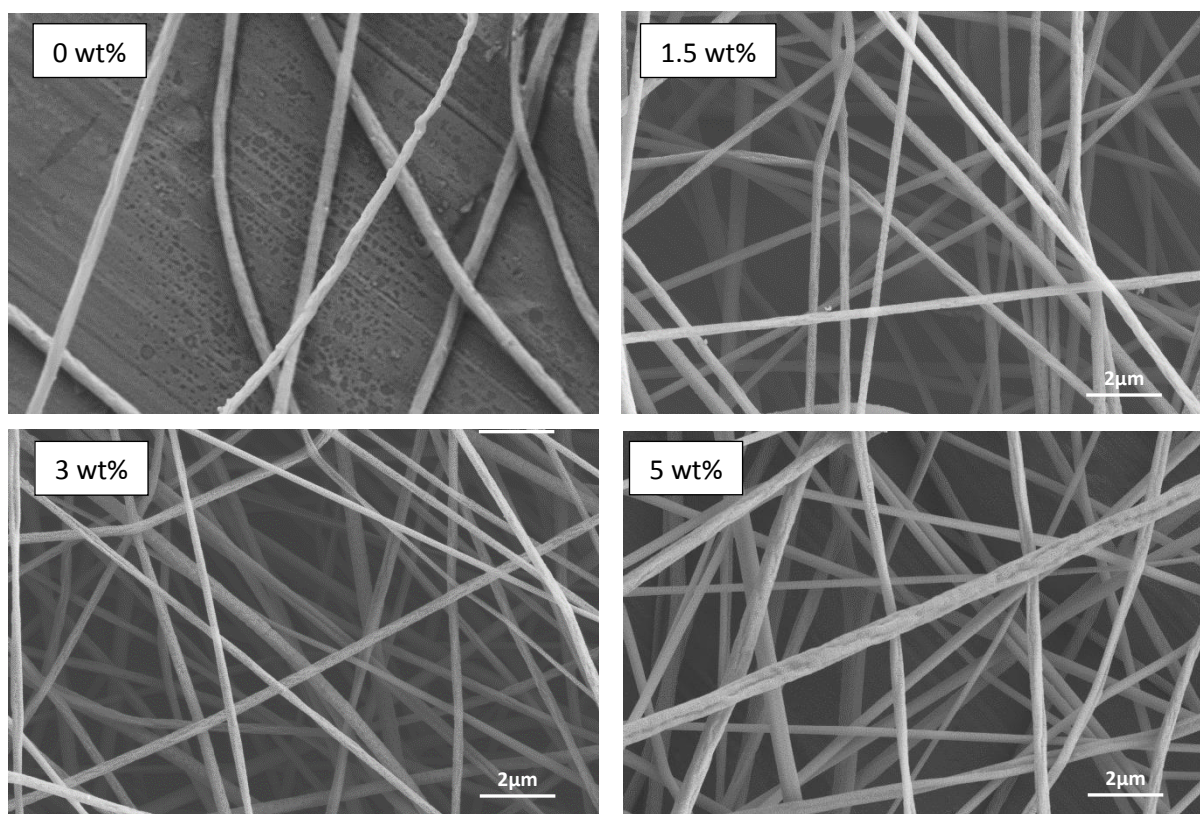


Figure 4.29: SEM imaging of fibrous composites of 0 wt%, 1.5 wt%, 3 wt% and 5 wt% EG composition in PAN matrix by noncovalent incorporation using 1.22 mol% PyMMP comprised multi-functional copolymer.

The SEM images present relatively homogeneous fibers in the same general diameter range as presented for the MWCNT filled composites. From these images fiber diameters are measured and presented as individual average values to be plotted as filler composition is increased (Figure 4.30).

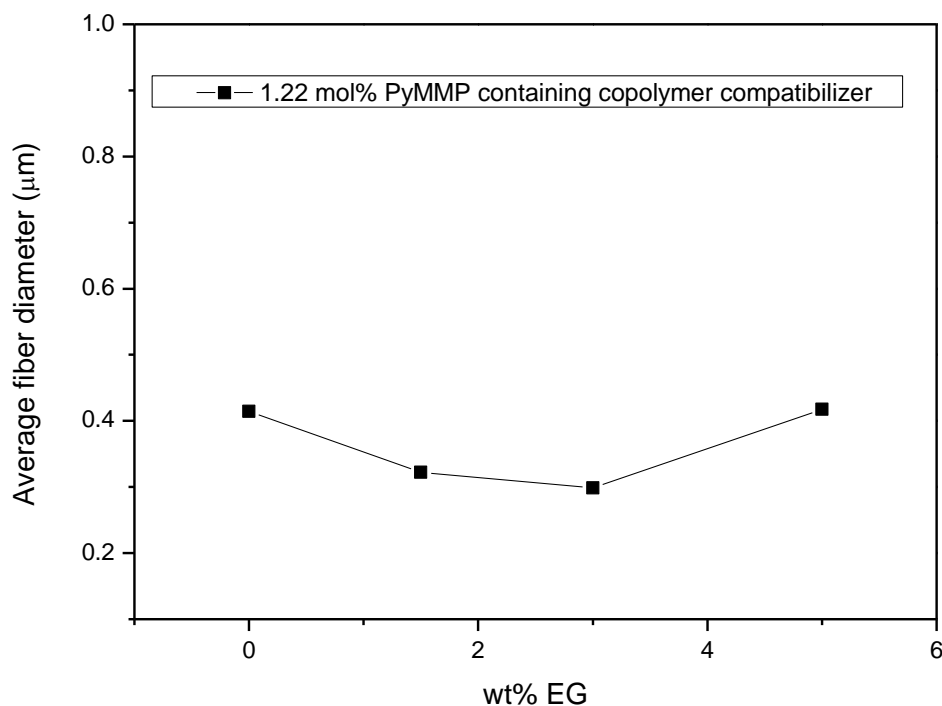


Figure 4.30: Representation of altering fiber diameters resulting from increasing EG filler content as noncovalently compatibilized by 1.22 mol% functional PAN.

The presented fiber diameter follows the same general trend as shown for the incorporation of MWCNT filler and more specifically falls in the same region as the presented trend for the noncovalently compatibilized composite making use of the compatibilizer with the smallest degree of functionality (0.43 mol% mono pyrene functional PAN). TEM analysis on the produced fibers are presented in Figure 4.31 below

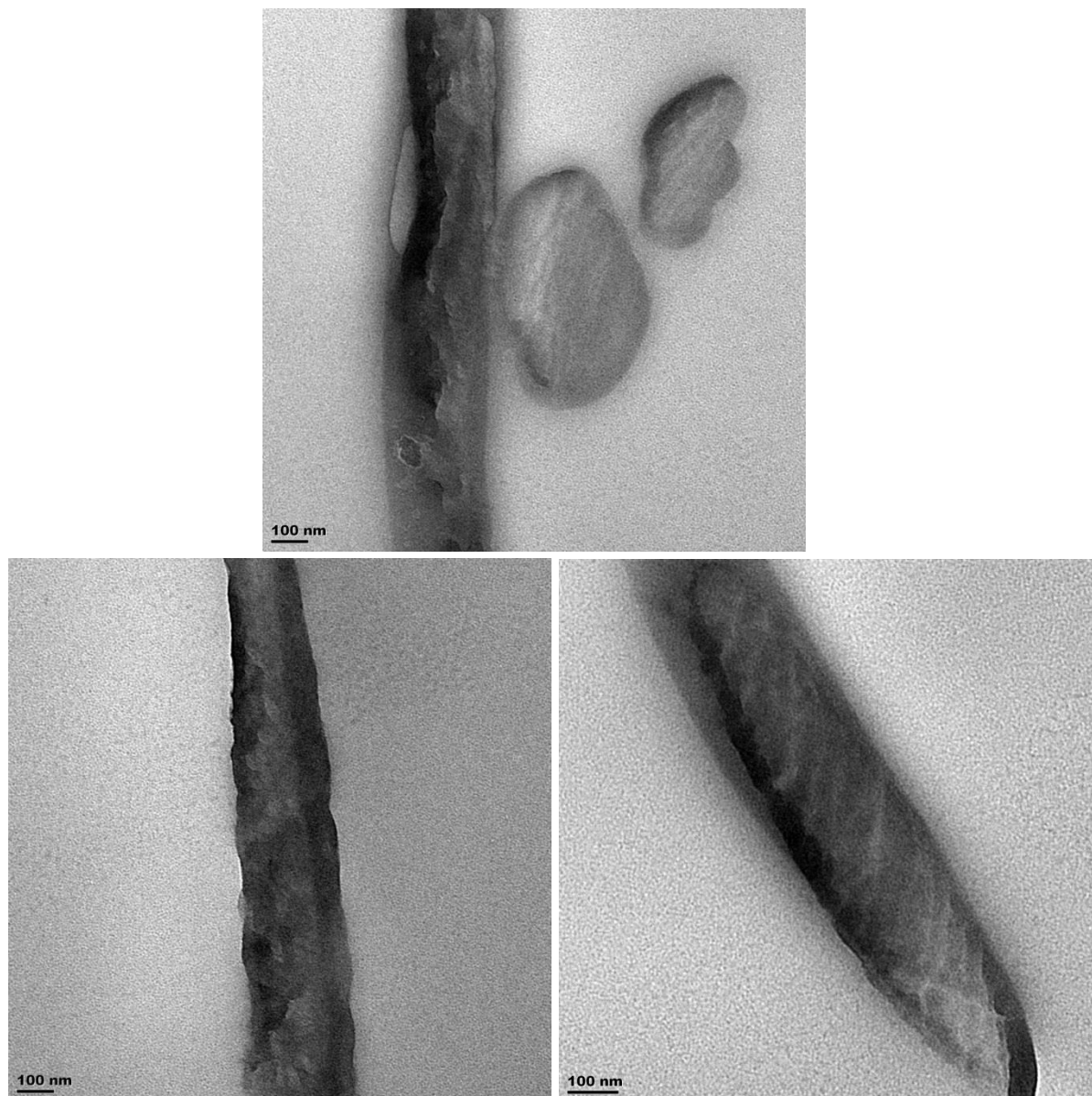


Figure 4.31: TEM imaging of nanofiber composites imbedded with 5 wt% of pristine EG by noncovalent compatibilization using PAN-co-PyMMP:2 (1.22 mol% PyMMP content) multi-functional copolymer.

The TEM analysis shows the incorporation of the EG filler to the fibrous matrix appearing as darkened areas in the fiber. The graphene, however, does not seem to be effectively dispersed throughout the matrix and appear as unexfoliated agglomeration in the fiber. This can be expected considering the weak association of the graphene filler with the compatibilizers as expressed in this section.

4.7 Carbonization of MWCNT/PAN precursor fibers

As the MWCNT fillers were successfully incorporated to the PAN fibrous matrix via the noncovalent incorporation methods, the possibility is explored to produce carbon fibers from

these noncovalently functionalized PAN/MWCNT nanocomposites. Fibers making use of both the mono (Py-PAN-3) and multi (PAN-co-PyMMP-3) pyrene functional compatibilizers and a loading of 5 wt% MWCNT fillers is as well as a PAN fibers of 5 wt% oxidized MWCNTs together with homo PAN fibers were subjected to carbonization. Figure 4.32 represents the SEM imaging of the nanofibers both before and after carbonization, as well as graphically illustrates the average fiber diameter distribution of each.

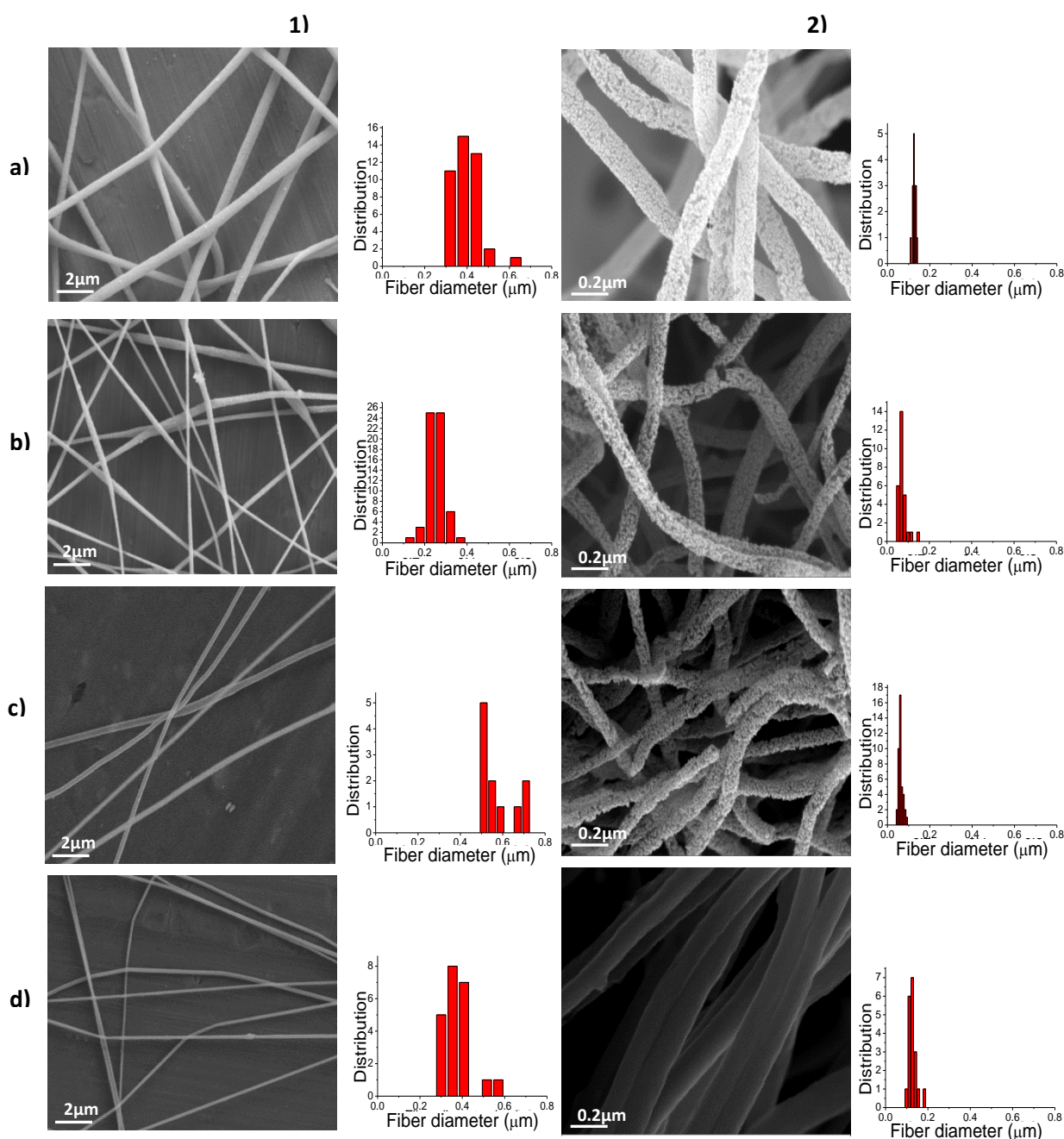


Figure 4.32: Images of PAN fibers as spun by electrospinning with a) no MWCNTs, b) oxidized MWCNTs c) PAN-co-PyMMP-3 and d) Py-PAN-3 for compatibilization of 5wt% of the MWCNT fillers before (1) and after (2) carbonization, with each image accompanied by a graphical representation of the fiber diameter distribution.

As illustrated in Figure 4.32, all the fibers were successfully converted to carbon nanofibers following the heat treatment. The fibers present homegenious fiber diameters at decreased fiber diameters from the uncarbonized precursor fibers, as can generally be expected from carbonized fibers. The average fiber diameters of each fibrous composite and resultant carbonized nanofiber together with the obtained fiber shrinkage is numerically represented in Table 4.21.

Table 4.21: Average fiber diameters ofbained befor and after carbonizatio of PAN/MWCNT nanocomposite fibers.

| <i>Filler specifications</i> | <i>Average fiber diameter before carbonization (μm)</i> | <i>Average fiber diameter after carbonization (μm)</i> | <i>Shrinkage (%)</i> |
|----------------------------------|---|--|----------------------|
| No MWCNTs | 0.43 | 0.16 | 63 |
| Oxidized MWCNTs | 0.28 | 0.21 | 25 |
| PAN-co-PyMMP·3 functional MWCNTs | 0.59 | 0.12 | 80 |
| Py-PAN·3 functional MWCNTs | 0.40 | 0.24 | 40 |

A definite decrease in fiber shrinkage is seen following caronization of the PAN nanofibers as oxidized MWCNTs are incorporated to the PAN fibers. The mono pyrene functional compatibilizer shows a shrinkage 23% less than represented by the shrinkage of the homo PAN fibers, however, shows 15% more shrinkage than seen by the PAN/MWCNT fibers compatibilized by the conventional covalent functionalization by oxidized MWCNTs. Strangely the composite fibers compatibilized by the multi pyrene functional PAN indicated a 17% greater fiber shrinkage following carbonization. Nevertheless, the production of pristine MWCNT imbedded carbon nanofibers by noncovalent functionalization proves successful from the precursor PAN/MWCNT nanocomposite nanofibers as produced in this project.

4.8 References

- 1) M. Degirmenci, E. Taskesen, S. Hicri and H. Yilmaz, *J. Polym. Sci. Part A*, 2008, **46**, 5404-5413.
- 2) N. Köken, S. Karagöz, N. Kizilcan and B. Ustamehmetoglu, *J. Appl. Polym. Sci.*, 2013, **127**, 3790-3797.
- 3) L. Ma, X. Yang, L. Gao, M. Lu, C. Guo, Y. Li, Y. Tu and X. Zhu, *Carbon*, 2013, **53**, 269-276.
- 4) K. Matyjaszewski and J. Xia, *Chem. Rev.*, 2001, **101**, 2921-2990.
- 5) J. K. Oh and K. Matyjaszewski, *J. Polym. Sci. A Polym. Chem.*, 2006, **44**, 3787-3796.
- 6) M. A. Semsarzadeh and M. Abdollahi, *J. Appl. Polym. Sci.*, 2012, **123**, 2423-2430.
- 7) H. E. Gottlieb, V. Kotlyar and A. Nudelman, *J. Org. Chem.*, 1997, **62**, 7512-7515.
- 8) S. A. Ross and G. Lowe, *Tetrahedron Lett.*, 2000, **41**, 3225-3227.
- 9) G. Rokicki, P. Rakoczy, P. Parzuchowski and M. Sobiecki, *Green Chem.*, 2005, **7**, 529-539.
- 10) X. Lou, R. Daussin, S. Cuenot, A. Duwez, C. Pagnoulle, C. Detrembleur, C. Bailly and R. Jérôme, *Chem. Mater.*, 2004, **16**, 4005-4011.
- 11) S. Perrier and D. M. Haddleton, *Effect of water on copper mediated living radical polymerization*, Wiley Online Library, 2002.
- 12) K. L. Beers, S. Boo, S. G. Gaynor and K. Matyjaszewski, *Macromolecules*, 1999, **32**, 5772-5776.
- 13) N. V. Tsarevsky, T. Pintauer and K. Matyjaszewski, *Macromolecules*, 2004, **37**, 9768-9778.
- 14) T. Ogoshi, Y. Takashima, H. Yamaguchi and A. Harada, *J. Am. Chem. Soc.*, 2007, **129**, 4878-4879.
- 15) J. Zou, L. Liu, H. Chen, S. I. Khondaker, R. D. McCullough, Q. Huo and L. Zhai, *Adv. Mater.*, 2008, **20**, 2055-2060.
- 16) N. Nakashima, Y. Tomonari and H. Murakami, *Chem. Lett.*, 2002, **31**, 638-639.
- 17) J. Chen, H. Liu, W. A. Weimer, M. D. Halls, D. H. Waldeck and G. C. Walker, *J. Am. Chem. Soc.*, 2002, **124**, 9034-9035.
- 18) A. Star, J. F. Stoddart, D. Steuerman, M. Diehl, A. Boukai, E. W. Wong, X. Yang, S. Chung, H. Choi and J. R. Heath, *Angew. Chem. Int. Ed.*, 2001, **40**, 1721-1725.
- 19) T. V. Sreekumar, T. Liu, B. G. Min, H. Guo, S. Kumar, R. H. Hauge and R. E. Smalley, *Adv. Mater.*, 2004, **16**, 58-61.

- 20) D. M. Guldi, G. A. Rahman, N. Jux, D. Balbinot, U. Hartnagel, N. Tagmatarchis and M. Prato, *J. Am. Chem. Soc.*, 2005, **127**, 9830-9838.
- 21) Y. Yan, J. Cui, P. Pötschke and B. Voit, *Carbon*, 2010, **48**, 2603-2612.
- 22) M. Assali, M. P. Leal, I. Fernández, R. Baati, C. Mioskowski and N. Khier, *Soft Matter*, 2009, **5**, 948-950.
- 23) T. J. Simmons, J. Bult, D. P. Hashim, R. J. Linhardt and P. M. Ajayan, *ACS Nano*, 2009, **3**, 865-870.
- 24) D. Wang, W. Ji, Z. Li and L. Chen, *J. Am. Chem. Soc.*, 2006, **128**, 6556-6557.
- 25) D. Tasis, N. Tagmatarchis, A. Bianco and M. Prato, *Chem. Rev.*, 2006, **106**, 1105-1136.
- 26) M. T. Byrne and Y. K. Gun'ko, *Adv. Mater.*, 2010, **22**, 1672-1688.
- 27) Z. Spitalsky, D. Tasis, K. Papagelis and C. Galiotis, *Prog. Polym. Sci.*, 2010, **35**, 357-401.
- 28) Y. Sun, K. Fu, Y. Lin and W. Huang, *Acc. Chem. Res.*, 2002, **35**, 1096-1104.
- 29) Y. Ju, G. Choi, H. Jung and W. Lee, *Electrochim. Acta*, 2008, **53**, 5796-5803.
- 30) E. J. Ra, K. H. An, K. K. Kim, S. Y. Jeong and Y. H. Lee, *Chem. Phys. Lett.*, 2005, **413**, 188-193.
- 31) Z. M. Huang, Y. Z. Zhang, M. Kotaki and S. Ramakrishna, *Composites Sci. Technol.*, 2003, **63**, 2223-2253.
- 32) F. Ko, Y. Gogotsi, A. Ali, N. Naguib, H. Ye, G. Yang, C. Li and P. Willis, *Adv. Mater.*, 2003, **15**, 1161-1165.
- 33) Y. Dror, W. Salalha, R. L. Khalfin, Y. Cohen, A. L. Yarin and E. Zussman, *Langmuir*, 2003, **19**, 7012-7020.
- 34) Y. Wang and Y. Bu, *J. Phys. Chem. B*, 2007, **111**, 6520-6526.
- 35) G. Zuo, X. Zhou, Q. Huang, H. Fang and R. Zhou, *J. Phys. Chem. C*, 2011, **115**, 23323-23328.
- 36) F. Tournus and J. Charlier, *Phys. Rev. B: Condens. Matter*, 2005, **71**, 165421.

Chapter 5

Conclusion and future prospects

This final chapter summarizes the findings of this study by presenting a condensed summary of the results and conclusions that are drawn thereof. The chapter is concluded with possible prospects for further work related to this project

5.1 Conclusion

The aim of the project was to produce fibrous PAN/MWCNT composites of theoretically enhanced properties, ranging from mechanical strength to both thermal and electrical conductivity. In optimizing the property transfer from MWCNT filler to composite material it was imperative that the surface morphology should not be chemically altered by disruption of the sp^2 hybridized structure. Maintaining the conjugated structure of the MWCNTs preserves the conductive and mechanical properties along the tubular axis, however, it presents problems in dispersing these fillers in an organic matrix due to the inert surface character and resultant self-agglomerative properties of these graphitic structures. In an effort to maintain the surface architecture of the MWCNT surfaces, the fillers were proposed to be subjected to a non-destructive noncovalent functionalization. Compatibilizing polymers were successfully prepared of both mono as well as multi-functional chemical architecture to serve as an interface between MWCNT fillers and PAN matrix. Pyrene functionality was incorporated as functional moiety to PAN polymer in achieving a compatibilizer capable of associating with the graphitic surface of MWCNTs via a π - π stacking interaction while allowing for the concurrent association with the polymer matrix. These noncovalently compatibilized composites were electrospun to composite fibrous mats of high surface area.

The PAN polymers of α -chain end pyrene functionality were successfully synthesized by means of both a CAN catalyzed redox polymerization as well as an ATRP polymerization. Multi pyrene functional PAN copolymers were successfully prepared by means of CFR copolymerization.

Polymerization by the redox initiated system was investigated by doing a systematic method development consisting of the investigation and variation in parameters such as the solvent, temperature, reaction runtime and catalyst concentration. The system proved redundant for every alteration in reaction variable tested from 1-pyrene-methanol and 1-pyrene-butanol initiators, based on unsatisfactory yields produced. As an alternate way of producing pyrene functional PAN, ATRP synthesis from pyrene functional initiators was attempted and achieved by the production of α -chain end functional polymer of sufficient yields at three variations of molecular weights. The initiators that were used presented similar general molecular geometry as those used for the redox initiated polymerization in being both 1-pyrenebutyl and 1-pyrenemethyl based bromoisobutyrate respectively. Multi-functional PAN was produced by the CRF mediated copolymerization of AN and PyMMP monomers to produce a poly(AN-co-PyMMP) polymer of chain-protruding pyrene functionality. Pyrene incorporation to functional polymer was established by SEC analysis connected to a dual

RI/UV detector system. The synthesis of functional polymers, initiators and PyMMP monomer was confirmed by $^1\text{H-NMR}$ spectroscopy.

The integrity or extent of the noncovalent π - π stacking interactions were investigated based on initial visual filler solubility followed by TGA as well as $^1\text{H-NMR}$ and UV-fluorescent quenching analysis. These analytical techniques were implemented to study the degree of these π - π stacking interactions. TGA analysis indicates an increased quantity of immobilized compatibilizer extracted on MWCNT surfaces as pyrene functionality is increased for the multi-functional copolymers.

Referring to the data presented by the signal quenching analysis by both $^1\text{H-NMR}$ spectroscopy and UV-fluorescence, the degree of quenching is representative of the degree of noncovalent interaction or association strength between MWCNTs and functional polymer. From $^1\text{H-NMR}$ analysis an overall linear type quenching trend is observed for the mono-functional polymer when exposed to a gradual increase in MWCNT loading fractions. This is not the case for the multi-functional copolymers indicating a strong initial degree of quenching to a 20 wt% MWCNT loading fraction after which a less intense quenching extent is observed relative to nanotube content. The quenching of $^1\text{H-NMR}$ signals representing the protons protruding from the nonfunctional segments of the polymeric backbone suggests close association of these segments to MWCNT surfaces when compared to the mono-functional PAN. The successive quenching analysis by UV-fluorescence presents data supporting that of the quenching trends presented by $^1\text{H-NMR}$ analysis. During the fluorescent quenching analysis of mono and multi-functional polymers of similar pyrene functionality, a clear superiority in quenching extent is evident for the multi-functional polymer. This indicated the stronger association of MWCNTs with the polymer compatibilizer of multi-functional character. From these results, the most viable option of producing homogeneously dispersed MWCNT/PAN composites, by the noncovalent functionalization of MWCNT, is suggested by the use of these multi-functional polymer interfaces. The only potential negative of these multi-functional polymers is the possibility that they may act as “crosslinkers” between the MWCNTs leading to dramatic increases in the solution viscosity rendering the solutions “unspinnable”. However, results from this study suggest that at relatively low MWCNT and compatibilizer concentrations this does not present a significant problem. A further potential advantage of the multi-functional pyrene copolymer is the relatively simpler synthesis compared to the longer and more stringent synthetic method required to produce the mono-functional polymer via ATRP.

Following the investigation into the π - π stacking interaction degrees and trends presented for the various MWCNT/functional-PAN complexes, various PAN/MWCNT fibrous

composites are successfully prepared from the single needle electrospinning technique. The fibrous composites are prepared by the incorporation of noncovalently functionalized MWCNTs by the various mono- and multi-functional PAN polymers (Py-PAN and PAN-co-PyMMP polymers respectively) acting as interfacial compatibilizers to the PAN matrix. This is the first reported study on the inclusion of pristine MWCNTs into electrospun PAN nanofibers using pyrene based non-covalent compatibilizers. The influence of functional architecture of the compatibilizing species are compared by electrospinning of solutions containing an increasing pristine MWCNT filler content for each multi-functional compatibilizer as well as a mono-functional PAN and conventionally oxidized MWCNTs series. With gravimetrically varied compatibilizer, universally constant pyrene quantity is achieved and fibrous composite analysis was carried out by SEM and TEM. Analysis of the SEM imaging of fibrous composites presented a general fiber trend for all measured electrospun composites. An initial decrease in fiber diameter is seen following the increase in filler content to 30wt% relative to functional polymer followed by a steep increase in fiber diameters to 50 wt% filler loading. Fiber diameter analysis indicates two separate influences of fiber diameter suggested to be resulting from MWCNT incorporation. A decreasing fiber diameter is suggested to be resultant of increased whipping instability resulting from isolated charges in viscoelastic solution resulting from filler incorporation. The phenomenon of increasing diameter, however, seems to dominate in samples containing compatibilizers of increased pyrene functionality. The observation is made that the effect of increasing fiber diameter is dominant to increasingly greater extents as the pyrene composition of the compatibilizing polymers are increased. This suggests the likely possibility that the functional polymers may act as MWCNT crosslinking materials leading to an increased viscosity more notable in the cases of increased pyrene functionality of interfacial polymers, allowing for a greater possibility of inter filler association and resulting in greater fiber diameters.

Preliminary studies into the association of graphene fillers with the compatibilizers for the production of PAN/graphene composites presented data indicating weak π - π stacking interactions but with similar quenching trends as seen for the MWCNT analysis. SEM analysis showed the successful production of nanofibers. TEM analysis shows the successful incorporation of EG into the fiber matrix, however, suggests poor dispersion or exfoliation of graphene within the fibers.

The MWCNT/PAN fibrous composites prepared by noncovalent functionalization of MWCNTs were successfully carbonized to produce carbon fiber nanocomposites containing pristine MWCNTs as shown by SEC analysis.

5.2 Future prospects

Future work would involve the rheology analysis into the electrospinning solutions in an effort to better understand the effects of the compatibilizers on the viscosity of the solutions and in effect the fiber diameters. Investigation into the obtained electrical conductivity will be needed to establish the property gains of the composite materials from homo PAN fibers and the comparison of the noncovalent filler incorporation against the conventional covalent incorporation.

The preliminary investigation into the graphene filled composites will need to be furthered by investigation into different exfoliation options to achieve better graphene dispersion in the composite materials.

In regard to the carbonization of the composites, analysis into the mechanical and conductive properties is necessary to establish the industrial viability of the nanocomposite fibers.

Appendix

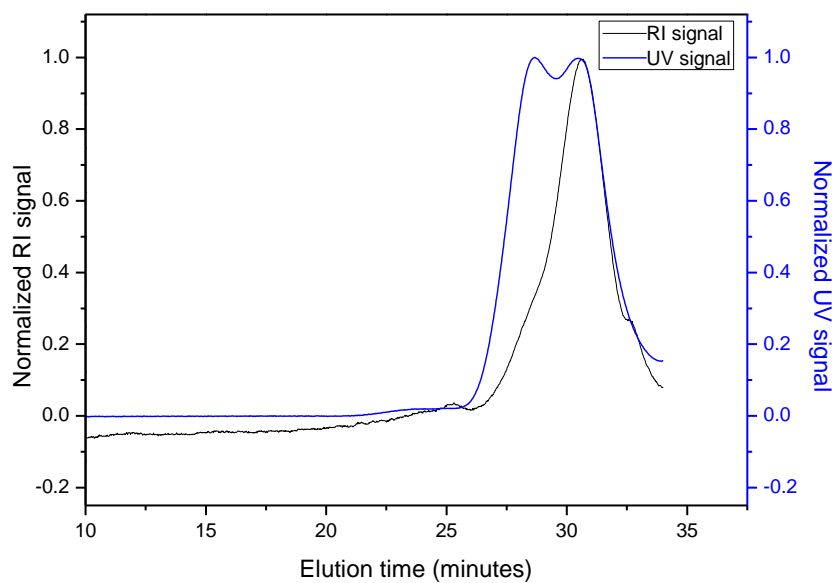


Figure A1: SEC elugrams of py-PAN·1 (1.97 mol% functionality) represented by dual RI/UV (365nm) detection.

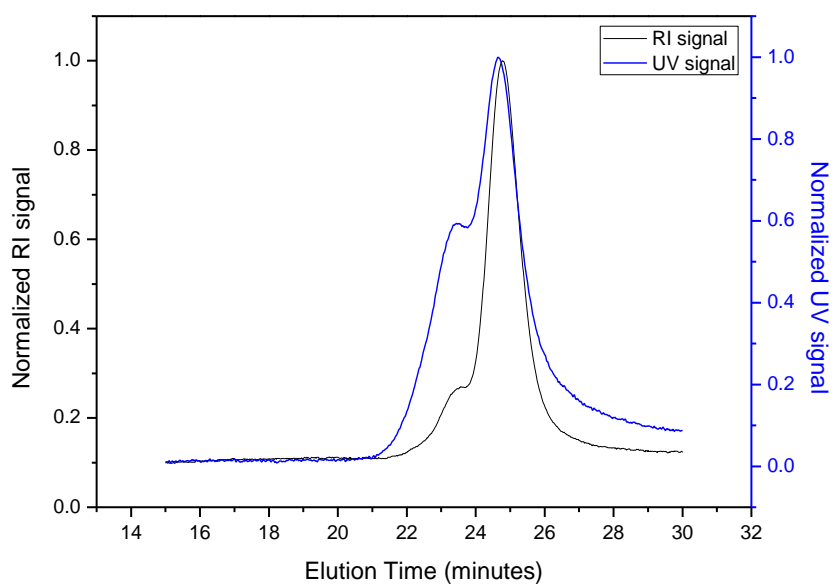


Figure A2: SEC elugrams of py-PAN·3 (0.43 mol% functionality) represented by dual RI/UV (365nm) detection.

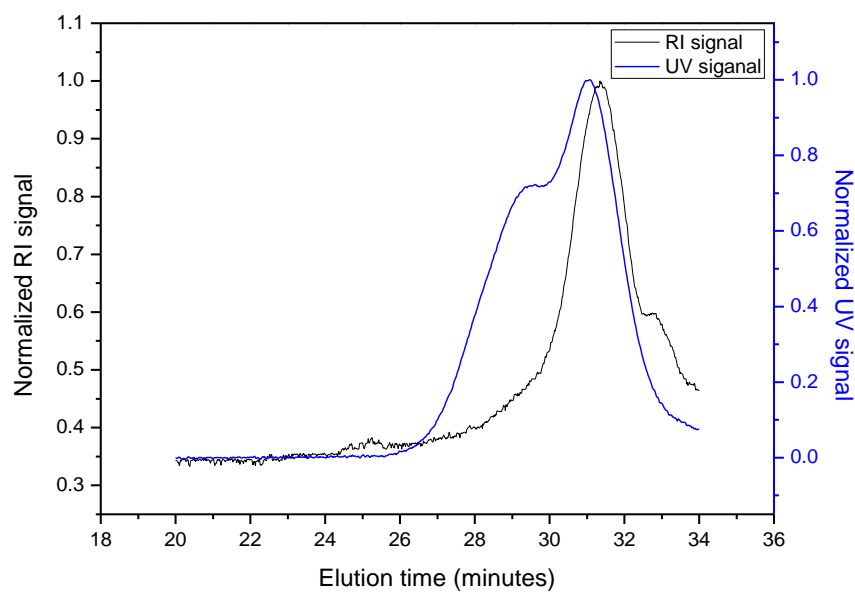


Figure A3: SEC elugrams of py-PAN-4 (7.14 mol% functionality) represented by dual RI/UV (365nm) detection.

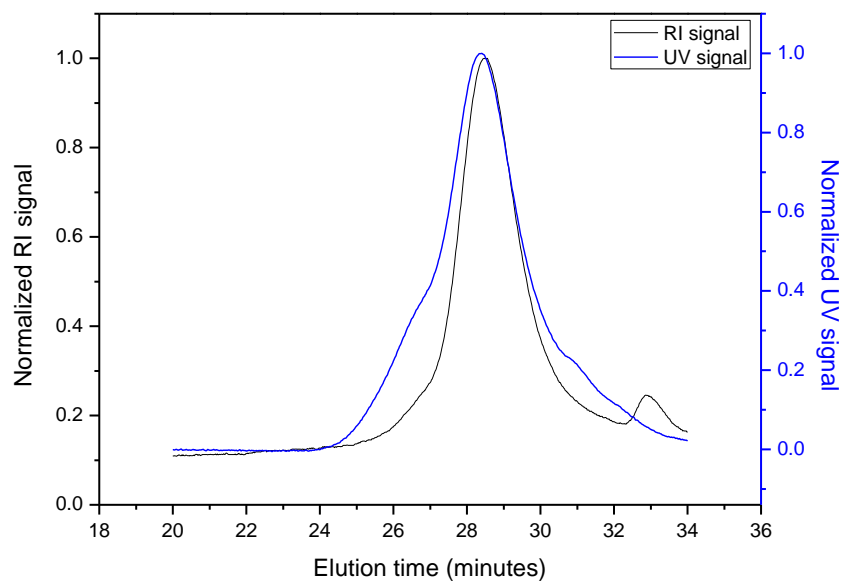


Figure A4: SEC elugrams of py-PAN-5 (2.86 mol% functionality) represented by dual RI/UV (365nm) detection.

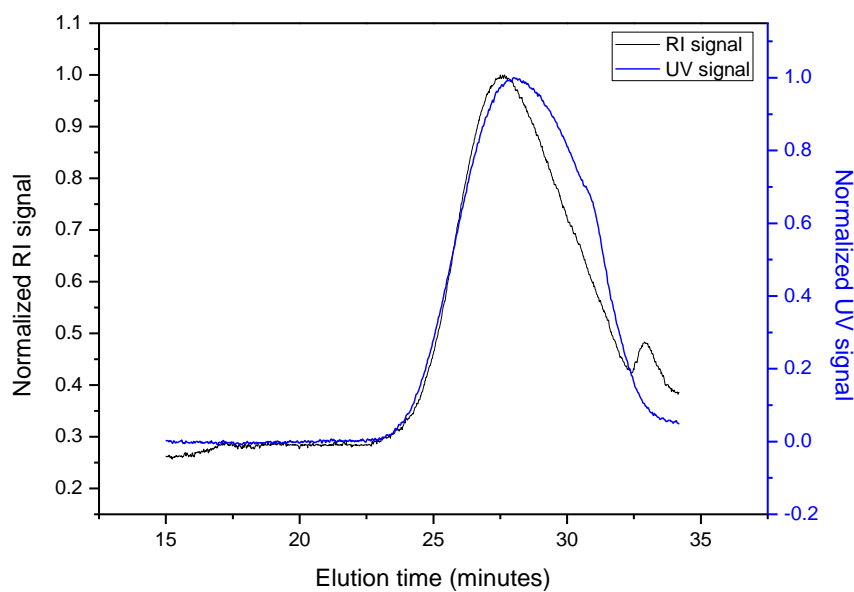


Figure A5: SEC elugrams of py-PAN·6 (2.78 mol% functionality) represented by dual RI/UV (365nm) detection.

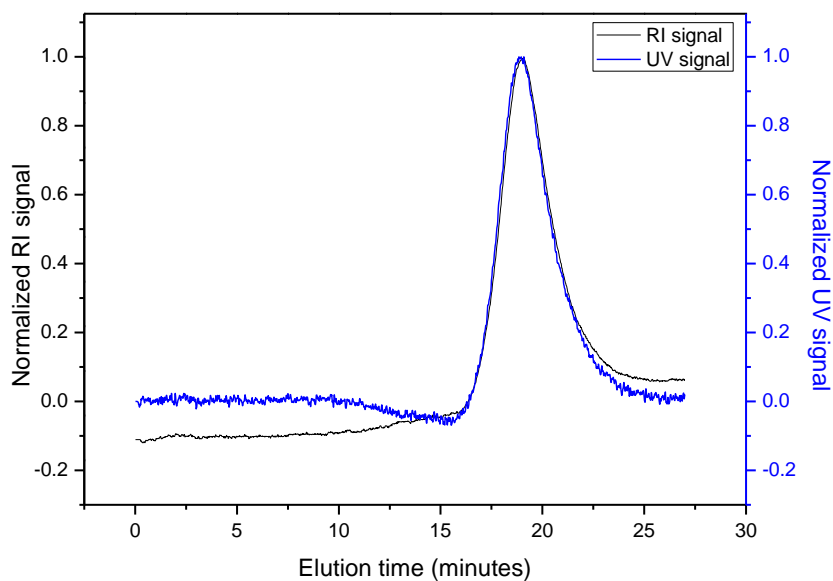


Figure A6: SEC elugrams of PAN-co-PyMMP·1 (0.45 mol% functionality) represented by dual RI/UV (365nm) detection.

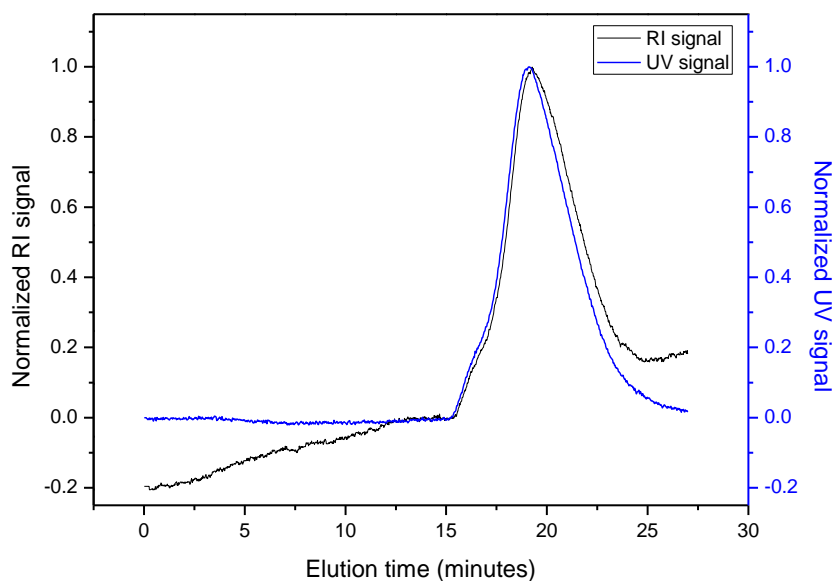


Figure A7: SEC elugrams of "PAN-co-PyMMP-3 (2.02 mol% functionality) represented by dual RI/UV (365nm) detection.

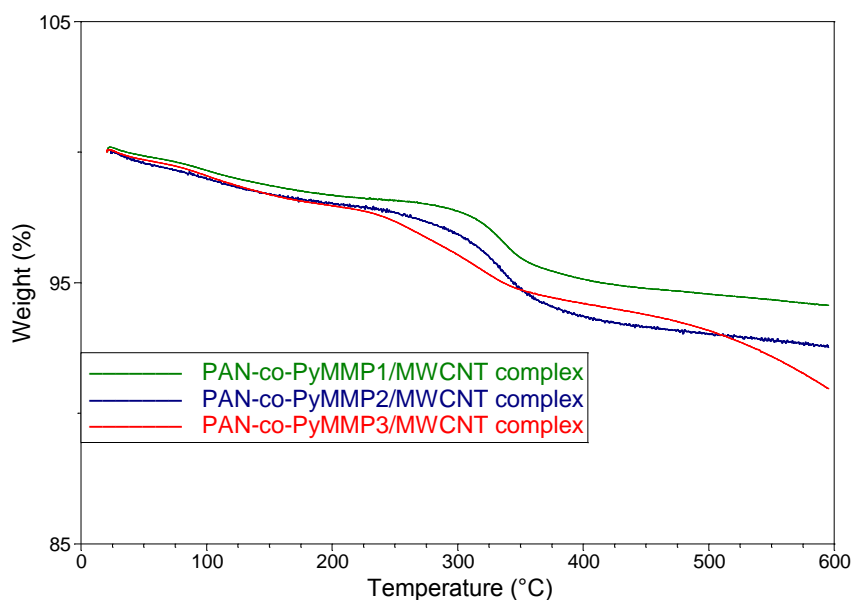


Figure A8: TGA thermograms representing % weight loss of extracted MWCNT complexes of multi pyrene functional polymers, PAN-co-PyMMP-1, PAN-co-PyMMP-2 and PAN-co-PyMMP-3 respectively.

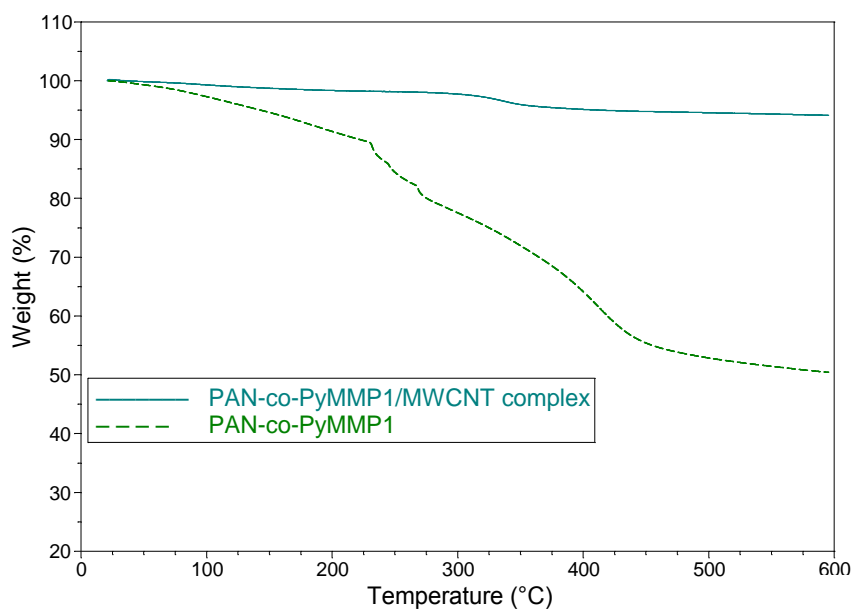


Figure A9: TGA thermograms representing gravimetric weight loss of PAN-co-PyMMP 1 polymer and PAN-co-PyMMP 1/MWCNT complex respectively.

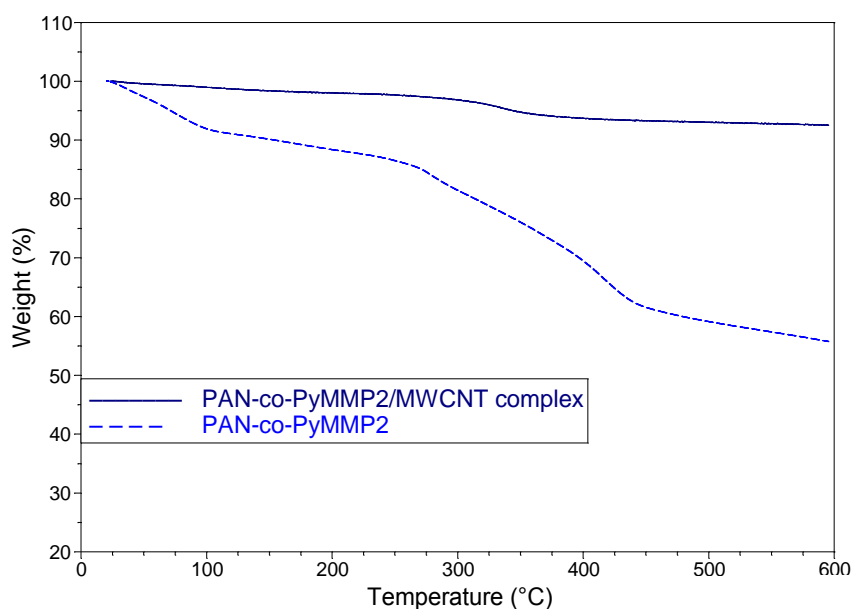


Figure A10: TGA thermograms representing gravimetric weight loss of PAN-co-PyMMP 2 polymer and PAN-co-PyMMP 2/MWCNT complex respectively.

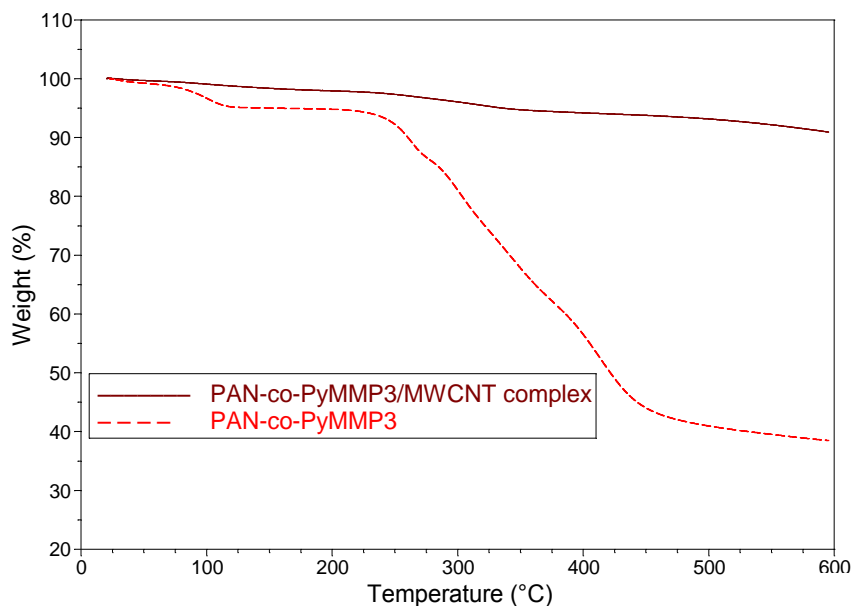


Figure A11: TGA thermograms representing gravimetric weight loss of PAN-co-PyMMP-3 polymer and PAN-co-PyMMP-3/MWCNT complex respectively.

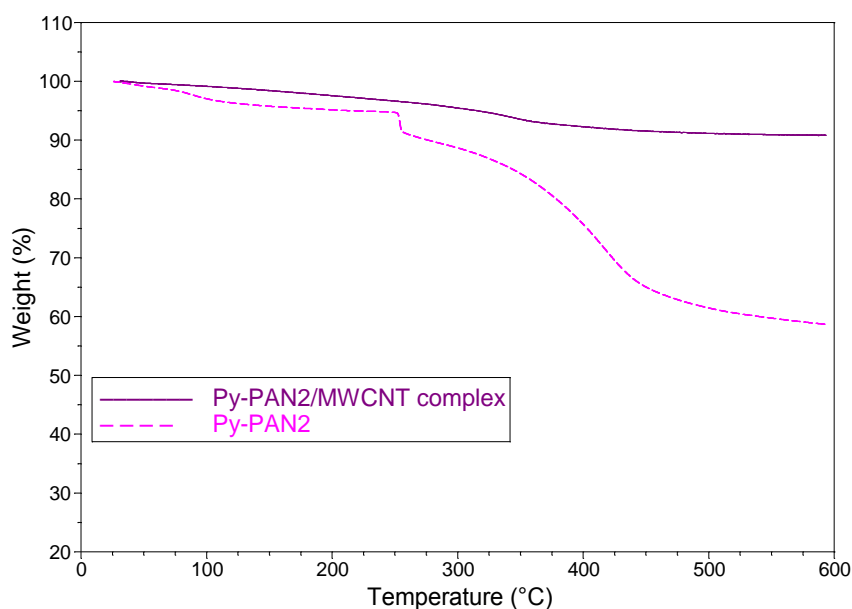


Figure A12: TGA thermograms representing gravimetric weight loss of Py-PAN-2 polymer and Py-PAN-2/MWCNT complex respectively.

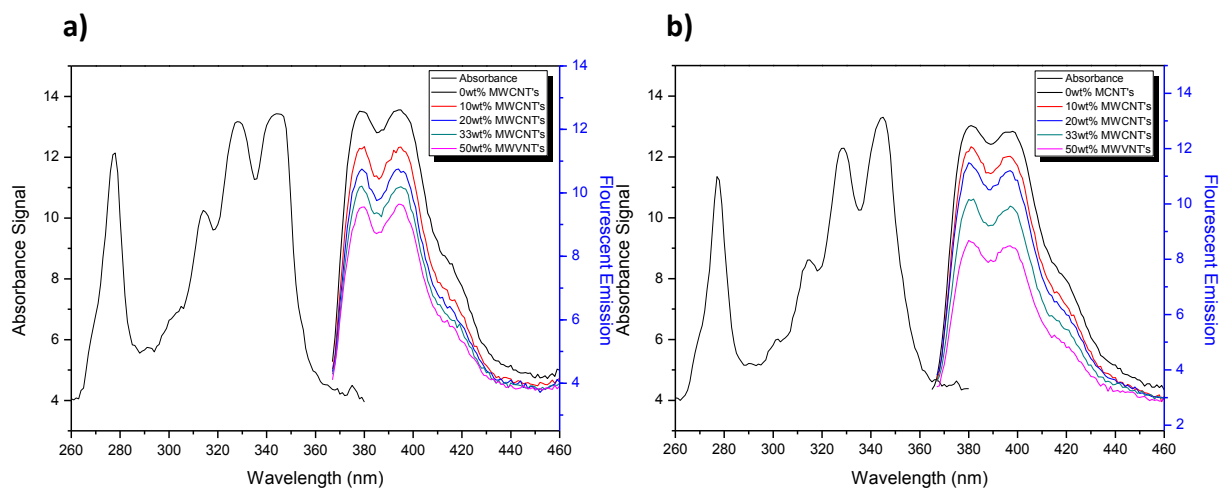


Figure A13: Representation of fluorescent quenching character observed for a) PAN-co-PyMMP-2 (1.22 mol% functionality) and b) py-PAN-3 (0.43 mol% functionality) polymers when exposed to various quantities of MWCNTs.

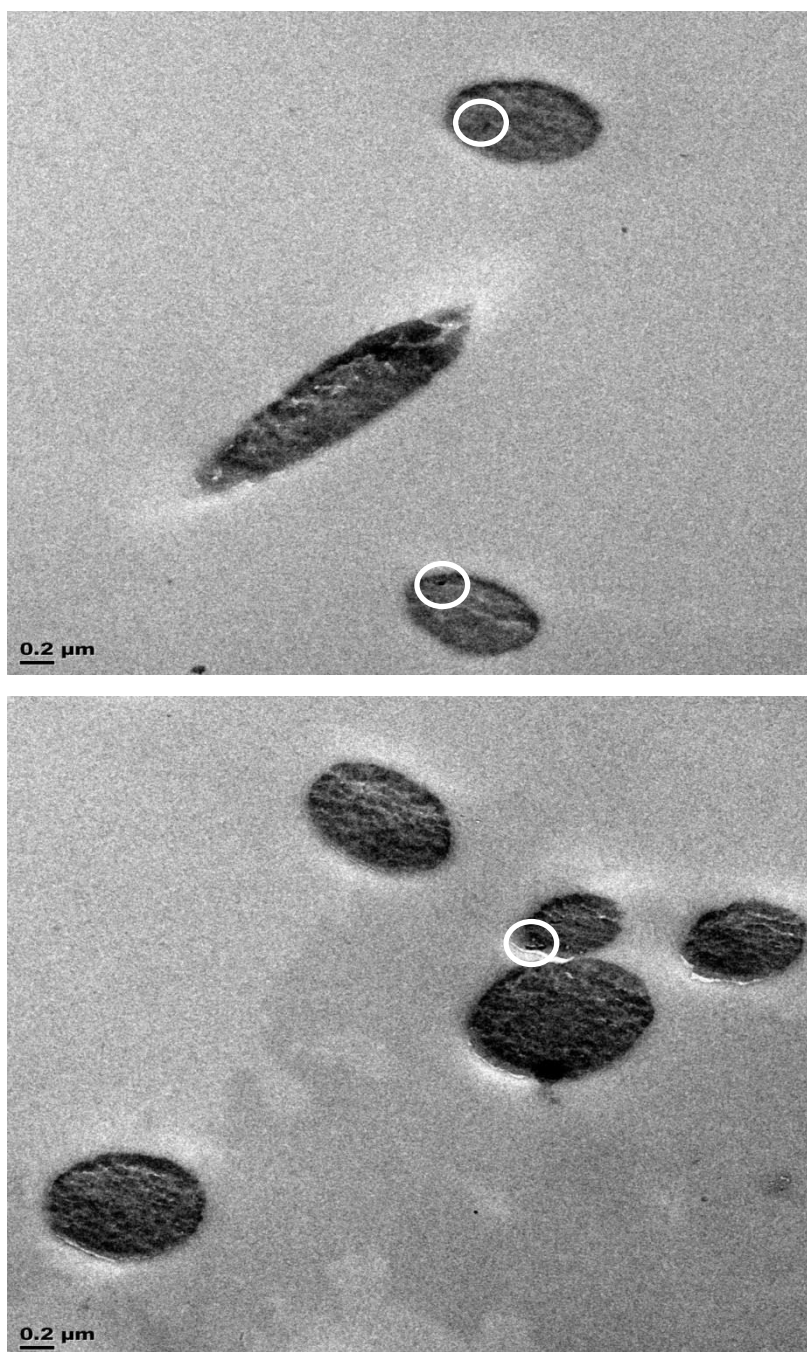


Figure A14: SEM images of PAN/MWCNT fibrous composites containing a 5 wt% loading fraction of MWCNTs as prepared with the PAN-co-PyMMP.1 compatibilizing specie.